I. Table of Contents

II. List of Tables

III. List of Figures

IV. List of Abbreviations

3-D	3-dimensional
A	Surface area
AAP	3-azido-1-aminopropane
AC	Alternating current
Ac.	Sodium acetate buffer
APTES	Amine (3-aminopropyl)triethoxy-silane
Ar-ion	Argon-ion
ASM	Average Surface Mass
A-SpA	Alkynated SpA
bIgG	Bovine immunoglobuline G
B-PER	Bacterial protein extraction reagent
Conc.final	Final concentration
COOH-	Carboxylic acid-
CPM	Close-packed Monolayer
C-terminus	Carboxyl-terminus
Cu(I)	Copper (I)
CuAAC	Copper(I)-catalysed azide alkyne cycloaddition
DMSO	Dimethyl sulfoxide
DNA	Deoxyribonucleic acid
E	Elastic modulus
E. coli	*Escherichia coli*
e.g.	Exempli gratia
EDC	1-ethyl-3-(3-dimethylaminopropyl) carbodiimide
et al.	*et alii*
Fab-domain	Fragment antigen binding domain
fA-MBP	Fully alkynated MBP species
fA-SpA	Theoretical fully alkynated SpA
Fc-domain	Fragment crystallizable region domain
GFP	Green fluorescent protein
H_2O	Water
hCG	Human chorionic gonadotropin
HEPES	4-(2-hydroxyethyl)-1-piperazine ethane sulfonic acid
HF	Hydrogen fluoride
hIgG	Human immunoglobulin G

His-Tag	Polyhistidine-tag
Hz	Hertz
i.e.	*id est*
IgA	Immunoglobulin A
IgE	Immunoglobulin E
IgM	Immunoglobulin M
IMPACT	Intein mediated purification with an affinity chitin-binding tag
intein-CBD	Intein-chitin binding domain
IPL	Intein-expressed protein ligation
IR	Infrared
ISFET	Ion-selective field-effect transistor
IUPAC	International Union of Pure and Applied Chemistry
Ka	Affinity constant
kDa	Kilodalton
kHz	Kilohertz
LB Medium	Luria Bertani Medium
M	Molar
MBP	Maltose binding protein
MES	2-(N-morpholino)ethanesulfonic acid
MESNA	2-mercaptoethanesulfonic acid
MHz	Megahertz
MIP	Molecularly imprinted polymers
MWCO	Molecular weight cut-off
Myc	v-myc avian myelocytomatosis viral oncogene homolog
N_2	Nitrogen gas
N_3	Azide
NaAsc	Sodium L-ascorbate
NHS	N-hydroxysuccinimide
Nm	Nanometer
N-terminus	Amino-terminus
O_3	Ozone
OD	Optical density
PAGE	Polyacrylamide gel electrophoresis
PBS	Phosphate buffered saline

pI	Isoelectric point
PPE	Poly(p-phenylene ethynylene
PVC	Poly Polyvinyl chloride
QCM	Quartz crystal microbalance
rA-MBP	Random alkynated MBP
RNA	Ribonucleic acid
RT	Room temperature
S.D.	Standard deviation
SAM	Self-assembled monolayer
sA-SpA	Single alkynated SpA
SDS	Sodium dodecyl sulfate
SELEX	Systematic evolution of ligands by exponential enrichment
SH-group	Thiol-group
SiO_2	Silicon oxide
SpA	*Staphyllococcus* Protein A
SPAAC	Strain-promoted alkyne-azide cycloadditions
SPIEDAC	Strain-promoted inverse electron-demand Diels-Alder cycloaddition
ssA-MBP	Site-specifically alkynated MBP
TBTA	Tris[(1-benzyl-1H-1,2,3-triazol-4-yl) methyl] amine
TCEP	Tris(2-carboxyethyl)phosphine
THPTA	Tris(3-hydroxypropyltriazolylmethyl) amine
TMS-EDTA	N-(Trimethoxysilylpropyl)ethylenediamine triacetic acid sodium acetate trihydrate
Trizma	Tris(hydroxymethyl)aminomethane
UV	Ultraviolet
v/v %	Volume/volume percentage
VCAM	Vascular cell adhesion protein
WB	Washing buffer

Chapter 1. General introduction

1.1 State-of-the-art of (protein) immobilisation strategies

In the modern world, a variety of surface modifications is being applied to improve the properties of materials. The trend of the last decade is to produce advanced materials that are more reliable, lighter and more sustainable. For instance, in healthcare prosthesis manufacturers are constantly developing their materials in order to improve properties such as density, strength and reliability [1, 2, 3]. When the first hip replacement was performed in 1951, the prostheses were made out of stainless steel and cobalt chrome molybdenum alloys [4]. Due to the fact that the manufacturing process was not yet optimised, precision was still a hurdle, and the prosthesis suffered from friction and wear. Currently, the surface roughness of these implants can be controlled and the shape of the artificial joint resembles the original, decreasing the amount of stress and wear on the implant. As more and more younger people are struggling with joint issues, the operating life of the implant needs to increase as well. By improving the alloys towards a higher wear resistance and a reduced coefficient of friction, its lifespan can be increased.

Furthermore, the chemical surface properties of other biomedical devices are becoming more and more important. Well-known examples are dental implants that are functionalised with biological material. These titanium implants, modified with peptides and collagen are being introduced into the bone structure of the patient's jaw. The applied surface modifications improve the bone formation to enhance the integration of the 'foreign' material into the bone tissue [5, 6].

In case of cardiovascular implants, there are two needs. First, for the insertion of a stent in a cardiac artery or vein, surgeons use catheters in order to get the stent into the right place [7]. To minimise complications, these catheters need to be made of materials that are biocompatible, stable, very lubricious and traceable while using certain imaging techniques. At the same time the interaction with the body's own molecules needs to be kept to a minimum. However, after applying the stent that is made of a biocompatible alloy of cobalt and chromium, and removing the catheter, the medical device has to interact with its surroundings. By biofunctionalising the stent, endothelialisation of the metal surface will be enhanced and the long-term efficacy of the stents is increased [8]. In literature several polymeric and metallic implantable devices are being described of which the surfaces were modified to improve their integration into the human body [9].

Another application in the healthcare industry, which is gaining interest lately, are nanoparticles functionalised with a biological material. These nanohybrids can be used for different purposes such as diagnostics or as therapeutic tools. In literature this conjugation of antibodies to inorganic nanoparticles and the importance of their orientation is described [10]. Different immobilisation approaches, such as physical adsorption, covalent binding *via* endogenous functional groups and biotin binding, their advantages and disadvantages were extensively described.

Biotextiles are examples of a less invasive application which requires surface modifications [11]. This type of textile can serve as a haemostatic wound dressing, preventing patients from bleeding to death. Especially in case patients, who are treated with anticoagulants, are having a seriously bleeding wound, this type of textiles is highly desirable.

A final very interesting example, which has been recently reported in the literature, describes surface modified nanoparticles containing anticancer drugs [12]. In the report, a modified porous silicon is described, which contains Tamoxifen, a drug used for the treatment of breast cancer. By chemically modifying the silicon nanoparticles with this drug, the drug release was prolonged over several weeks. A chitosan gel, containing the same drug, had not such an ideal release profile. All previous examples demonstrate how important it is to have a reliable immobilisation method in order to obtain surfaces with certain modifications, adapted to their application's specific needs.

Currently, different methods are being used to immobilise (bio) molecules in order to obtain (bio) functionalised layers which can be used for different applications such as (non-)adhesive surfaces and nanomedicines. Each immobilisation method has its specific properties, which might be beneficial in one case while being a drawback in another situation. Major differences between the current methods are the bond strength between the receptor molecule and the solid carrier, and the accessibility of the target binding sites in the receptor molecule.

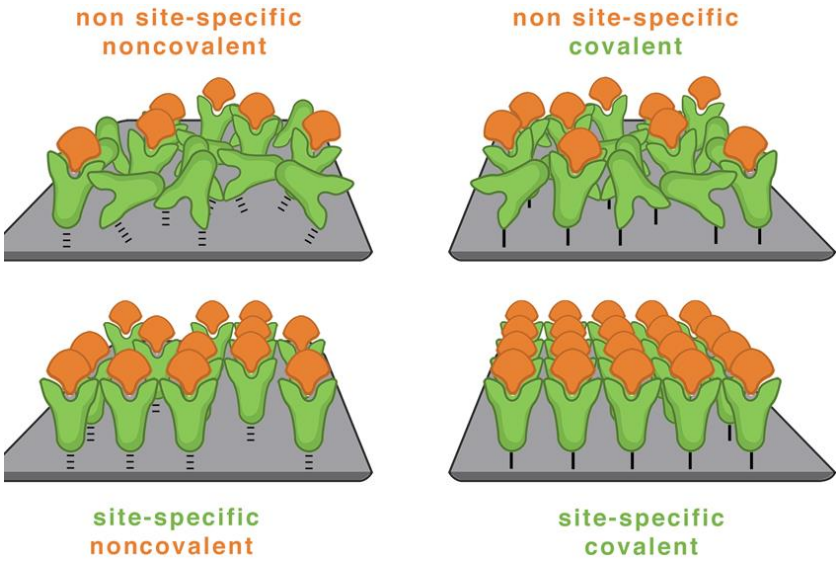

Figure 1.1: Schematic illustration of the different (non) covalently, (non) oriented immobilised biolayers obtained by various immobilisation methods and their influence on target binding [13].

The least expensive and most straightforward way to immobilise proteins onto solid carriers is by physical adsorption [14]. This type of immobilisation is based on weak interactions, *i.e.* hydrogen bonds, van der Waals, hydrophobic and electrostatic interactions, which are reversible [10]. Most often physical adsorption results in heterogeneous, disordered biolayers (**Figure 1.1**; top left) due to the multiple orientation possibilities of the receptor molecules. Proteins will keep their conformation after adsorption to a hydrophilic surface, while adsorption to a hydrophobic surface often results in conformational changes [15]. This can be explained by the fact that the hydrophobic part of the protein is pointed towards the protein's 'core', at a remote distance from the polar solvent in which it is dissolved. By interaction with a hydrophobic surface, the stable core will be affected due to strong protein-carrier interactions, resulting in conformational

changes which might result in activity loss of the protein [16]. In case of a hydrophilic surface, the protein will tend to unfold its hydrophobic core to a lesser degree. A conformational shift will be less likely, and its functioning will be influenced less. In addition to the conformational issues, the accessibility of the binding sites cannot be guaranteed.

A second immobilisation approach is based on complementary affinity interaction between biomolecules. Artificially introduced bio affinity tags show increased affinity towards each other leading to a strong, but non-covalent bond between the functionalised biomolecule and the complementary functionalised surface (**Figure 1.1**; bottom left). Although the strength of the bond is weaker than a covalent coupling, the stability of this layer is more definite than an adsorbed protein layer. Furthermore, a site-specific introduction of these affinity tags is possible, which allows the formation of oriented biofilms [17]. A well-known example of this bio-affinity immobilisation is the interaction between biotin, also known as vitamin B7, which is involved in many biochemical processes, and (strept) avidin. Biotin binding proteins, such as (strept)avidin, exhibit the highest possible affinity that can be achieved between ligand (receptor molecule) and target ($Ka \approx 10^{15}\ M^{-1}$) [18]. They are used for the conjugation of a wide variety of target-binder pairs to a solid support, ideally without hindering the biologically active compound of the biotin/(strept)avidin functionalised receptor [19-24]. Also polyhistidine is a very commonly used affinity tag, which has to be recombinantly introduced to the C- or N-terminus of the protein. When exposing these polyhistidine-tagged proteins to a metal treated substrate a reversible but oriented interaction between protein and surface occurs [25]. Another possibility is the introduction of a specific epitope at the N- or C-terminus of a protein.

Examples of well-known epitopes are FLAG-tags (with sequence motive DYKDDDDK), which can be recognized by a scala of anti-FLAG poly- and monoclonal antibodies, or myc-tags (polypeptide protein tag derived from the c-myc gene), which can be recognized by anti-c-myc antibodies [24, 26]. An interesting approach as an alternative to the previously mentioned tags is the conjugation of DNA to proteins. However, this still needs further optimisation concerning the site-specific introduction of DNA to the bio receptor [27].

A third immobilisation strategy utilizes the presence of endogenous functional groups present in the protein (**Figure 1.1** top right). Reactions can be performed between functionalised surfaces and a suitable counterpart inside the protein's backbone leading to a strong covalent bond. Most of the reactive functional groups can be found at the N- and C-terminus, or in the naturally occurring amino acids. Amines and thiols are frequently used to establish the stable bond between the biomolecule and the solid carrier, due to their nucleophilic characteristics. Amines found in lysines can make up to 10% of the overall amino acid sequence [28]. The thiol functionalities of cysteine are present in much lower amounts, more particular in free cysteines [29]. Coupling reactions with malemide, vinyl-sulfone or thiol-ene reactions are possible routes to covalently immobilise the proteins to the solid carrier [30, 31].

In addition, carboxylic groups, which are abundantly present in proteins, are used by converting them into an appealing, reactive counterpart. The reactive species is obtained by addition of 1-ethyl-3-(3-dimethylaminopropyl) carbodiimide or EDC. Since the half-life of the reactive carboxylic species is rather short, in general N-hydroxysuccinimide (NHS) is added to the reaction mixture. The acquired NHS ester 'stabilises' the reactive form until the primary amines appear and turns NHS

in a good leaving group [32]. The resulting covalent bond between receptor and surface improves the stability of the functionalised layer compared to a non-covalent functionalised bio surface. For example, this may offer the opportunity of manufacturing reusable sensing surfaces. Since no drastic preceding protein functionalisation has to be performed, the biomolecule's structure will undergo minimal, directly induced alterations after the coupling. However, the abundant presence of the endogenous functional groups, makes the formation of a homogeneous oriented biolayer after immobilisation highly unlikely. Obviously, the randomness in orientation will most likely affect the availability of the target binding sites.

In order to obtain stable layers with optimised availability of the target binding sites, a fourth and most ideal procedure combines all beneficial properties of the former mentioned. To acquire such biolayers, the coupling between biomolecule and carrier should be covalent and a single functionality should be site-specifically introduced into the biomolecule of interest, preferably without affecting its activity. This site-directed, covalent immobilisation is depictured in **Figure 1.1** (bottom right). This site-directed coupling needs functionalities, which are site-specifically applied into the protein's structure. For example, bioengineering makes it possible to functionalise a protein of interest during expression in cells like yeasts or bacteria, *e.g. Escherichia coli* (*in vivo*), or post-translational by appending a functionality at, for example, the C- or N-terminus of the protein (*in vitro*).

The straightforward approach to introduce functional groups in a protein is by linking a bifunctional molecule to a functional group of which only one is present in the wild-type proteins. One functionality of the bi-linker will be involved in

creating a bond between linker and protein, while the other will be involved in protein immobilisation reaction. Targets of the protein modification are, for example, thiols, carboxyls, hydroxyl and amines. The ideal situation is when the amino acid containing the targeted functional group, is unique *and* distant from the active side, leading to an active, mono functionalised protein.

Another approach uses enzymes (*e.g.* sortase A [33]) in order to introduce functionalities in a post-translational way. This implies that the used enzyme is able to recognize a certain peptide at a certain point in the protein. Depending on the enzyme species it will catalyse a reaction leading to functionalisation or it will be directly involved by covalently reacting with the protein and thereby labelling it in one single step [34].

The alternative to post-translational modification implies inserting/deleting fragments or replacing parts of the DNA sequence present in the cell which lead to the introduction of a unique, bio-orthogonal (not naturally present) amino acids in the protein's structure. The term bio-orthogonal refers to the fact that this group can be introduced into a living system without interfering with any native biochemical processes [30]. In this specific case, it would not affect the functioning of the protein or cause any side reactions with other biomolecules that are not bearing the complementary functional group. To achieve such functionalised proteins, living cells are being used as small factories, which manufacture proteins based on a genetic template. This template is inserted into the cell by transfecting with a DNA vector. After transcription and translation of the genetic code, recombinant proteins are obtained by extraction from the cells [35, 36]. Ultimately this 'engineering' of proteins offers opportunities to append a new functionality in the biomolecule's structure at a location that is not involved

in the target binding processes. This functionality can serve as a unique chemical handle to immobilise proteins in an oriented and covalent way.

Because of the large variety of potential functional groups that can be embedded into biomolecules, an appropriate immobilisation method should be chosen satisfying certain properties. Minimising the chance of side reactions, bio-orthogonality and formation of stable covalent bonds under aqueous conditions, are key criteria to which the reaction method has to match. Furthermore, it is a self-evident truth that, to maintain the original conformation and activity, an aqueous environment with, if possible, physiological conditions, is preferred. All this will create a situation at which only the bio-orthogonal moieties will react with their counterparts, minimising crosslinking between the different proteins and, in a more advanced stage, giving the opportunity to couple the protein in a site-directed manner, *i.e.* paving the way towards advanced hybrid biomaterials containing proteins with a uniform orientation.

1.2 'Click' Chemistry

According to the abovementioned key criteria for finding proper immobilisation chemistry, many chemical reactions can already be excluded such as those that take place in organic, denaturing solvents. A next hurdle for many reactions is the bio-orthogonality, which is very important considering the goal of obtaining uniform oriented proteins. By introducing a unique, non-natural functional group, of which it is certain that it will not react intra- or intermolecularly with other functionalities, the opportunity is created to obtain a uniformly loaded bio surface. Reactions relying on functional groups already present in nature, which are therefore not unique, will not be considered.

Although 'Click' chemistry has already existed for a considerable time, it did not gather a lot of attention until Sharpless published an article entitled *"Click chemistry: diverse chemical function from a few good reactions"* [37]. 'Click' chemistry encloses a whole set of different coupling reactions with very specific characteristics. The reaction conditions need to be simple, modular, wide in scope and without harmful side-products. Furthermore, the reaction yields need to be high enough. Separation of the product after the synthesis reaction should be very straightforward and the reaction has to be able to be carried out under physiological conditions. When all these requirements are fulfilled, the reaction can be categorised as a 'click' reaction [37]. As described by Sharpless 'click' chemistry can be divided in three subgroups: nucleophilic opening of highly strained rings (*e.g.* epoxides, aziridines, cyclic sulphates), 'protecting group' reactions (reversible carbonyl chemistry) and cycloadditions (acetyls, ketals, aza-analogs). In this thesis an archetypal example of a cycloaddition will be studied extensively.

This cycloaddition is termed the Huisgen 1,3-dipolar azide-alkyne cycloaddition. Because of the stability of azides in aqueous environment they stay 'invisible' until the proper conditions are achieved. The azide groups will only start to form triazoles, 1,4 and 1,5 region-isomers, with alkynes at an elevated temperature. This selectivity is a very important advantage. However, the formation of two possible isomers is not favourable towards the formation of a uniform biolayer. By mediating the reaction using metal ions, *i.e.* copper (I), region-isomers are excluded, creating only 1,4 substituted 1,2,3-triazoles as shown in **Scheme 1.1**. In a first step copper(I) acetylide **I** is formed. Next a stepwise annealing *via* a six-membered copper(III) containing intermediate **III** leads to the 1,4 substituted 1,2,3-triazoles.

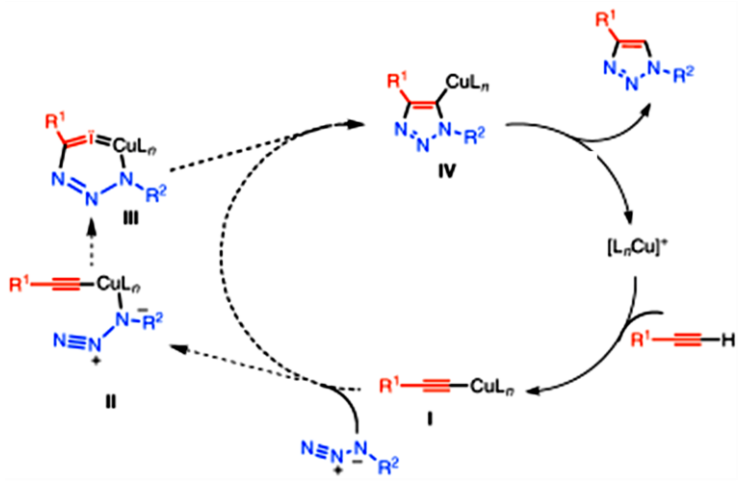

Scheme 1.1: Mechanism of the Cu(I) catalysed alkyne-azide 1,3 cycloaddition (CuAAC) adapted from reference [38].

Other 'click' chemistry reactions, such as the strain-promoted alkyne-azide cycloadditions (SPAAC), strain-promoted inverse electron-demand Diels-Alder cycloaddition (SPIEDAC), Diels-Alder, thiol-ene or Staudinger ligation, all have

their strengths and weaknesses. In general, their main strength is the same: they can be applied in the incorporation of functionalities in proteins and other biomolecules. For example, various bio-orthogonal functionalities, such as fluorescent labels, can be attached to a protein in this way.

The Staudinger ligation complies to the key criteria as mentioned above. However, it has been shown that the efficiency and reaction kinetics are a huge constraint when applied *in vivo* due to air oxidation of phosphine reagents [39]. The Diels-Alder reaction is a reversible reaction and has similar issues when taking the reaction rate into consideration, which is in general low at room temperature. Additionally, under physiological conditions the combination of proteins with unrestricted SH-groups and the use of malemides and furans hinders the Diels-Alder reaction, which makes this a less favourable method for coupling reaction [40].

The thiol-ene reaction is another alternative. By reaction of thiols and alkenes under UV radiation, a covalent bond between the protein and the surface can be created. Main restriction here is the fact that thiols are present in wild-type proteins, which most likely will lead to crosslinked proteins. Finally, Strain-promoted alkyne-azide cycloaddition (SPAAC) chemistry could be suitable because no catalyst needs to be added in order to chemically couple the azide and alkyne containing molecules and surface. However, the reaction rate is rather low and still more research is required considering how to introduce the required functionality and the effect thereof on the protein's functionality [41].

In this research the CuAAC technique will be evaluated and extensively tested to prove its advantages and suitability in the development of improved biofunctionalised surfaces.

1.3 Biofunctionalisation for biosensors

1.3.1 Biosensor platform

Not only medical devices that serve to treat people against diseases or life threatening conditions require further improvement of their surface characteristics, also devices which might sense or even predict upcoming diseases at a very early stage, *i.e.* without explicit symptoms, require optimisation to make them more sensitive and accurate. In addition, the food industry could use highly sensitive (bio) sensors for the detection of pathogens. Until 50 years ago, housewives and cooks decided whether food was unfit for consumption by using their senses, *i.e.* smell, taste and view. Even today people are still relying on several chemical senses (taste and olfaction) and the visual senses (sight) to decide whether food contains pathogens [42]. Because in this case, relying on our senses is only 'accurate' for larger quantities of bacteria, contaminated food at the earliest stages (containing only a few bacteria or toxic substances) can give the impression to be harmless but in reality be an actual threat to the individual's health. To detect the smallest amounts of contamination in food, drinks or inside living organisms, the development of sensitive artificial sensors is of interest. Therefore, researchers try to construct artificial sensors, based on biological or non-natural materials, which are extremely sensitive and very selective in order to detect the smallest amounts of pathogens or to search for the presence of certain biomarkers. Biomarkers are molecules that can be quantitatively measured and evaluated as an indicator of normal biological processes, pathogenic processes, or pharmacological responses to a therapeutic intervention [43]. Early detection of these molecules provides the opportunity for a rapid and appropriate intervention. By combining the advanced biological sensing system,

which has been optimised for millions of years, with the technological progression of the past 100 years, the best of both worlds can be combined in order to develop surfaces covered with biological material for diverse biomedical applications, *e.g.* adhesive for implants, anti-fouling surfaces for medical applications, biofunctionalised nanoparticles for tissue imaging [44-47], controlled drug delivery systems [48] or for bio based sensing purposes [49-51].

Currently at Hasselt University, research efforts are focussing on the development of sensor layers with improved sensitivity by controlling the orientation of the sensing elements. To obtain these stable, oriented layers, first the proper immobilisation approach needs to be chosen. However, at the beginning of the 20th century, oriented coupling was not yet a matter of interest. At that time researchers were about to discover the first sensing layers based on biologic material. The first steps towards a real biosensor appeared in 1916, when Nelson and Griffin reported the immobilisation of invertase on activated charcoal [52]. Six years later, the first glass pH-electrode was invented [53]. Then three decades past until L.C. Clark Jr. invented the first oxygen electrode in 1956 [54]. He was also the first who reported a definition and invented the first biosensor: an amperometric enzyme electrode for glucose [55]. In 1969 the first potentiometric biosensor was produced, which was able to detect urea due to immobilised urease on an ammonia electrode [56]. One year later, the first ion-selective field-effect transistor (ISFET) was discovered [57]. In 1972 the first commercial biosensor, a pen shaped single use glucose sensor, appeared on the market. In 1975 the first microbe-based biosensor using cells of *Acetobacter xynilum* to determine ethanol was developed [58], as was the first immuno sensor in which ovalbumin was coupled to a platinum wire for the detection of ovalbumin antibodies [59]. Later

that year an artificial endocrine pancreas was developed. The prototype consisted of an auto-analyser for blood glucose determination, a minicomputer system, and a pump driving system. Later, Miles Laboratory Inc. brought such a device with a reduced size on the market. These devices have been used to study the pathophysiology of diabetes mellitus [60]. From 1980 several devices were developed. Examples include a fibre optic pH-sensor for the *in vivo* measurement of blood gases, a fibre optic-based biosensor for glucose and surface plasmon resonance immuno sensors [61-63]. Nowadays, researchers are developing a broad variety of biosensors based on planar surfaces, nanoparticles, nanowires, nanotubes and quantum dots [64].

During the 20th century the definition of a biosensor altered a few times, resulting in the definition we know today. According to a recently proposed IUPAC definition a biosensor is "*a self-contained integrated device which is capable of providing specific quantitative or semi-quantitative analytical information using a biological recognition element (biochemical receptor) which is in direct spatial contact with a transducer element. A biosensor should be clearly distinguished from a bioanalytical system, which requires additional processing steps, such as reagent addition. Furthermore, a biosensor should be distinguished from a bio probe which is either disposable after one measurement, i.e. single use, or unable to continuously monitor the analyte concentration*" [65].

In **Figure 1.2** the basic elements of a biosensor are shown: a biological receptor (green), a transducer surface (blue), an amplifier (purple) and a data processing system. In order to determine whether the solution of interest (*e.g.* blood serum, urine, saliva) contains target molecules, the solution has to be applied to the biosensor's surface. When binding between the target analyte and the biological

receptor occurs, it will cause a chemical or physical change. The transducer will transfer this change into an electric signal, which on its turn will be amplified and recorded by the computer. After the data have been processed by a computing system, analysis can be performed.

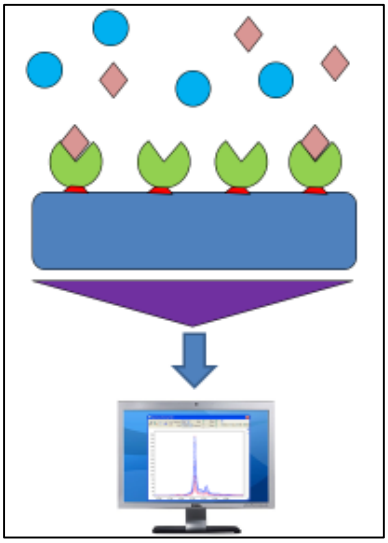

Figure 1.2: Basic scheme of a biosensing set-up: target analyte (pink), biological receptor (green), transducer surface (blue), signal amplifier (purple) and a data processing system.

1.3.2 Bio(-mimicking) receptor molecules

During evolution a large pool of different signalling molecules developed inside living cells in order to maintain proper intra- and extracellular conditions. To assure that all different cells/organs are working in harmony with each other, an appropriate signalling system had to be developed. This system is based on various very specific signalling molecules from all sizes and shapes, which transfer information from one cell to another or from one organ to another. These signalling molecules can vary from hormones excreted by endocrinal glands to inflammatory cytokines produced by damaged tissue. They do not only affect neighbouring cells, they also can have an impact on remote tissue, enhancing or inhibiting certain activities. In order to survive, cells/tissues organs have to interact properly with each other. Due to the large variety of circulating signal molecules, cells need to be sensitive to specific stimulants and stay unaffected by others. Therefore, every specific organ developed its very specific receptors. As shown in **Figure 1.3** specific stimuli activate receptors present in the membrane, cytoplasm or at the nucleus, leading to activation or inhibition of well-defined processes. Without the high specificity of these receptors the whole cellular signalling would end up in chaos and complex organisms could not exist.

As illustrated in **Figure 1.2** the primary layer of a biosensing device generates the initial signal after a target binding event. This biolayer is essential and determines the difference between a regular sensor and a 'bio' based sensor. In nature different target-receptor interactions can be found, *e.g.* enzyme-substrate interactions, antigen-antibody interactions, protein-protein and protein-DNA interactions, DNA-DNA binding and cell-cell binding interactions, which can be of use for countless biosensing applications.

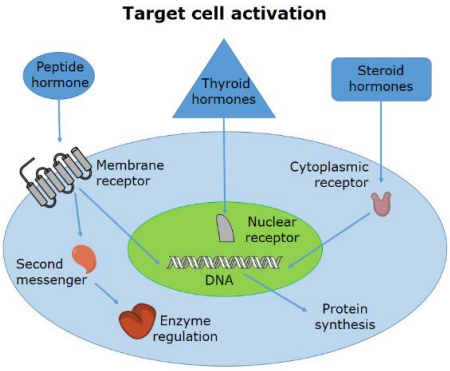

Figure 1.3: Hormonal activation of target cells *via* nuclear, cytoplasmic or membrane receptors.

The major advantages of biologic molecules are their high specificity. This specificity creates the opportunity to sense only the target of interest, and it is only this target binding that causes a positive signal. Until present, only nature is capable of producing such a variety of receptor molecules for such a large pool of possible target molecules and with such a high specificity.

Already many attempts have been made to mimic 'Nature's work' by the production of artificial (biomimetic) receptors, *e.g.* aptamers and molecularly imprinted polymers (MIPs). The word aptamer is derived from the Latin word "aptus", meaning fitting, and the word "meros", Greek for particles. Aptamers are short single stranded nucleic acid based (DNA aptamers, RNA aptamers) or peptide based oligomers with a very specific shape. This specific shape gives them the opportunity to bind a wide range of target molecules, varying from ions to proteins [66] and even complex organisms, *e.g.* bacteria and cells [67]. Specific binding aptamers are obtained by using systematic evolution of ligands by exponential enrichment (SELEX). The procedure starts from a pool of random nucleic acid sequences as presented in **Figure 1.4**.

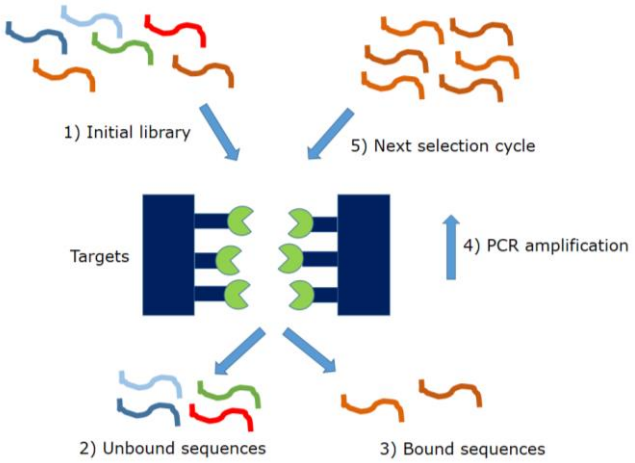

Figure 1.4: SELEX procedure for the development of aptamers which mimic antigen recognition of antibodies.

After several cycles of polymer chain reaction amplifications and target binding and washing process, a very selective aptamer species is obtained and will be cloned in an appropriate vector [68]. Their affinity towards targets are more or less comparable to the antibody-antigen affinity. However, in practice there is still no general, standardized procedure to produce and use aptamers in diagnostics. [69]. This means that in case one lab produces an aptamer against a target, they will get a slightly different aptamer with different properties compared to another lab. If it would be possible to create a standardised procedure this would lead to an optimised library of aptamers with excellent properties. Furthermore, the quality control of aptamers is still in development while for antibodies this is already well developed [70].

MIPs are another type of artificial (biomimetic) receptor. MIPs made from synthetic material also mimic the functioning of antibodies [71-73]. In a MIP, the target molecule functions as a template around which a receptor molecule will be

assembled (**Figure 1.5**). After polymerisation the template will be removed and an empty mould remains, which is complementary in shape and functionality. This mould is capable of selectively binding the target molecule when present in a solution of interest. Disadvantages of these artificial receptors are their rigidity and large size and their incapability of being soluble. This is not the case when using biomolecules: they are flexible, much smaller in size and most of the time soluble. Furthermore, the number of binding sites in biomolecules is determined whereas this is not the case for MIPs which can possess thousands of binding possibilities. Additionally, the accessibility of these binding places can vary from molecule to molecule.

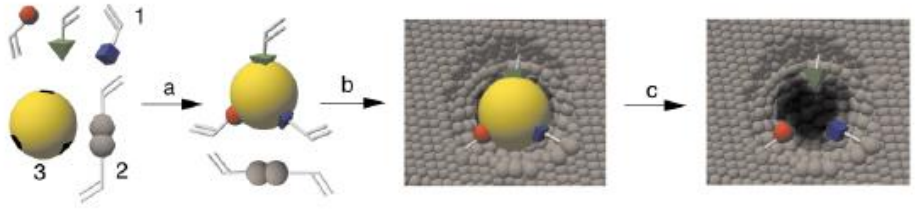

Figure 1.5: Schematic representation of the synthesis of molecular imprinted polymers. a) assembly of building blocks (1,2) around the target molecule (3); b) polymerisation resulting in a MIP; c) removal of the target molecule by bond breakage between the MIP and its target [77].

In view of these drawbacks of artificial receptors, this work will focus on the use of protein based layers, which can be used in biosensing devices.

Initially target and receptor molecule of interest will be selected to serve as model molecules. Secondly, the proper CuAAC conditions have to be found to immobilise the proteins on a transducer surface in such a way that the advantages of both, biomolecules and the CuAAC immobilisation strategy, are maximally manifested.

1.4 Directed immobilisation of the biolayer

CuAAC as a (site-directed) immobilisation method could offer great opportunities, especially towards the improvement of devices that would benefit from oriented biolayers, such as biosensing applications. As mentioned before, currently used methods very often result in random oriented biolayers of which the accessibility of target binding sites is far from optimal. Considering the fact that only a small percentage of the target binding sites is actually available for the effective target recognition, the measured signals will not represent the actual presence of the target molecules inside the sample which has to be measured. By directing the orientation of the receptor molecules, the accessibility will be improved, leading to higher, more accurate signals with a better signal-to-noise ratio.

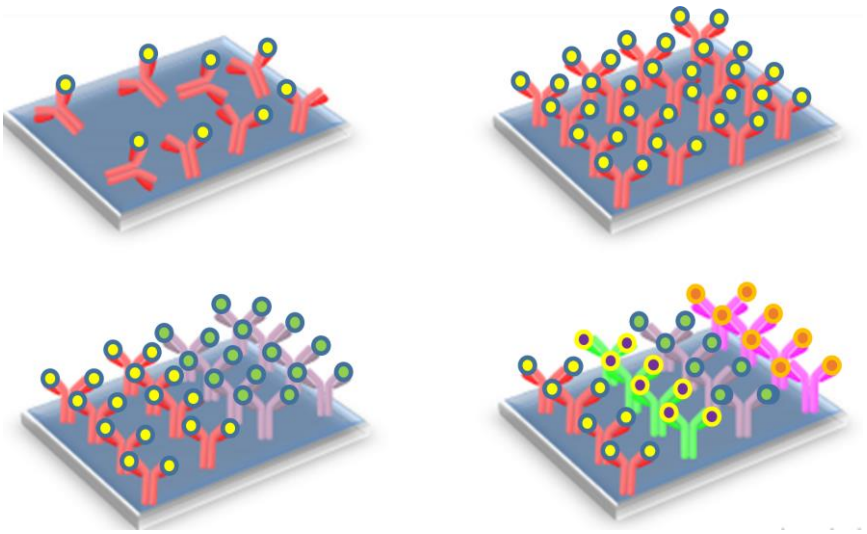

Figure 1.6: Random immobilisation of antibody followed by antigen binding (top left). Possible opportunities offered by site-directed immobilisations towards higher sensitivity and higher efficient use of sensor surface; oriented antibody layer (top right and bottom); Bottom: Future opportunities for antibody layers allowed by site-directed coupling by CuAAC. Antibody ; Antigen .

In **Figure 1.6** (top left) an example is depicted with only a limited amount of target binding sites are available for effective target recognition. When an oriented layer is obtained, as shown in **Figure 1.6** (top right), not only more antibodies can be bound to the transducer surface, also more antigen binding sites will point towards the solution. Considering the fact that the random oriented layer already offered sufficient results in quite a few of the previously reported investigations, reducing the occupied area for a certain receptor by using a directed coupling method would lead to a surface which still possesses the same number of target binding sites, but the surface area is smaller. This creates the opportunity to use the remaining area for other receptor molecules with different targets as showed in **Figure 1.6** (bottom). In addition to the above mentioned advantages of utilising CuAAC for protein immobilisation, another advantage is that a 1,2,3-triazole bond will be formed upon coupling, which resembles a natural occurring peptide bond while being stable to enzymatic degradation [74]. Especially for protein engineering purposes, 1,2,3-triazoles are of particular interest due to the fact that they are planar and similar in size as amides. They possess a high dipolar moment, have similar H-bonding capabilities and are resistant to cleavage by proteases [75, 76].

1.5 Aims of the thesis

The primary focus of this thesis is the covalent coupling of molecules, whether or not from biologic origin, to planar surfaces by means of a fast, reliable and reproducible 'click' chemistry termed as CuAAC or the Huisgen copper(I) catalysed alkyne azide cycloaddition. At the start of this research, this was the first attempt to utilise the CuAAC for biosensor purposes.

First, both functionalised Alexa Fluor® ^{488}, a fluorescent dye, and bovine Immunoglobulin G (bIgG) protein will be used to demonstrate the viability of using CuAAC as an immobilisation strategy to functionalise planar surfaces. In this initial stage, fluorescence will serve as a qualitative analysis of the functionalised surface.

In a next step, *in situ* ellipsometry will be used to monitor and optimise the initial immobilisation conditions by using a functionalised model protein, *Staphylococcus* protein A (SpA). In addition, maltose binding protein (MBP) will be used to demonstrate the high specificity of the immobilisation reaction. By alkynating MBP at a single location, the objective is to obtain homogeneous oriented biolayers. The expectation of these homogeneously oriented layers is that all the proteins are having an identical orientation, which would increase their binding capacity towards antigen or antibodies.

The final objective of this thesis is to produce an optimal biolayer used in an actual biosensing setting, making use of all the advantages that CuAAC can offer in terms of immobilisation efficiency, homogeneity of the created layer, high binding capacity and excellent specificity towards targets.

1.6 Thesis Outline

Prior to the discussion of the experimental parts of this thesis, a general overview concerning the current "state-of-the-art" of surface modifications and their applications was given in **Chapter 1** "General introduction".

Chapter 2 summarizes the different surface characterisation methods to study the coupling reactions, which are being used throughout this thesis. Contact angle measurements, fluorescence surface analysis and label-free surface characterisation, such as *in situ* ellipsometry and Quartz Crystal Microbalance (QCM), will be concisely described. The coupling experiments described in this thesis, in combination with the characterisation methods, are schematically represented in (Figure 1.7).

In **Chapter 3**, the CuAAC immobilisation of an alkynated, fluorescent dye Alexa Fluor® ^{488} to an azidified glass surfaces will be discussed. Different aspects of the immobilisation protocol such as the azidification of carboxyl and amine silanised glass surfaces, the concentration of the model molecules, the determination of the optimal buffer, the impact of the different 'click' reagents and the first attempts towards a biofunctionalised surface are presented.

Subsequently, in **Chapter 4** the alkynation of *Staphylococcus aureus* protein A (SpA) resulting in SpA molecules bearing different amounts of alkyne functionalities by targeting different amounts of lysines will be discussed. Furthermore, the CuAAC immobilisation on azidified silicon wafers of these different alkynated SpA species will be compared with currently used immobilisation procedures. In addition, the CuAAC immobilisation reaction will be monitored in real-time using *in situ* ellipsometry to optimise the immobilisation

process. The most important aims are to ensure that the obtained SpA layers are covalently and reproducibly bound to the surface in a reduced reaction time, consuming a minimised amount of randomly alkynated SpA.

In **Chapter 5,** the reaction conditions, which were optimised for the randomly alkynated SpA in Chapter 4, have been tested for a second protein, being the maltose binding protein (MBP). Initially, MBP is randomly alkynated as well. Afterwards, MBP is site-specifically alkynated by Intein-expressed protein ligation (IPL) and immobilised on an azidified silicon wafer. The influence of the site-specific functionalisation and site-directed immobilisation of MBP on the antibody binding capacity are also presented in this chapter.

Chapter 6 discusses the implementation of the CuAAC immobilisation in a sensing platform consisting of a Quartz Crystal Microbalance (QCM). For this application the SpA molecules are being immobilised on an azide functionalised quartz crystal platform and their antibody binding capacity is being quantified in real-time.

Finally, the last part of this thesis contains a general discussion, the major conclusions regarding the previously described experiments, the results thereof and an outlook to future work.

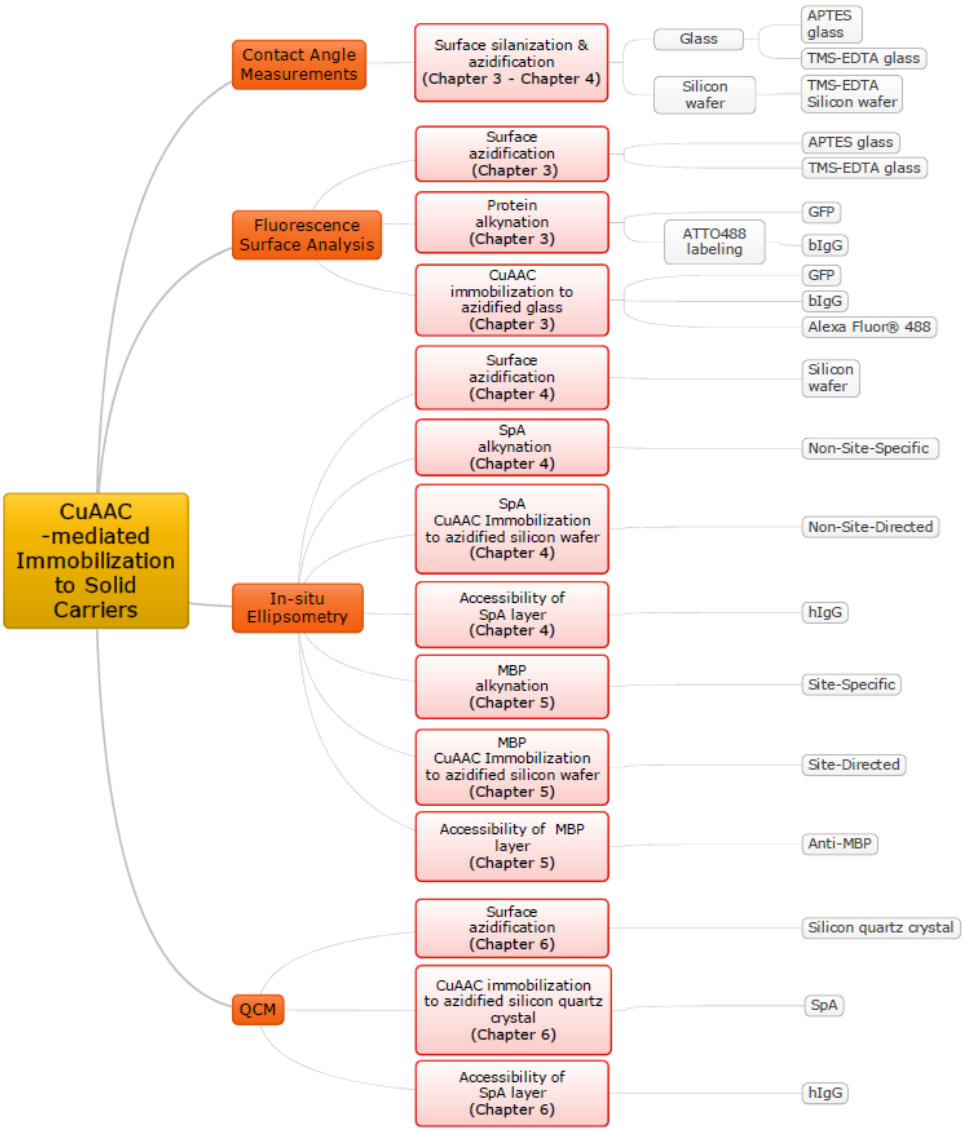

Figure 1.7: Schematic description of the thesis outline.

1.7 References

1. Boyer RR, Briggs RD. The use of β titanium alloys in the aerospace industry. Journal of Materials Engineering and Performance. 14(6):681-5.

2. Digby RP, Packham DE. Pretreatment of aluminium: topography, surface chemistry and adhesive bond durability. International Journal of Adhesion and Adhesives. 1995;15(2):61-71.

3. Prabhu TR. An overview of high-performance aircraft structural Al alloy-AA7085. Acta Metallurgica Sinica (English Letters). 2015;28(7):909-21.

4. Schmalzried TP, Peters PC, Maurer BT, Bragdon CR, Harris WH. Long-duration metal-on-metal total hip arthroplasties with low wear of the articulating surfaces. The Journal of Arthroplasty.11(3):322-31.

5. Hanawa T. Biofunctionalization of titanium for dental implant. Japanese Dental Science Review. 2010;46(2):93-101.

6. Raita Y, Komatsu K, Hayakawa T. Pilot study of gingival connective tissue responses to 3-dimensional collagen nanofiber-coated dental implants. Dent Mater J. 2015;34(6):847-54.

7. Burl M, Coutts GA, Young IR. Tuned fiducial markers to identify body locations with minimal perturbation of tissue magnetization. Magnetic Resonance in Medicine. 1996;36(3):491-3.

8. Castellanos MI, Zenses AS, Grau A, Rodriguez-Cabello JC, Gil FJ, Manero JM, *et al.* Biofunctionalization of REDV elastin-like recombinamers improves endothelialization on CoCr alloy surfaces for cardiovascular applications. Colloids and surfaces B, Biointerfaces. 2015;127:22-32.

9. Wise SG, Waterhouse A, Kondyurin A, Bilek MM, Weiss AS. Plasma-based biofunctionalization of vascular implants. Nanomedicine (London, UK). 2012; 7(12):1907-16.

10. Montenegro J-M, Grazu V, Sukhanova A, Agarwal S, de la Fuente JM, Nabiev I, *et al.* Controlled antibody/(bio-) conjugation of inorganic nanoparticles for targeted delivery. Advanced Drug Delivery Reviews. 2013;65(5):677-88.

11. Gajjar CR, McCord MG, King MW. 19 - Hemostatic wound dressings. Biotextiles as medical implants: Woodhead Publishing; 2013. p. 563-89.

12. Haidary SM, Mohammed AB, Córcoles EP, Ali NK, Ahmad MR. Effect of coatings and surface modification on porous silicon nanoparticles for delivery of the anticancer drug tamoxifen. Microelectronic Engineering. 2016;161:1-6.

13. Steen Redeker E, Ta DT, Cortens D, Billen B, Guedens W, Adriaensens P. Protein engineering for directed immobilization. Bioconjugate Chemistry. 2013;24(11):1761-77.

14. Passos MLC, Ribeiro DSM, Santos JLM, Saraiva MLMFS. Physical and chemical immobilization of choline oxidase onto different porous solid supports: Adsorption studies. Enzyme and Microbial Technology. 2016;90:76-82.

15. Roach P, Farrar D, Perry CC. Interpretation of protein adsorption: surface-induced conformational changes. Journal of the American Chemical Society. 2005;127(22):8168-73.

16. Anand G, Sharma S, Dutta AK, Kumar SK, Belfort G. Conformational transitions of adsorbed proteins on surfaces of varying polarity. Langmuir. 2010;26(13):10803-11.

17. Howarth M, Takao K, Hayashi Y, Ting AY. Targeting quantum dots to surface proteins in living cells with biotin ligase. Proceedings of the National Academy of Sciences of the United States of America. 2005;102(21):7583-8.

18. O L, EA B, M W, JL S, inventors; Three-dimensional structures of avidin and the avidin-biotin complex.

19. Yu C-C, Kuo Y-Y, Liang C-F, Chien W-T, Wu H-T, Chang T-C, *et al.* Site-specific immobilization of enzymes on magnetic nanoparticles and their use in organic synthesis. Bioconjugate Chem. 2012;23(4):714-724.

20. Holland-Nell K, Beck-Sickinger AG. Specifically immobilised aldo/keto reductase AKR1A1 shows a dramatic increase in activity relative to the randomly immobilised enzyme. Chembiochem. 2007;8(9):1071-1076.

21. Alves NJ, Mustafaoglu N, Bilgicer B. Oriented antibody immobilization by site-specific UV photocrosslinking of biotin at the conserved nucleotide binding site for enhanced antigen detection. Biosensors and Bioelectronics. 2013;49(0):387-93.

22. Wang J, Aki M, Onoshima D, Arinaga K, Kaji N, Tokeshi M, *et al.* Microfluidic biosensor for the detection of DNA by fluorescence enhancement and the following streptavidin detection by fluorescence quenching. Biosensors and Bioelectronics. 2014;51(0):280-5.

23. Wingren C, Steinhauer C, Ingvarsson J, Persson E, Larsson K, Borrebaeck CA. Microarrays based on affinity-tagged single-chain Fv antibodies: sensitive detection of analyte in complex proteomes. Proteomics. 2005;5(5):1281-91.

24. Sudheer PD, Pack SP, Kang TJ. Cyclization tag for the detection and facile purification of backbone-cyclized proteins. Anal Biochem. 2013;436(2):137-41.

25. Ganesana M, Istarnboulie G, Marty JL, Noguer T, Andreescu S. Site-specific immobilization of a (His)6-tagged acetylcholinesterase on nickel nanoparticles for highly sensitive toxicity biosensors. Biosensors and Bioelectronics. 2011;30(1):43-8.

26. Hopp TP, Prickett KS, Price VL, Libby RT, March CJ, Pat Cerretti D, *et al.* A short polypeptide marker sequence useful for recombinant protein identification and purification. Nat Biotech. 1988;6(10):1204-10.

27. Niemeyer CM. Semisynthetic DNA-protein conjugates for biosensing and nanofabrication. Angew Chem Int Ed Engl. 2010;49(7):1200-1216.

28. Jonkheijm P, Weinrich D, Schroder H, Niemeyer CM, Waldmann H. Chemical strategies for generating protein biochips. Angew Chem Int Ed Engl. 2008;47(50):9618-9647.

29. Kim Y, Ho SO, Gassman NR, Korlann Y, Landorf EV, Collart FR, *et al.* Efficient site-specific labeling of proteins via cysteines. Bioconjug Chem. 2008;19(3):786-791.

30. Sletten EM, Bertozzi CR. Bioorthogonal chemistry: Fishing for selectivity in a sea of functionality. Angewandte Chemie International Edition. 2009;48(38): 6974-98.

31. Basle E, Joubert N, Pucheault M. Protein chemical modification on endogenous amino acids. Chemistry & Biology. 2010;17(3):213-227.

32. Pei Z, Anderson H, Myrskog A, Dunér G, Ingemarsson B, Aastrup T. Optimizing immobilization on two-dimensional carboxyl surface: pH dependence of antibody orientation and antigen binding capacity. Anal Biochem. 2010;398(2):161-168.

33. Massa S, Vikani N, Betti C, Ballet S, Vanderhaegen S, Steyaert J, *et al.* Sortase A-mediated site-specific labeling of camelid single-domain antibody-fragments: a versatile strategy for multiple molecular imaging modalities. Contrast Media & Molecular Imaging. 2016:328-339.

34. Milles S, Lemke EA. What precision-protein-tuning and nano-resolved single molecule sciences can do for each other. BioEssays: News and reviews in molecular, cellular and developmental biology. 2013;35(1):65-74.

35. Vijayan V, Giersberg M, Chamas A, Mehrotra M, Chelikani V, Kunze G, *et al.* Use of recombinant oestrogen binding protein for the electrochemical detection of oestrogen. Biosensors and Bioelectronics. 2015;66:379-384.

36. Beladiya C, Tripathy RK, Bajaj P, Aggarwal G, Pande AH. Expression, purification and immobilization of recombinant AiiA enzyme onto magnetic nanoparticles. Protein Expression and Purification. 2015;113:56-62.

37. Kolb HC, Finn MG, Sharpless KB. Click Chemistry: diverse chemical function from a few good reactions. Angew Chem Int Ed Engl. 2001;40(11):2004-2021.

38. Rostovtsev VV, Green LG, Fokin VV, Sharpless KB. A stepwise huisgen cycloaddition process: copper(I)-catalyzed regioselective "ligation" of azides and terminal alkynes. Angewandte Chemie International Edition. 2002;41(14):2596-2599.

39. Baskin JM, Prescher JA, Laughlin ST, Agard NJ, Chang PV, Miller IA, *et al.* Copper-free click chemistry for dynamic *in vivo* imaging. Proceedings of the National Academy of Sciences. 2007;104(43):16793-16797.

40. Wiessler M, Waldeck W, Kliem C, Pipkorn R, Braun K. The Diels-Alder-reaction with inverse-electron-demand, a very efficient versatile click-reaction concept for proper ligation of variable molecular partners. International Journal of Medical Sciences. 2009;7(1):19-28.

41. Prescher JA, Bertozzi CR. Chemistry in living systems. Nat Chem Biol. 2005;1(1):13-21.

42. Hendry SH, Hsiao SS. Chapter 22 - Fundamentals of Sensory Systems. Spitzer *et al.*, editor. Fundamental Neuroscience (Fourth Edition). San Diego: Academic Press; 2013. p. 499-511.

43. Group BDW. Biomarkers and surrogate endpoints: preferred definitions and conceptual framework. Clin Pharmacol Ther. 2001;69(3):89-95.

44. Ĉulić-Viskota J, Dempsey WP, Fraser SE, Pantazis P. Surface functionalization of barium titanate SHG nanoprobes for *in vivo* imaging in zebrafish. Nat Protocols. 2012;7(9):1618-1633.

45. Ravindran A, Chandran P, Khan SS. Biofunctionalized silver nanoparticles: Advances and prospects. Colloids and Surfaces B: Biointerfaces. 2013;105:342-352.

46. Dumont MF, Hoffman HA, Yoon PRS, Conklin LS, Saha SR, Paglione J, *et al.* Biofunctionalized gadolinium-containing prussian blue nanoparticles as multimodal molecular imaging agents. Bioconjugate Chemistry. 2014;25(1): 129-137.

47. Kim E, Steinbrück A, Buscaglia MT, Buscaglia V, Pertsch T, Grange R. Second-harmonic generation of single $BaTiO_3$ nanoparticles down to 22 nm diameter. ACS Nano. 2013;7(6):5343-5349.

48. Wang L-S, Wu L-C, Lu S-Y, Chang L-L, Teng IT, Yang C-M, *et al.* Biofunctionalized phospholipid-capped mesoporous silica nanoshuttles for targeted drug delivery: Improved water suspensibility and decreased nonspecific protein binding. ACS Nano. 2010;4(8):4371-9.

49. Lautenschläger C, Schmidt C, Fischer D, Stallmach A. Drug delivery strategies in the therapy of inflammatory bowel disease. Advanced Drug Delivery Reviews. 2014;71(0):58-76.

50. Ma Z, Mao Z, Gao C. Surface modification and property analysis of biomedical polymers used for tissue engineering. Colloids and Surfaces B: Biointerfaces. 2007;60(2):137-157.

51. Ahuja T, Mir IA, Kumar D, Rajesh. Biomolecular immobilization on conducting polymers for biosensing applications. Biomaterials. 2007;28(5):791-805.

52. Nelson JM, Griffin EG. Adsorption of invertase. Journal of the American Chemical Society. 1916;38(5):1109-1115.

53. Hughes WS. The potential difference between glass and electrolytes in contact with the glass. Journal of the American Chemical Society. 1922;44(12):2860-7.

54. Clark LCJ. Monitor and control of blood and tissue oxygen tensions. ASAIO Journal. 1956;2(1):41-8.

55. Clark LC, Lyons C. Electrode systems for contious monitoring in cardiovascular surgery. Annals of the New York Academy of Sciences. 1962;102(1):29-45.

56. Willimas D. Urea determination and electrode therefor. Patent US 3776819 A; 1973

57. Bergveld P. Development, operation, and application of the ion-sensitive field-effect transistor as a tool for electrophysiology. Biomedical Engineering, IEEE Transactions on. 1972;BME-19(5):342-51.

58. Divies C. Ethanol oxidation by an "*Acetobacter xylinum*" microbial electrode Annales de Microbiologie. 1975;126(2):175-86.

59. Diviès C. Remarques sur l'oxydation de l'éthanol par une electrode microbienne d'*Acetobacter zylinum*. Ann Microbiol. 1975 (126A):175–86.

60. Nishida K. What is artificial endocrine pancreas? Mechanism and history. World Journal of Gastroenterology. 2009;15(33):4105.

61. Peterson JI, Goldstein SR, Fitzgerald RV, Buckhold DK. Fiber optic pH probe for physiological use. Analytical Chemistry. 1980;52(6):864-9.

62. Schultz JS, Inventor. The United States Of America As Represented By The Department Of Health, Education And Welfare, Owner. Optical sensor of plasma constituents. Patent number US4344438; 1982.

63. Liedberg B, Nylander C, Lunström I. Surface plasmon resonance for gas detection and biosensing. Sensors and Actuators. 1983;4:299-304.

64. Jianrong C, Yuqing M, Nongyue H, Xiaohua W, Sijiao L. Nanotechnology and biosensors. Biotechnology Advances. 2004;22(7):505-18.

65. Thévenot DR, Toth K, Durst RA, Wilson GS. Electrochemical biosensors: recommended definitions and classification. Biosensors and Bioelectronics. 2001;16(1–2):121-31.

66. Cox JC, Ellington AD. Automated selection of anti-Protein aptamers. Bioorganic & medicinal chemistry. 2001;9(10):2525-31.

67. Sefah K, Shangguan D, Xiong X, O'Donoghue MB, Tan W. Development of DNA aptamers using Cell-SELEX. Nat Protoc. 2010;5(6):1169-85.

68. Gopinath S. Methods developed for SELEX. Analytical and Bioanalytical chemistry. 2007;387(1):171-82.

69. Lakhin AV, Tarantul VZ, Gening LV. Aptamers: Problems, solutions and prospects. Acta Naturae. 2013;5(4):34-43.

70. McKeague M, DeRosa MC. Challenges and opportunities for small molecule aptamer development. Journal of Nucleic Acids. 2012;2012:20.

71. Horemans F, Alenus J, Bongaers E, Weustenraed A, Thoelen R, Duchateau J, *et al.* MIP-based sensor platforms for the detection of histamine in the nano- and micromolar range in aqueous media. Sensors and Actuators B: Chemical. 2010;148(2):392-8.

72. Horemans F, Diliën H, Wagner P, Cleij TJ. Book: Chapter 5 - MIP-based sensor platforms for detection of analytes in nano- and micromolar range, edited by …. Molecularly Imprinted Sensors, S;J. Li Y. Ge, S.A. Piletsky, J. Lunec, editors. Elsevier, Amsterdam. 2012:91-124.

73. Horemans F, Weustenraed A, Spivak D, Cleij TJ. Towards water compatible MIPs for sensing in aqueous media. Journal of molecular recognition. 2012; 25(6):344-51.

74. Valverde IE, Mindt TL. 1,2,3-Triazoles as amide-bond surrogates in peptidomimetics. Chimia. 2013;67(4):262-6.

75. Ko E, Liu J, Perez LM, Lu G, Schaefer A, Burgess K. Universal Peptidomimetics. Journal of the American Chemical Society. 2011;133(3):462-77.

76. Hua Y, Flood AH. Click chemistry generates privileged CH hydrogen-bonding triazoles: The latest addition to anion supramolecular chemistry. Chemical Society Reviews. 2010;39(4):1262-71.

77. Haupt K. Molecularly imprinted polymers: The next generation. Anal Chem. 2003;75(17):376A-383A.

Chapter 2. Experimental

2.1 Introduction

This chapter presents the principles of the various surface analysis techniques used for the characterisation of the chemical and physical properties of the functionalised substrates, *i.e.* silanised glass and silicon. In addition to the azidification of these substrates, alkynated small molecules and proteins were covalently linked to the substrates. Several analytical techniques were used to investigate the resulting surface-protein hybrids.

2.2 Contact Angle Measurements

Contact angle measurements are a fast and straightforward technique to demonstrate the wettability, *i.e.* the ability of a liquid to interact with a solid surface [1-3]. As presented in **Figure 2.1** (middle), the contact angle θ between the vector of the solid-liquid interfacial tension (γ_{sl}) and the vector of the liquid-vapour interfacial tension (γ_{lv}) will be the indicator of the wettability of the surface [4]. Under ideal circumstances, in a static state, the relation between all the interfacial tensions can be described as stated by Thomas Young [4] (Equation 2.1):

$$cos\theta = \frac{\gamma sv - \gamma sl}{\gamma lv} \qquad \text{Equation 2.1}$$

However, the contact angle is not only depending on the surface tensions. Gravity and hysteresis (determined by dynamic contact measurements [5]) influence the shape of the droplet and thus its angle as well. Under ideal circumstances the hysteresis, which is determined by the difference between advancing and receding angle measurements is zero, which indicates a very smooth surface. Under these circumstances the dynamic contact angle will almost equal the static state angle,

which is the Young contact angle θ_Y. In general, when applying a drop of a polar liquid to a surface, a low contact angle ($\theta<90°$) corresponds to a high degree of wettability, *i.e.* a hydrophilic surface (**Figure 2.1**; left). In case the contact angle equals zero, due to a total spreading of the liquid, one may conclude that the surface is extremely hydrophilic. Higher contact angles ($\theta>90°$) indicate that the surface is hydrophobic (**Figure 2.1**; right), resulting in a spherical drop on top of the surface. Contact angles of 90° indicate that the surface is as hydrophilic as it is hydrophobic (**Figure 2.1**; middle). If an apolar liquid is used for contact angle measurements instead of water, low contact angles point towards high hydrophobicity, while high contact angles indicate the surface is hydrophilic.

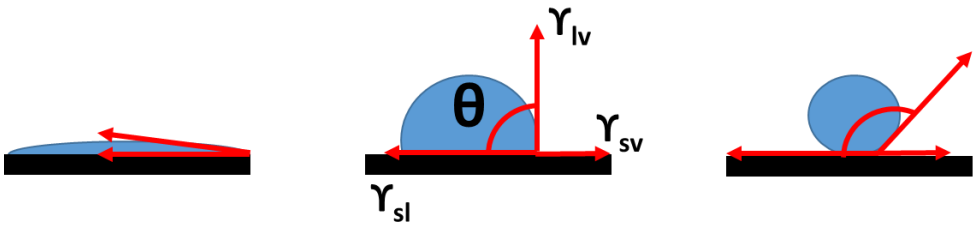

Figure 2.1: Representation of the contact angles θ (°) formed by a drop of a polar liquid on smooth surfaces differing in wettability. The vector of the different interfacial tensions is represented by γ_{sl} (solid-liquid), γ_{lv} (liquid-vapour) and γ_{sv} (solid-vapour).

In addition, contact angle measurements provide information on the wettability of a surface at a certain point in time. However, a surface can be exposed to external factors, which might change the properties of the surface as such. Exposure to strong acidic solutions or solutions containing certain reagents or proteins can modify the outer layer of the surface, resulting in a different wettability. By monitoring changes in contact angle, evidence of surface modifications can be

derived [6-9]. In this thesis static contact angles are measured and presented to demonstrate the wettability of the different surfaces.

2.3 Fluorescent surface analysis

The proper functioning of a biomedical application is determined by the exact configuration of its biolayer [10-13]. Furthermore, it is of considerable importance that the interaction between receptor molecules on the surface of the biolayer and targets in solution can occur without obstruction. It is desirable that the target-receptor binding events only cause physicochemical changes, which can be translated into electric, recordable signals. In case of fluorescence, a photodetector receives and translates the emitted signals coming from the fluorescent labels into electrical signals, demonstrating the presence of labels at the surface.

When labelling techniques are used, both fluorescent and radioactive labels can be readily detected. To measure a response, such labels have to be attached to the molecule of interest. Detection of the emitted light or radioactive radiation will lead to electrical pulses that are recorded and visualised by a computing system. A possible disadvantage is the interaction of the label with the activity of the proteins. Quantification of the emitted signals can be very delicate due to possible signal loss caused by quenching or by the instability of the label during longer excitation periods. Moreover, auto-fluorescence and fluorescence overlap might also result in wrong impressions and conclusions [14]. Reorientation of the immobilised proteins could cause changes in fluorescent signal, resulting in wrong conclusions [15]. Notwithstanding, this type of analysis is very suitable for rapidly gathering qualitative information. The presence of labelled molecules inside cells [16-18], on top of solid supports [19-22] or in a solution [23-25] can be verified

very easily. However, quantification may sometimes be difficult. Although prudence is called when analysing the results, labelling can offer good qualitative indications about a certain process or event. In this thesis fluorescence was used to rapidly gain information about the presence of labelled proteins on solid glass substrates.

Two different devices are used to measure the presence of fluorescent (bio) molecules on glass substrates, *i.e.* an Ettan DIGE fluorescence spectrometer and a confocal microscope. A third apparatus is used to measure the fluorescent excitation and emission spectrum of a solution *i.e.* Spex Fluorolog Tau Lifetime Spectrofluorometer. The Ettan DIGE and confocal microscope are both devices that excite a fluorescent dye and measure the fluorescent signal emitted by the dye. The excitation occurs at a certain wavelength, with a certain intensity, for a certain time period. By adjusting the frequency of the light beam to the excitation wavelength of the dye, the maximal fluorescence intensity can be obtained. However, the intensity of the excitation period should not be too strong and the duration should also be limited, otherwise the excitation might induce a photo bleaching effect, resulting in reduction or absence of a measurable signal [26-28].

When all parameters are properly chosen, the photodetector records a signal with a longer wavelength, emitted by the dye. This change in wavelength is caused by the loss of energy due to vibrational relaxation and internal conversion [29], leading to a shift in wavelength, called the Stokes shift [30, 31]. The dyes are chosen in such a way that the difference in energy between excitation wavelength and emission wavelength is large enough in order to get a proper signal-to-noise ration by minimising cross excitation. In case a signal can be measured, this will be a clear indication that the surface is containing a fluorescent dye. Both devices,

DIGE scanner and the confocal microscope, can provide a quantitative analysis of the substrates. On the other hand, the Spex spectrofluorometer, is a very sensitive apparatus, which is able to measure excitation and emission spectra of dyes in solution. If a dye is used without knowing its optimal excitation wavelength, this can be determined by the apparatus. The advantage is that by recording the excitation spectrum, the optimal excitation wavelength can be determined. By exciting the dye with this wavelength, the maximal fluorescent signal will be obtained. Another advantage of the Spex is that it is able to detect a fluorescent signal coming from a 50 femtomolar dye solutions, proving its high sensitivity [32]. This device easily discovers changes of the dye's fluorescent absorption and emission spectra.

2.4 Label-free surface analysis

In addition to labelled detection, label-free methods can provide qualitative and quantitative data. No additional steps are required in order to detect and quantify the molecule of interest, as compared to labelled assays. The label-free techniques can be divided in different categories, such as electrochemical [33, 34], calorimetric [35, 36], optical [37-39], acoustic [40, 41] and nanostructure- based analysis techniques [42, 43]. In this thesis data will be acquired by label-free detection based on optical (null-ellipsometry) and acoustic (QCM) analysis techniques.

2.4.1 Ellipsometry

Binding events of molecules to solid carriers can be recorded by direct optical analysis. In this way, biomolecules interact with an incoming light beam, thereby influencing certain parameters such as the reflection [44] or polarisation [45]. By

monitoring one or multiple parameter changes, these binding events can be quantified. Ellipsometry, which will be extensively used throughout the thesis, is a non-invasive, non-destructive optical technique to obtain the properties of planar, reflecting samples [46]. This technique determines the relative changes in polarisation after reflection without being dependent on the absolute light intensity. By monitoring the state of polarisation of the light beam on both the uncovered surface and on the biofunctionalised surface, it becomes possible to convert the change in polarisation into a thickness of the adsorbed biolayer with a high precision and reproducibility. Depending on the light source, ellipsometry can be split into two main groups: the single wavelength ellipsometry [47] and the spectroscopic ellipsometry [48]. In case of single wavelength ellipsometry, the used light source is a laser (in the visible spectrum), focused on a very minute area of the sample. The output, obtained from the measurements usually only results in one value for ψ (analyser) and one for Δ (polarizer). In case of spectroscopic ellipsometry light sources with a broad range of wavelengths, *i.e.* UV, visible and infrared light, are used, hereby gaining more information about the physical properties of the sample.

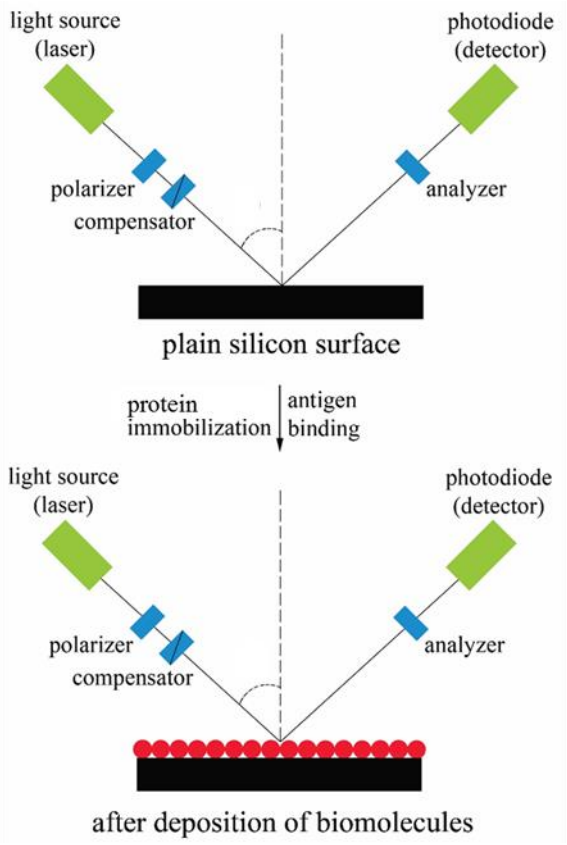

Figure 2.2: Schematic representation of the ellipsometer.

In **Figure 2.2** a schematic representation of the single wavelength ellipsometer is presented. As can be seen, the radiation source is a laser (λ = 632.8 nm), which passes through a polarizing prism and a compensator before reaching the reflecting sample. The reflected beam then passes through a second prism, the analyser, and is detected by a photodiode (detector).

In the experiments described in this thesis, null-ellipsometry will be performed, meaning that the signal reaching the detector will be zero by setting the polariser and analyser in the proper configuration. The polariser will alter the light originating from the laser beam into an elliptic beam. After passing through the

sample, the reflected, linear beam will be directed towards the analyser, which on its turn will be configured in such a way that (almost) no signal will reach the detector. Due to the fact that the coupling of organic molecules to a silicon surface will result in large changes in polarizing angle and only in minor changes in analyser angle, the change in polariser angle will be proportional to the immobilised surface mass density or 'Γ' [49]. Using the quantity 'Γ' (µg/cm²) as the final result implies a reduction of the obtained information as it combines two quantities, *i.e.* thickness and refractive index. From a physical and chemical point of view, these two quantities offer the opportunity to gain insight into many properties, such as the nature of the material of the surface and the thickness of deposited layers. In a life science context, combining them offers information about the protein layer expressed in surface density [47]. Equation 2.2 describes the relation the between surface density Γ and polariser angle before Δ and after Δ' protein deposition, when performing null-ellipsometry with an angle of incidence of 68 degrees of the used laser beam to the substrate.

$$\Gamma\left(\frac{\mu g}{cm^2}\right) = 0.085\,(\Delta' - \Delta) \qquad \text{Equation 2.1}$$

A major advantage of ellipsometry is the fact that it allows studying layers in model systems, which mimic their normal environment in biological systems. Furthermore, the dynamics of layers can be studied *in situ*, no molecular labelling is required and, most importantly, it allows the monitoring of the coupling procedure in real-time [50]. This asset offers the unique opportunity to get an accurate representation of what is actually happening during the coupling process. This real-time insight gives the opportunity to optimise the immobilisation process for parameters, such as reaction time and protein concentration.

All described experiments using ellipsometry for real-time analysis as depictured in **Figure 2.3**, were executed in 'null mode'. This means that the intensity detected by the photodiode will be kept to a minimum by changing polarizer and analyser. The ellipsometer was developed by the research group of Professor Hermens (former Delbia B.V.) and was setup with the following settings: the filter (creating a ellipsometric light beam) is set at 16; offset is 0, (when working in off-null mode this value will change depending on how much de polariser will differ from its minimum used in null-mode); gain (amplification of the diode signal) is kept at 1; polariser sweep angle and analyser sweep angle are respectively 10 and 6 (sweep angles represent the degrees that polariser and analyser change during changes at the surface of the reflecting substrate in order to keep the intensity detected by the photodiode to a minimum).

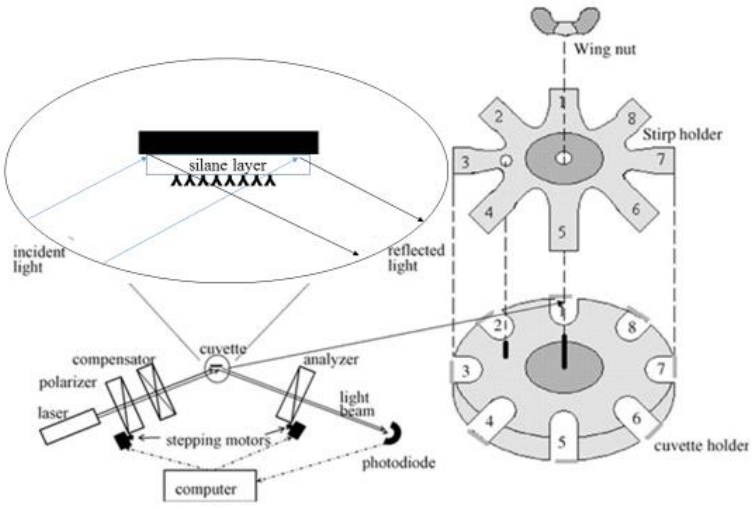

Figure 2.3: Schematic illustration of the customised ellipsometer showing the sample holder for eight silicon slides fitting vertically into eight buffer containing cuvettes [51].

2.4.2 Quartz crystal microbalance

Quartz crystal microbalance (QCM) is a technique used to determine changes in surface mass by measuring differences in acoustic resonance frequency of a piezo-electric crystal [52]. This resonance frequency is generated by applying an AC voltage to a crystal, resulting in a transverse acoustic wave, which propagates across the material. By adding or removing molecules from the surface, the resonance frequency will change. The Sauerbrey equation (Equation 2.3) describes the relationship between the frequency changes and the mass changes in a rigid system [52].

$$\Delta f = -\frac{2f_0^2}{A\sqrt{\rho_q \mu_q}}\Delta m \qquad \text{Equation 2.2}$$

In this equation the frequency change, Δf (Hz), depends on the properties of the crystal and the difference in surface mass Δm (g). The properties of the crystal which have their influence on the frequency are the resonant frequency f_0 (Hz), the density of quartz ρ_q (g/cm³), the active crystal area *A (*cm²*)* and the shear modulus of quartz for an AT-cut crystal μ_q ($g \cdot cm^{-1} \cdot s^{-2}$). An AT-cut crystal is widely used for electronic instruments and has a frequency range between 500 kHz and 300 MHz with a good thermal stability. However, the described relationship (Equation 2.3) is only true for rigid layers, measured in air. In case the measurements are performed in a liquid a damping effect will occur, which means that the frequency will decrease slightly, as is presented below (Equation 2.4), due to the density ρ_L and viscosity η_L of the liquid itself [53]. When performing QCM measurements in a liquid, only one side of the crystal, *i.e.* the functionalised side, gets in contact with the liquid [54].

$$\Delta f = -f_0^{\frac{3}{2}}\left(\frac{\eta_L \rho_L}{\pi \rho_q \mu_q}\right)^{\frac{1}{2}}$$ Equation 2.3

Equation 2.3 offers the opportunity to calculate the increase in surface mass of a rigid layer. However, when immobilising proteins to a surface, the absorbed or covalently bound layer will not behave as a rigid layer, but as a viscoelastic layer, as proteins are not rigid molecules at all [55]. By modelling the obtained data, using the Voigt-Kelvin viscoelastic model [56], information about the surface mass can nevertheless be obtained. This model is used for layers having elasticity and viscosity properties, which is typical for biofilms. Very often, this Voigt model is represented as parallel arranged spring and dashpot as depicted in **Figure 2.4**. The principle of this model becomes clearer by representing it as a mechanical circuit, in which elastic energy (E) is being stored and a certain amount of this energy is dissipated during each vibration due to viscous friction. When vibrating, the protein layer will behave as a spring which would deform immediately if it was not dissolved in a solution. The liquid surrounding the protein slows this elastic deformation down. When the force applied to the protein is removed, the 'spring' will return to its original state, again with a certain delay.

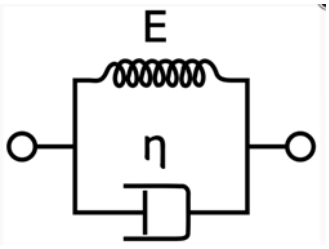

Figure 2.4: Schematic mechanical representation of the Voigt-Kelvin model where η is the viscosity of the dashpot causing the damping effect and E is the elastic modulus.

When extrapolating this to the QCM, it means that when the AC voltage is switched off, the oscillation decreases exponentially. After recording this decay, the frequency and the energy dissipation factor of different overtones can be extracted [57]. As mentioned before this dissipation is the ratio between the dissipated energy during one vibration cycle and the total kinetic and potential energy of the crystal at that moment. When absorbing proteins to a surface it will behave like a viscoelastic hydrogel composed of the proteins and the surrounding water together, meaning that the dissipation factor D will increase. By modelling these results, information such as layer thickness and layer density can be obtained in a quantitative way.

2.5 References

1. Gu H, Wang C, Gong S, Mei Y, Li H, Ma W. Investigation on contact angle measurement methods and wettability transition of porous surfaces. Surface and Coatings Technology. 2016;292:72-77.

2. Kallury KMR, Cheung M, Ghaemmaghami V, Krull UJ, Thompson M. Silanization of oxidized silicon and aluminum surfaces with functionalized silanes with characterization by wettability, ellipsometry, XPS and quartz crystal microbalance studies. Colloids and Surfaces. 1992;63(1–2):1-9.

3. Vistas CR, Águas ACP, Ferreira GNM. Silanization of glass chips—A factorial approach for optimization. Applied Surface Science. 2013;286:314-8.

4. Young T. An essay on the cohesion of fluids. Philosophical Transactions of the Royal Society of London. 1805;95:65-87.

5. Schmitt M, Grub J, Heib F. Statistical contact angle analyses; "slow moving" drops on a horizontal silicon-oxide surface. Journal of Colloid and Interface Science. 2015;447:248-53.

6. Williams DL, Mittal KL. Chapter 10 - Wettability techniques to monitor the cleanliness of surfaces. Developments in Surface Contamination and Cleaning (Second Edition). Kohli R, Mittal K.L., editors. Elsevier, Inc. 2016.445-76.

7. Rana D, Matsuura T. Surface modifications for antifouling membranes. Chemical Reviews. 2010;110(4):2448-71.

8. Abdul-Kader AM. Surface modifications of PADC polymeric material by ion beam bombardment for high technology applications. Radiation Measurements. 2014;69:1-6.

9. Gérard E, Bessy E, Salvagnini C, Rerat V, Momtaz M, Hénard G, *et al.* Surface modifications of polypropylene membranes used for blood filtration. Polymer. 2011;52(5):1223-33.

10. Zhen G, Eggli V, Vörös J, Zammaretti P, Textor M, Glockshuber R, *et al.* Immobilization of the enzyme β-lactamase on biotin-derivatized poly(l-lysine)-g-poly(ethylene glycol)-coated sensor chips: A study on oriented attachment and surface activity by enzyme kinetics and *in situ* optical sensing. Langmuir. 2004;20(24):10464-73.

11. Raghav R, Srivastava S. Immobilization strategy for enhancing sensitivity of immunosensors: L-asparagine–AuNPs as a promising alternative of EDC–NHS activated citrate–AuNPs for antibody immobilization. Biosensors and Bioelectronics. 2016;78:396-403.

12. Ye S, Nguyen KT, Boughton AP, Mello CM, Chen Z. Orientation difference of chemically immobilized and physically adsorbed biological molecules on poly-mers detected at the solid/liquid interfaces *in situ*. Langmuir. 2010;26(9):6471-7.

13. Steen Redeker E, Ta DT, Cortens D, Billen B, Guedens W, Adriaensens P. Protein engineering for directed immobilization. Bioconjugate Chemistry. 2013;24(11):1761-77.

14. Mosiman VL, Patterson BK, Canterero L, Goolsby CL. Reducing cellular autofluorescence in flow cytometry: An *in situ* method. Cytometry. 1997;30(3): 151-6.

15. Daly SM, Przybycien TM, Tilton RD. Coverage-dependent orientation of lysozyme adsorbed on silica. Langmuir. 2003;19(9):3848-57.

16. Kim HM, Cho BR. Two-photon probes for intracellular free metal ions, acidic vesicles, and lipid rafts in live tissues. Accounts of Chemical Research. 2009;42(7):863-72.

17. Tang B, Yu F, Li P, Tong L, Duan X, Xie T, *et al.* A near-infrared neutral pH fluorescent probe for monitoring minor pH changes: Imaging in living HepG2 and HL-7702 Cells. Journal of the American Chemical Society. 2009;131(8): 3016-23.

18. Brock R, Hink MA, Jovin TM. Fluorescence correlation microscopy of cells in the presence of autofluorescence. Biophysical Journal. 1998;75(5):2547-57.

19. Uygun A, Oksuz L, Chowdhury S, Bhethanabotla V. Fluorescence study of protein immobilization on poly(4-hydroxyphenyl thiophene-3-carboxylate)-coated electrodes. Materials Science and Engineering: C. 2010;30(6):868-72.

20. Rossi AM, Wang L, Reipa V, Murphy TE. Porous silicon biosensor for detection of viruses. Biosensors and Bioelectronics. 2007;23(5):741-5.

21. Volle JN, Chambon G, Sayah A, Reymond C, Fasel N, Gijs MAM. Enhanced sensitivity detection of protein immobilization by fluorescent interference on oxidized silicon. Biosensors and Bioelectronics. 2003;19(5):457-64.

22. Li H, Qiang W, Vuki M, Xu D, Chen H-Y. Fluorescence enhancement of silver nanoparticle hybrid probes and ultrasensitive detection of IgE. Analytical Chemistry. 2011;83(23):8945-52.

23. Waldo GS, Standish BM, Berendzen J, Terwilliger TC. Rapid protein-folding assay using green fluorescent protein. Nat Biotech. 1999;17(7):691-5.

24. Kneen M, Farinas J, Li Y, Verkman AS. Green fluorescent protein as a noninvasive intracellular pH Indicator. Biophysical Journal. 1998;74(3):1591-9.

25. Sackett DL, Wolff J. Nile red as a polarity-sensitive fluorescent probe of hydrophobic protein surfaces. Analytical Biochemistry. 1987;167(2):228-34.

26. Hess ST, Girirajan TPK, Mason MD. Ultra-High resolution imaging by fluorescence photoactivation localization microscopy. Biophysical Journal. 2006;91(11):4258-72.

27. Shaner NC, Lin MZ, McKeown MR, Steinbach PA, Hazelwood KL, Davidson MW, *et al.* Improving the photostability of bright monomeric orange and red fluorescent proteins. Nat Meth. 2008;5(6):545-51.

28. Eggeling C, Widengren J, Rigler R, Seidel CAM. Photobleaching of fluorescent dyes under conditions used for single-molecule detection: Evidence of two-step photolysis. Analytical Chemistry. 1998;70(13):2651-9.

29. Mataga N, Shibata Y, Chosrowjan H, Yoshida N, Osuka A. Internal conversion and vibronic relaxation from higher excited electronic state of porphyrins: Femtosecond fluorescence dynamics studies. The Journal of Physical Chemistry B. 2000;104(17):4001-4.

30. Stokes GG. On the change of refrangibility of light. Philosophical Transactions of the Royal Society of London. 1852;142:463-562.

31. Vollmer F, Rettig W, Birckner E. Photochemical mechanisms producing large fluorescence stokes shifts. Journal of Fluorescence. 1994;4(1):65-9.

32. Atzeni, Sal. Fluorolog-3 Operation Manual. 2002; 11-3.

33. Lohrengel MM, Moehring A, Pilaski M. Electrochemical surface analysis with the scanning droplet cell. Fresenius' Journal of Analytical Chemistry. 2000;367(4):334-9.

34. Hansen JA, Wang J, Kawde A-N, Xiang Y, Gothelf KV, Collins G. Quantum-dot/aptamer-based ultrasensitive multi-analyte electrochemical biosensor. Journal of the American Chemical Society. 2006;128(7):2228-9.

35. Danielsson B. Biosensors calorimetric biosensors. Journal of Biotechnology. 1990;15(3):187-200.

36. Bhand SG, Soundararajan S, Surugiu-Wärnmark I, Milea JS, Dey ES, Yakovleva M, *et al.* Fructose-selective calorimetric biosensor in flow injection analysis. Analytica Chimica Acta. 2010;668(1):13-8.

37. Endo T, Kerman K, Nagatani N, Takamura Y, Tamiya E. Label-free detection of peptide nucleic acid−DNA hybridization using localized surface plasmon resonance based optical biosensor. Analytical Chemistry. 2005;77(21):6976-84.

38. Arsov L, Ramasubramanian M, Popov BN. Ellipsometry. Characterization of Materials: John Wiley & Sons, Inc.; 2002.

39. Tengvall P, Jansson E, Askendal A, Thomsen P, Gretzer C. Preparation of multilayer plasma protein films on silicon by EDC/NHS coupling chemistry. Colloids and Surfaces B: Biointerfaces. 2003;28(4):261-72.

40. Zhou A, Muthuswamy J. Acoustic biosensor for monitoring antibody immobilization and neurotransmitter GABA in real-time. Sensors and Actuators B: Chemical. 2004;101(1–2):8-19.

41. Tsortos A, Papadakis G, Gizeli E. Shear acoustic wave biosensor for detecting DNA intrinsic viscosity and conformation: A study with QCM-D. Biosensors and Bioelectronics. 2008;24(4):836-41.

42. Tougaard S. Accuracy of the non-destructive surface nanostructure quantification technique based on analysis of the XPS or AES peak shape. Surface and Interface Analysis. 1998;26(4):249-69.

43. Kim K-H, Xing H, Zuo J-M, Zhang P, Wang H. TEM based high resolution and low-dose scanning electron nanodiffraction technique for nanostructure imaging and analysis. Micron. 2015;71:39-45.

44. Kumawat N, Pal P, Varma M. Diffractive optical analysis for refractive index sensing using transparent phase gratings. Scientific Reports. 2015;5:16687.

45. I Tinoco J, W Mickols, M F Maestre a, Bustamante C. Absorption, scattering, and imaging of biomolecular structures with polarized light. Annual Review of Biophysics and Biophysical Chemistry. 1987;16(1):319-49.

46. Rothen A. The ellipsometer, an apparatus to measure thicknesses of thin surface films. Review of Scientific Instruments. 1945;16(2):26-30.

47. Cuypers PA, Corsel JW, Janssen MP, Kop JM, Hermens WT, Hemker HC. The adsorption of prothrombin to phosphatidylserine multilayers quantitated by ellipsometry. J Biol Chem. 1983;258(4):2426-31.

48. Marsillac S, Sestak MN, Li J, Collins RW. Spectroscopic Ellipsometry. Advanced characterization techniques for thin film solar cells: Wiley-VCH Verlag GmbH & Co. KGaA; 2011. p. 125-49.

49. Speijer H, Laterveer-Vreeswijk RH, Glatz JFC, Nieuwenhuizen W, Hermens WT. One-step immunoassay for measuring protein concentrations in plasma, based on precipitate-enhanced ellipsometry. Analytical Biochemistry. 2004; 326(2):257-61.

50. Arwin H. 12 - Ellipsometry in Life Sciences. Handbook of ellipsometry. 2005. p. 799-855.

51. Damen CWN, Speijer H, Hermens WT, Schellens JHM, Rosing H, Beijnen JH. The bioanalysis of trastuzumab in human serum using precipitate-enhanced ellipsometry. Analytical Biochemistry. 2009;393(1):73-9.

52. Sauerbrey G. Verwendung von Schwingquarzen zur Wägung dünner Schichten und zur Mikrowägung. Zeitschrift für Physik. 1959;155(2):206-22.

53. Kanazawa KK, Gordon JG. Frequency of a quartz microbalance in contact with liquid. Analytical Chemistry. 1985;57(8):1770-1.

54. Auge J, Hauptmann P, Hartmann J, Rösler S, Lucklum R. New design for QCM sensors in liquids. Sensors and Actuators B: Chemical. 1995;24(1–3):43-8.

55. Reed CE, Kanazawa KK, Kaufman JH. Physical description of a visco-elastically loaded AT-cut quartz resonator. Journal of Applied Physics. 1990;68(5):1993-2001.

56. Voinova MV, Rodahl M, Jonson M, Kasemo B. Viscoelastic acoustic response of layered polymer films at fluid-solid interfaces: Continuum mechanics approach. Physica Scripta. 1999;59(5):391.

57. Keller JM, Swarthout RF, Carlson BK, Yordy J, Guichard A, Schantz MM, *et al.* Comparison of five extraction methods for measuring PCBs, PBDEs, organochlorine pesticides, and lipid content in serum. Analytical and Bioanalytical Chemistry. 2009;393(2):747-60.

Chapter 3. CuAAC mediated immobilisation of proteins functionalised with fluorescent probes on glass

3.1 Introduction

For more than a century, internal and terminal alkynes together with organic azides are being used in thermal reactions resulting in the formation of 1,2,3-triazoles. In 1893 Arthur Michael was the first researcher who was able to synthesize this triazole ring starting from a phenyl azide and diethyl acetylene-dicarboxylate [1]. From the fifties of the last century Rolf Huisgen and his research group started their research on the mechanism of the 1,3-dipolar cycloaddition of azides and alkynes [2, 3]. Half a century later, Sharpless *et al.* introduced copper(I) to overcome the activation energy barrier without heating: the copper(I) catalysed alkyne azide cycloaddition (CuAAC) [4]. Its presence enhances the reaction speed and only results in 1,4-region specific 1,2,3-triazoles. Furthermore, it offers the opportunity to perform reactions at room temperature, in protic and aprotic solvents resulting in chemically stable hetero-cycles [5]. All the above resulted in the extensive use of CuAAC in many fields, *e.g.* organic chemistry, polymers and bio conjugation.

In a first stage, to gain further fundamental insights of its potential concerning bio conjugated surface chemistry, a small fluorescent molecule, alkynated Alexa Fluor® ^{488} will be immobilised on an appropriate functionalised carrier surface that has a minimal interference with the fluorescent signals. Alexa Fluor® ^{488} is a fluorescent marker which is frequently used for intracellular tracking of a wide variety of cellular molecules and processes. Excitation of this dye occurs at 495 nm after which a fluorescent signal is emitted at 519 nm.

All experiments are performed with glass substrates. The latter have been functionalised using two different silanisation protocols, leading to amine (3-aminopropyl)triethoxy-silane (APTES) or N-(Trimethoxysilylpropyl)ethylenedi-

amine triacetic acid (TMS-EDTA) functionalised surfaces (see trisodium salt of TMS-EDTA in **Figure 3.1**).

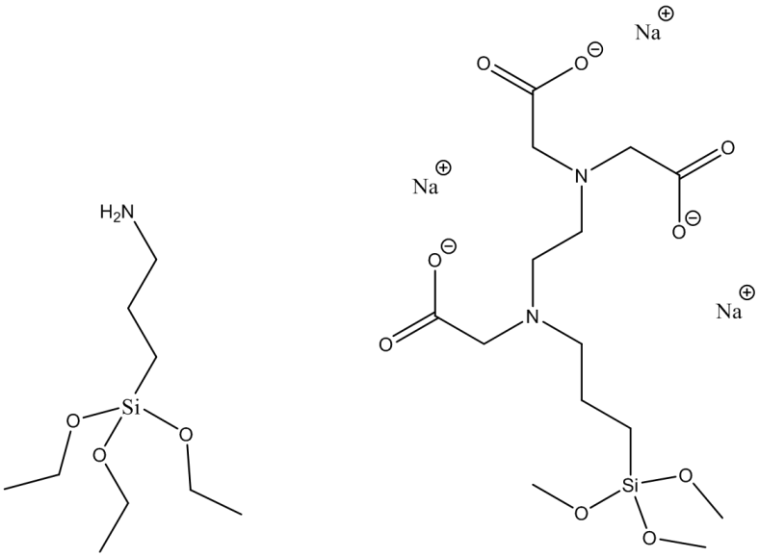

Figure 3.1: Chemical structure of APTES (left) and TMS-EDTA trisodium salt (right).

Subsequently, these silanes are modified with the required azide groups using two slightly different protocols, both based on EDC/NHS coupling. On one hand, a surface with carboxylic functional groups will be used as an anchor point which will be modified with an azide functionality. On the other hand, an amine functionalised surface will be modified to an azide functionalised surface. The azidified substrates will serve as the basis to couple them with the alkynated Alexa Fluor® ^{488} (**Figure 3.2**) *via* CuAAC. Because of the high solubility of the dye in polar aprotic solvents, dimethyl sulfoxide (DMSO) will be used to perform the immobilisation reactions towards the glass substrates. Since this type of solvents can possibly affect the activity of biomolecules, such as antibodies and enzymes, it is recommended to use a minimal amount of these solvents mixed in an aqueous buffer.

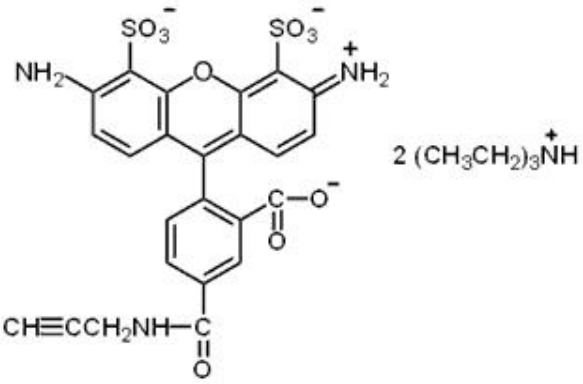

Figure 3.2: Chemical structure of alkynated Alexa Fluor® [488].

Next to the immobilisation of a dye, a protein was selected to prove that CuAAC can be used for protein immobilization purposes. Green fluorescent protein (GFP, see **Figure 3.3**) originates from the jellyfish *Aequorea victoria*. GFP absorbs light at 395 nm (with a smaller peak at 475 nm) and emits green light at 508 nm [6]. GFP is a relatively small protein (27 kDa; 20 lysines) and is used as a model compound for the biofunctionalisation of the azidified glass substrates *via* CuAAC.

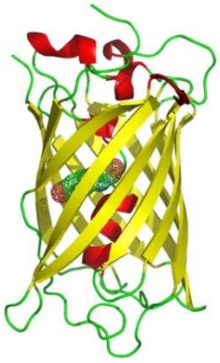

Figure 3.3: 3-D structure of wild-type green fluorescent protein. β-strands (yellow), α-helices (red), loops (green) and the chromophoric centre are presented [7].

The optimised coupling conditions, as will be discussed in sections 3.3.3 - 3.3.5, for the alkynated fluorescent dye and alkynated GFP immobilisation will later be used as a starting point for further biofunctionalisation of planar glass substrates with bovine immunoglobulin G (bIgG; **Figure 3.4**), a Y-shaped antibody with a molecular mass of ±150 kDa containing approximately 83 lysines per molecule [8]. A dye (ATTO^{488}-NHS), and alkyne groups are being introduced to the IgG molecules in order to allow fluorescent detection.

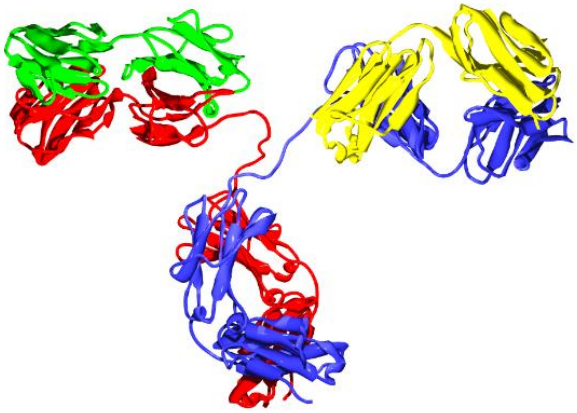

Figure 3.4: 3-D structure of IgG [9].

3.2 Materials & Methods

3.2.1 Reagents

N-[(3-trimethoxysilyl)propyl]ethylenediamine triacetic acid trisodium was obtained from ABCR. Sodium azide, 1-ethyl-3-(3-dimethylaminopropyl) carbodiimide (EDC), N-hydroxysuccinimide, copper sulphate pentahydrate and bromopropylamine hydrobromide were purchased from Acros. Zeba micro spin desalting columns (7K MWCO, 0.5 mL) were obtained from Thermo Scientific. Tris[(1-benzyl-1H-1,2,3-triazol-4-yl)methyl] amine (TBTA) (3-aminopropyl)triethoxysilane (APTES), bovine immunoglobulin G (bIgG), tris(2-carboxyethyl) phosphine (TCEP), sodium L-ascorbate, 4-(2-hydroxyethyl)-1-piperazineethanesulfonic acid (HEPES), ATTO^{488}-NHS, sodium acetate trihydrate, tetrakis acetonitrile Cu(I) hexafluorophosphate, 5-hexynoic acid, tris(2-carboxyethyl)phosphine (TCEP) were obtained from Sigma-Aldrich. Green fluorescent protein (GFP) is obtained from Millipore S.A./N.V.. Alkynated Alexa Fluor® ^{488} was obtained from Life Technologies.

3.2.2 Solutions

For the coupling buffer, 2 mM tetrakis acetonitrile Cu(I) hexafluorophosphate in DMSO; 2 mM TBTA in DMSO; 2.6 mM sodium L-ascorbate in H_2O; 6.5 mM alkynated Alexa Fluor® ^{488} in DMSO; 10 mM sodium acetate buffer pH 4; 100 mM tris(2-carboxyethyl) phosphine (TCEP) in sodium acetate buffer pH 4; 200 mM copper sulphate ($CuSO_4$) in sodium acetate buffer pH 4. All buffers were prepared with Milli-Q water.

For cleaning, 1:3 H_2O_2/H_2SO_4; 4:1:1 $H_2O/H_2O_2/NH_4OH$ solution; 2 % (v/v) APTES solution in 95:5 ethanol/water; 6 % in 0.2 M sodium acetate buffer pH 4; 200 mM

solution of azide-NHS ester in DMSO was added to 50 mM borate buffer pH 8 resulting in a 20 mM azide-NHS solution; mixture of EDC (0.2 M), NHS (0.05 M) and 3-azido-1-aminopropane (AAP; 0.1 M) in H_2O; alkyne-NHS ester in acetonitrile (1 mg/mL); PBS; 10 mM IgG solution.

3.2.3 Instruments

Fluorescence measurements were performed with an Ettan DIGE scanner and a confocal microscope. Fluorescent spectra were recorded by a Spex Fluorolog Tau Lifetime Spectrofluorometer. Contact angle measurements were performed with a dataphysics OCA 15+ goniometer (Filderstadt, Germany). Contour ellipse fitting of the water droplets was done by the SCA 1.0 software. The droplet size was 1 µL dispensed at 0.1 µL/s.

Ettan DIGE scanner

A mounted glass cassette was used to load the fluorescent substrates into the scanner. In between substrate and the cassette, water was applied for optimal fluorescent signals. The wavelengths for excitation and emission were chosen depending on the used fluorophore. For the dyes, Alexa Fluor® ^{488}, ATTO^{488}-NHS and GFP, the filter settings were λ_{ex}: 480 nm/30 nm λ_{em}: 530 nm/40 nm. The exposure time was set up to 0.9 s and the pixel size was 100.0 µm.

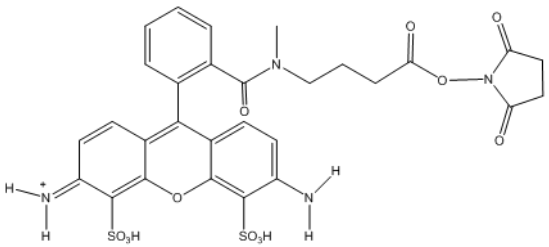

Figure 3.5: Chemical structure of ATTO^{488}-NHS.

Confocal microscope

The laser beam emitted by a 30 mW 488 nm Ar-ion laser in the confocal microscope was filtered up to 10 % by a 488 nm 'clean-up' interference filter. *Via* a dichroic mirror and a 10x/0.3 objective the laser beam was lead to the sample. A second dichroic mirror collected the fluorescence signal and this signal was on its turn filtered by a 505 nm long-pass filter. The scanning speed was 3.2 µs per pixel and the resolution was 512 by 512 pixels with a pixel size of 1.76 µm. The pinhole-diameter was 1 Airy unit (72 µm). The recording time, needed for an entire frame amounts to 1.97 s.

Spex Fluorolog Tau Lifetime Spectrofluorometer

Crystal cuvettes were filled with the fluorophore solution. Excitation occurred at 395 nm (λ_{ex}) while an emission spectrum was recorded from 500 to 650 nm. The signals of the buffer reference spectrum were subtracted from those of the actual fluorescence measurements.

UV-Ozone apparatus

A PSD Benchtop UV/Ozone System was used for the dry cleaning of glass substrates before silanising them. A mercury vapour lamp was used to generate UV radiation with varying wavelengths for different purposes: 185 nm generates ozone from oxygen and 254 nm excites organic molecules on the sample, producing free radicals which are being removed as CO_2 and H_2O vapour. The machine was heated up to 110 °C during the cleaning cycle during 1 hour.

3.2.4 Substrate functionalisation

Glass cleaning before APTES silanisation

Before functionalising the glass samples with azide groups, a wet and dry cleaning was performed. First the samples were incubated in a 1:3 H_2O_2/H_2SO_4 (Piranha) solution for 30 minutes at room temperature and consequently washed with H_2O. In a next step, the samples were put in a 4:1:1 $H_2O/H_2O_2/NH_4OH$ solution for 15 minutes at 70 °C, excessively flushed with water and ethanol, and finally dried with N_2. Following to the wet cleaning, the samples were further cleaned with UV-ozone for 20 minutes at 110 °C and stored in N_2 atmosphere, at room temperature until further functionalisation.

Glass cleaning before TMS-EDTA silanisation

The glass slides were firstly cleaned in a 3:1 mixture (v/v) of H_2SO_4:H_2O_2 for 5 min and then treated with 6 % (v/v) HF for a few seconds to create a hydrophobic surface. Subsequently, the slides were oxidized by treating them with chromic acid (8 % potassium dichromate (w/v) in 25 % H_2SO_4 (v/v)) at 80 °C for 1 hr to make them hydrophilic. The oxidized slides were washed with Milli-Q water and ethanol, dried with N_2 and stored in N_2 atmosphere, at room temperature until further use.

Silanisation with APTES and TMS-EDTA

The samples, cleaned as described earlier, were functionalised with amine groups using APTES. A falcon tube was completely filled with a 2 % (v/v) APTES solution in 95:5 ethanol/water. The clean glass (amorphous SiO_2) slides were put into this solution for 30 minutes. Afterwards the samples were washed repeatedly with ethanol and H_2O, dried with N_2, placed in the oven at 110 °C for 15 minutes and

stored under N_2. **Figure 3.6** depicts the schematic overview of both silanisation procedures resulting in the amine functionalised APTES surface or in the TMS-EDTA silanised surface.

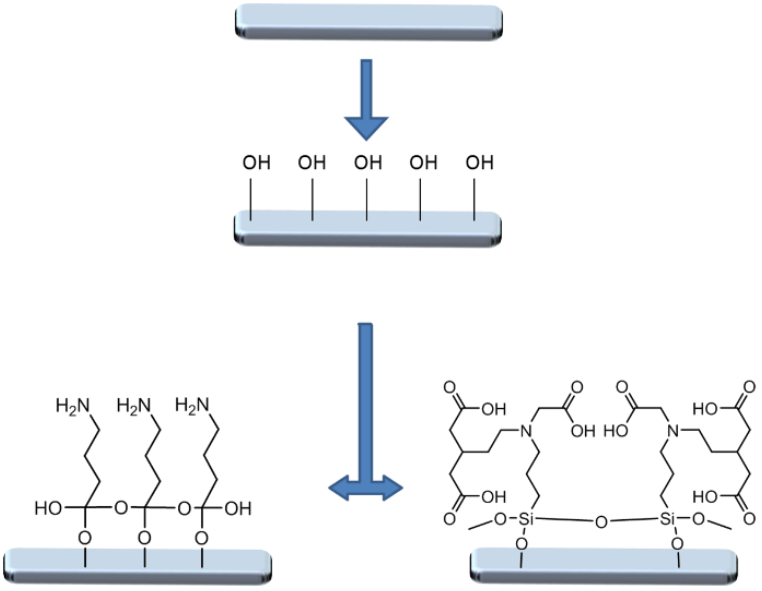

Figure 3.6: Schematic representation of the amino and carboxyl silanised glass surfaces (ideal model) after pre-treatment with strong oxidising solutions and UV-O_3.

In addition to the amine functionalised glass substrates, carboxyl functionalised substrates were prepared. To this end, first the glass slides were cleaned as previously described. In the following step, the slides were entirely covered with TMS–EDTA containing solution (6 % (v/v) in 0.2 M sodium acetate buffer pH 4) and placed in the oven at 110 °C for 1 hour. Afterwards the slides were flushed with water and dried with N_2. After silanisation, contact angles were measured for both silanisation protocols.

Azidification of APTES- and TMS-EDTA functionalised surfaces

After amino silanising the glass samples, the surface needs to be modified with azide functionalities. Azidified glass can be obtained *via* an azide containing NHS ester, succinimidyl 4-azidobutyrate synthesised according to a literature protocol [10] (**Figure 3.7**). A 200 mM solution of azide-NHS ester in DMSO was added to 50 mM borate buffer pH 8 resulting in a 20 mM azide-NHS solution. The amine modification towards azide functionalities occurred by covering the substrates entirely with the NHS containing solution in a water vapour saturated environment, overnight, at room temperature. Afterwards the substrates were excessively washed with water to remove all the remaining reactants and ethanol in order to facilitate the drying. Contact angle measurements confirmed the azidification of the used surfaces.

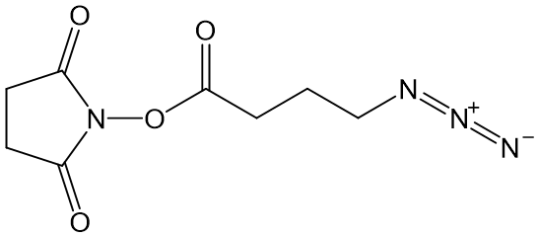

Figure 3.7: Chemical structure of succinimidyl 4-azidobutyrate (azide-NHS ester).

In addition to functionalising the surface with azide moieties using the azide-NHS ester, a second linker molecule has been used, based on the same chemistry between carboxyl and amine groups induced by EDC and NHS. To a carboxylated glass slide a linker, 3-azido-1-aminopropane (AAP; **Figure 3.8**) synthesised as described by Hatzakis [11], was attached using EDC/NHS chemistry. To this end, the glass slides were immersed into a mixture of EDC (0.2 M), NHS (0.05 M) and

AAP (0.1 M) in H_2O for 3 hours at room temperature. The slides were then rinsed for 30 minutes with Milli-Q water and dried under N_2 gas flow.

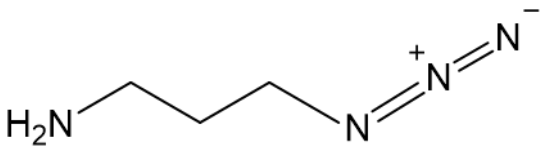

Figure 3.8: Chemical structure of 3-azido-1-aminopropane (AAP).

The following **Figure 3.9** is a schematic representation of the azide modification of both silanised surfaces as described above.

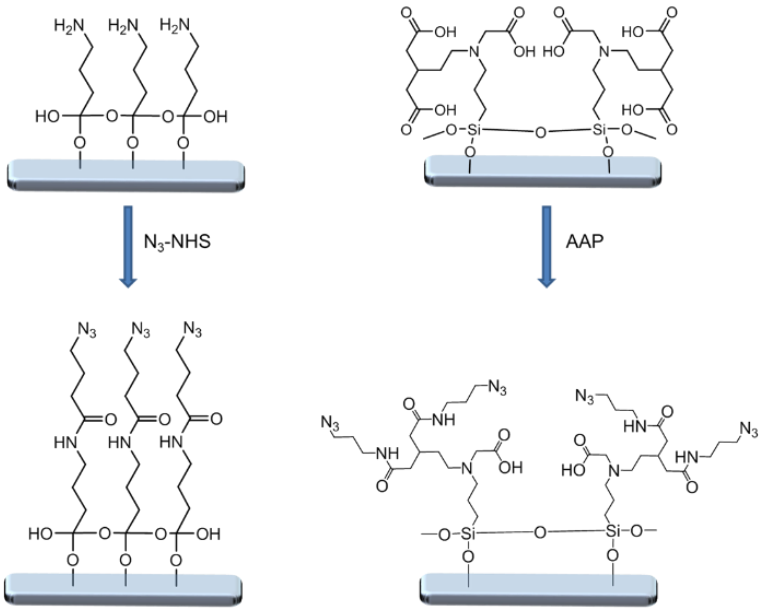

Figure 3.9: Schematic representation of the azide functionalisation by succinimidyl 4-azidobutyrate (azide-NHS) of the APTES (NH_2) functionalised glass (left) and by 3-azido-1-aminopropane (AAP) of the TMS-EDTA (COOH) functionalised glass (right).

It should be noted that organic azides, as depicted in **Figure 3.8**, are known for their explosive properties. When the number of nitrogen atoms does not exceed

the number of carbons and the equation $(N_C + N_O)/N_N \geq 3$ (N =number of atoms) is fulfilled, the organic azide is not explosive and manageable [12]. In AAP the number of nitrogen atoms exceeds the amount of carbon atoms and $(N_C + N_O)/N_N = (3 + 0)/4 = 0.75$ which is smaller than 3. The synthesis and handling of the AAP linker should be done with care, preferably in small amounts and at low temperatures!

3.2.5 Protein alkynation and subsequent fluorescent labelling

The silanised and azidified glass surfaces will serve as the base carrier to which different molecules will be coupled. These different molecules will need to contain the required alkyne functionality. Due to the fact that in the first stage, detection of the molecules will be performed by means of fluorescence, the molecule will not only need an alkyne functionality, but it will also require a fluorescent label, unless the molecule of interest emits a fluorescent signal itself when excited.

Alkynation of GFP and IgG

To a 5,5 µM GFP solution in PBS, a 3.2 molar excess of 2,5-dioxopyrrolidin-1-yl hex-5-ynoate or alkyne-NHS ester (**Figure 3.10**) in acetonitrile was added in order to functionalise just over 3 of the 20 (about 16 %) endogenous lysines [13]. It should be noted that a 5.5 µM GFP solution equals a lysine concentration of 110 µM. As a result, to functionalise 16 % of present lysines the final concentration of added alkyne NHS has to be 17,6 µM. After 3 hours of incubation in the dark, at room temperature, the protein solution was filtered by Zeba micro spin desalting columns. Subsequently, the alkynated GPF solution was stored in PBS at 4 °C until further use during the substrate immobilisation reaction. Due to the auto

fluorescence properties of GFP an additional functionalisation step with a dye is not required.

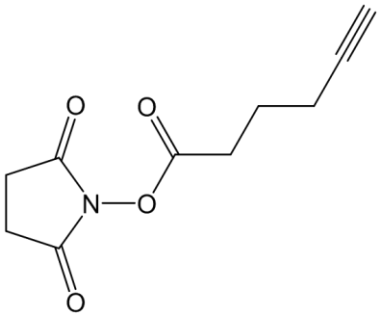

Figure 3.10: Chemical structure of 2,5-dioxopyrrolidin-1-yl hex-5-ynoate (alkyne-NHS) used for the alkyne functionalisation of proteins.

Analogous to the alkyne functionalisation of GFP, 16 % of the 83 lysines [8] present in a 10 mM IgG solution were functionalised with alkyne-NHS. The alkyne functionalised IgG molecules were filtered by Zeba micro spin desalting columns and stored in PBS at 4 °C until further use. In order to be able to detect the coupling of IgG to the solid carrier, the introduction of a dye is required as is described below.

Labelling of alkyne functionalised IgG with a fluorescent dye

In order to be detectable by fluorescence spectroscopy, to the 10 mM alkynated IgG solution in PBS, ATTO^{488}-NHS in PBS was added in a 1:1 (m/m) ratio (**Figure 3.5**). After incubation for 3 hours in the dark at room temperature, the solution was filtered with a Zeba micro spin desalting column. The protein was stored in PBS at 4 °C in the dark until further use.

3.2.6 CuAAC mediated coupling of alkynated Alexa Fluor® ^{488} to N_3-functionalised APTES surfaces

Determination of the optimal alkynated Alexa Fluor® ^{488} concentration for CuAAC immobilisation

First of all, an alkynated version of the fluorescent dye Alexa Fluor® ^{488}, will be immobilised on the azidified surface. To the azide functionalised amino silanised glass substrate two series of four spots are applied. The first series contains the alkyne functionalised 500 µM alkynated Alexa Fluor® ^{488} dye (dissolved in DMSO), 0.5 mM tetrakis acetonitrile Cu(I) hexafluorophosphate (dissolved in DMSO), 0.65 mM sodium L-ascorbate (in H_2O) and 0.5 mM TBTA (in DMSO). Tetrakis acetonitrile Cu(I) hexafluorophosphate is providing the Cu(I) to the reaction. Without adding a reducing agent as sodium L-ascorbate, Cu(I) will oxidize to Cu(II). To enhance the 'click' reaction and to keep the Cu(I) from reacting with other structures, TBTA is added to the mixture. For each spot, 10 µL of a mixture of all four components is prepared in a 1:1:1:1 ratio. Depending on the intended end concentration of alkynated Alexa Fluor® ^{488}, a stock solution of 2000, 200, 20 or 2 µM is used. The second series contains the alkynated Alexa Fluor® ^{488} and the identical solvents used in the first series, without the CuAAC components tetrakis acetonitrile Cu(I) hexafluorophosphate, sodium L-ascorbate and TBTA). This series will serve as the negative control for possible aspecific adsorption to the azide substrate. Both series are spotted on an azide functionalised glass as shown in **Table 3.1**.

Table 3.1: Eight 'Click' reaction mixtures containing similar amounts of copper catalyst, reducing agent and ligand with a serial dilution of the alkynated Alexa Fluor® ^{488} (500, 50, 5 and 0.5 µM).

Conc.$_{final}$ Alexa Fluor ^{488}	**500 µM**	**50 µM**	**5 µM**	**0,5 µM**
Cu(I)+NaAsc + TBTA (3:1 DMSO/H_2O)	1	2	3	4
3:1 DMSO/H_2O	5	6	7	8

In both series a range of alkynated Alexa Fluor® ^{488} concentrations is applied, varying from 500 to 0.5 µM. The coupling reaction took place overnight at room temperature in a dark, with water/DMSO vapour saturated environment. After coupling, the samples were washed in several steps in order to remove unbound dye. First, the samples were washed with 3 x 3 mL DMSO. Subsequently, they were put for 1 hour in a beaker containing enough DMSO to cover the samples entirely. Next the samples were dried. Subsequently, the fluorophore was excited at an excitation wavelength of 480 nm ±30 nm. The emitted fluorescent signal was measured at a wavelength of 530 nm ±40 nm with an Ettan DIGE scanner. In addition, fluorescence signals were detected using the confocal microscope.

Determination of optimal DMSO/Sodium acetate buffer ratio for the CuAAC immobilisation of alkynated Alexa Fluor® ^{488}

As the aim of the entire research, is to develop a procedure to immobilise biomolecules to solid carriers, the solution in which the immobilisation will take place, will need to be the least harmful as possible. Therefore, the amount of (harmful) organic solvents has to be kept at a level as low as possible.

The solvent ratios used for the coupling of alkynated Alexa Fluor® ^{488} varied from 20:80 DMSO/sodium acetate buffer to 5:95 DMSO/sodium acetate buffer in steps of 5 %. 10 µL spots of each mixture were applied on one common azide functionalised glass slide. The end concentration of the different components present in the reaction mixtures were 0.5 mM, 0.65 mM, 0.5 mM and 0.5 µM for tetrakis acetonitrile copper(I) hexafluorophosphate, sodium L-ascorbate, TBTA and alkynated Alexa Fluor® ^{488}, respectively. Simultaneously, a negative control was performed for each condition overnight. Afterwards the slide was washed as described under 3.2.6 and a fluorescence scan in water was recorded with the Ettan DIGE scanner.

The impact of the catalyst, reducing agent and ligand using CuAAC on the fluorophore immobilisation

Since it was found that Alexa Fluor® ^{488} can be immobilised in a solution of 95:5 sodium acetate/DMSO, seven different mixtures of Alexa Fluor® ^{488} in 95:5 sodium acetate/DMSO, were prepared in order to determine the impact of each of the different components in the reaction mixture (see **Table 3.2**). For each condition three spots were applied on the azide modified surface and the reaction took place overnight (saturated environment; room temperature). Afterwards, the sample was washed as described under 3.2.6 and a fluorescence scan in water was recorded with the Ettan DIGE scanner.

Table 3.2: Overview of the different reagents present in the reaction mixture of Alexa Fluor® 488 in 95:5 sodium acetate/DMSO and their impact on the CuAAC coupling of the alkynated dye to the azide functionalised glass surface. (√: reagent is present in reaction mixture; • not present in reaction mixture)

0.5 µM Alexa^{488} mixture	0.5 mM Cu(I)-catalyst	0.65 mM Sodium L-ascorbate	0.5 mM TBTA
1	√	√	√
2	√	√	•
3	√	•	•
4	•	√	√
5	√	•	√
6	•	•	√
7	•	•	•

Sodium L-ascorbate *vs.* TCEP as a reducing agent

Both sodium L-ascorbate and TCEP have been reported as the ideal reducing agents. In order to make sure that in this research the coupling conditions are optimal, both reducing agents have been tested. To a mixture, labelled C_1 in **Table 3.3**, containing 0.5 mM tetrakis acetonitrile copper(I) hexafluorophosphate and 0.5 mM TBTA in 95:5 sodium acetate buffer/DMSO, either 0.65 mM TCEP or 0.65 mM sodium L-ascorbate was added as the reducing agent. Furthermore, a serial dilution (2x, 4x and 10x) starting from C_1 was prepared. After the final preparation of the solutions, alkynated Alexa Fluor® ^{488} was added until a final dye concentration of 0.5 µM was achieved. Out of these eight reaction mixtures, 10

µL was spotted on an azide functionalised glass substrate. The reaction took place overnight in the dark (saturated environment; room temperature). Afterwards the sample was washed as described on 3.2.6 and a fluorescence scan in water was recorded with the Ettan DIGE scanner.

Table 3.3: Two alkynated Alexa Fluor® ^{488} containing solutions, differing in reducing agent (sodium ascorbate or TCEP), were prepared and spotted in threefold to azide functionalised glass (C_1). Further three solutions (C_2, C_3 and C_4) containing respectively 2x, 4x and 8x less Cu(I), reducing agent and TBTA compared to C_1, were also applied to the azide surface in threefold.

SOLUTION	**C_1**		**C_2**		**C_3**		**C_4**	
SPOT NR	**Reducing agent**							
1	NaAsc	TCEP	NaAsc	TCEP	NaAsc	TCEP	NaAsc	TCEP
2	NaAsc	TCEP	NaAsc	TCEP	NaAsc	TCEP	NaAsc	TCEP
3	NaAsc	TCEP	NaAsc	TCEP	NaAsc	TCEP	NaAsc	TCEP
ALEXA FLUOR® 488	**0.5 µM**							

3.2.7 CuAAC coupling of alkynated Alexa Fluor® ^{488} to N_3-functionalised TMS-EDTA surfaces

Since a hydrophilic surface most likely will lead to lower amounts of unfolded and hydrophobic bound proteins, a more hydrophilic surface, containing azide functionalities was tested. The catalyst concentrations remain unchanged for the coupling of alkynated Alexa Fluor® ^{488} to the azide modified TMS-EDTA glass surface. The immobilisation of the fluorescent dye was performed in 95:5 sodium acetate buffer/DMSO containing 0.5 mM acetonitrile copper(I)

hexafluorophosphate, 0.65 mM sodium L-ascorbate, 0.5 mM TBTA and 0.5 µM alkynated Alexa Fluor® ^{488}. A control solution without copper(I) was prepared as well. For both solutions 2 drops of 10 µL were applied on top of four azide functionalised carboxylated substrates. Fluorescence was measured at a wave-length of 367 nm ±8 nm by the Ettan DIGE scanner.

3.2.8 Coupling of alkynated GFP to N_3-glass

Immobilisation of GFP *via* CuAAC

In a next level of experiments, biomolecules were being used for the bio-functionalisation of the solid azidified carrier. The immobilisation of alkyne functionalised GFP was performed identical to the procedure as was used for alkynated Alexa Fluor® ^{488}. The reaction was performed in 95:5 sodium acetate buffer pH 4/ DMSO. The final concentration of tetrakis acetonitrile copper (I) hexafluorophosphate, TCEP, TBTA and alkyne functionalised GFP were 0.5 mM, 0.65 mM, 0.5 mM and 0.5 µM, respectively. A second solution containing only the alkyne functionalised GFP was prepared as the negative control experiment. Four spots of 10 µL from both solutions were applied to an azide functionalised carboxylic silanised glass surface (overnight; saturated environment; room temperature). Afterwards the samples were washed with washing buffer and a fluorescence scan was taken with the Ettan DIGE scanner.

Fluorescence inhibiting effect of CuAAC reaction mixture

Since the results from the GFP experiments did not meet the expectations several additional tests were performed. The fluorescence spectra of four different solutions were measured in order to get an impression of the potential effect on the fluorescent signal of GFP. In **Table 3.4** an overview is presented of the content

of all solutions: 1) a buffer solution of 95:5 sodium acetate buffer pH 4/DMSO, 2) 0.5 µM alkyne functionalised GFP in 95:5 acetate buffer pH 4/DMSO, 3) 0.5 µM alkyne functionalised GFP and 0.5 mM tetrakis acetonitrile copper (I) hexafluorophosphate in 95:5 acetate buffer/DMSO and 4) 0.5 µM alkyne functionalised GFP, 0.5 mM tetrakis acetonitrile copper(I) hexafluorophosphate, 0.65 mM TCEP and 0.5 mM TBTA in 95:5 acetate buffer/DMSO. The fluorescence spectra were measured with the Spex Fluorolog Tau Lifetime Spectro-fluorometer.

Table 3.4: Overview of the reactants present in the different solutions for demonstrating their potential inhibiting effect on the fluorescent signal. √: present in the solution •: not present in the solution.

Solution	Na Acetate/DMSO	GFP	Cu(I)	TCEP	TBTA
1	√	•	•	•	•
2	√	√	•	•	•
3	√	√	√	•	•
4	√	√	√	√	√

3.2.9 Immobilisation of ATTO-^{488} alkynated IgG to N_3-glass

Since GFP is a fluorescent protein and immobilizing might slightly influence certain intramolecular interaction, a second protein containing an artificially applied fluorescent molecule was used for immobilisation. Six spots from two different solutions were applied on one azide functionalised TMS-EDTA silanised glass substrate. The first mixture contained 0.5 mM $CuSO_4$, 0.65 mM TCEP, 0.5 mM

TBTA and 1 µM ATTO-^{488} labelled alkyne IgG in PBS while the second solution only contained the labelled alkyne IgG in PBS. The incubation was performed overnight (saturated environment; room temperature).

3.3 Results & Discussion

3.3.1 Substrate functionalisation

Before silanising the glass substrates with APTES, dust particles and organic contaminants such as bacteria and sebum coming from the skin (*e.g.* fingerprints, skin fluids, body lotion), had to be removed. Prior to silanisation, two different cleaning procedures were used, to facilitate the formation of homogenous silane layers on the glass slides.

The first procedure was a wet cleaning starting with piranha, a strong oxidising agent, to remove organic molecules. Afterwards a mixture of hydrogen peroxide, water and ammonia was used to further remove organic material. Due to the basic conditions of this additional cleaning step, small particles, which may have been strongly attached to the glass surface, were slowly etched away. Subsequently, the samples were treated with UV-O_3. This dry cleaning using ultraviolet rays and O_3 is known for its conversion of remaining organic compounds into volatile substances, *e.g.* nitrogen, carbon dioxide and water. After the cleaning steps, contact angles were measured and compared to the angles measured before cleaning. The untreated substrates had an average contact angle of 25°. The contact angles (<4°) for the clean substrates were hardly measurable due to a strongly increased hydrophilicity.

As an alternative, in the second cleaning procedure only the wet steps from the first cleaning procedure were utilised. Also after this cleaning step, surfaces with a contact angle lower than 4° were obtained.

The hydrophilic glass substrates obtained from both procedures were functionalised using two different silanes, *i.e.* APTES or TMS-EDTA, as presented in **Figure 3.6**. The slides cleaned by the dry-wet cleaning procedure were functionalised with APTES, the other samples obtained after the wet-only cleaning procedure were silanised with TMS-EDTA.

Silanisation can be performed in various ways. A first method is to dip the substrate in the silane containing solution. A second method is by drop casting the silane solution on top of the substrate. Spincoating is a third option which can be used. Finally, a fourth method is the vapour deposition of the silane on the substrates under vacuum or at elevated temperatures. In this work the dip method was used because it had to be performed in an environment without oxygen to obtain more homogeneous layers. By dipping the sample in a closed container, flushed with nitrogen, the oxygen could be excluded. In case of the EDTA silane, the silanisation was performed using the drop cast procedure as described in literature [14].

One of the best known and commonly used amino silanes is (3-aminopropyl) triethoxysilane or APTES. The amino silanisation protocol, as described in 3.2.4, was performed by dipping the clean glass samples in a degassed 2 % APTES solution dissolved in 95:5 ethanol/water solution. In **Table 3.5** the contact angles of five samples are shown before and after silanisation. Amine substrates with an average contact angle of 49° ±0.5° were obtained, which are comparable to angles realised with alternative APTES silanisation protocols [15, 16]. In view of

this contact angle the conclusion can be made that a functionalisation with APTES has indeed occurred. The obtained substrates, as schematically represented in **Figure 3.9**, were further modified to azide functionalised surfaces. As an alternative to the amine functionalised surfaces, TMS-EDTA was used to silanise the substrates to provide them with carboxyl functionalities. In this case, the silanisation was not performed by dipping the substrate into the solution, but *via* drop casting. The acidic solution, in which the silane was dissolved, was needed to hydrolyse the methoxy groups of TMS-EDTA into silanols. These silanols were covalently coupled to the hydroxylated surface. For this coupling reaction, the success of the silanisation could not be confirmed by contact angle measurements due to the fact that the carboxyl silanisation also results in a very hydrophilic surface of which the contact angles (<4°) were hardly measurable (**Table 3.5**.).

Finally, two types of azide functionalised surfaces were obtained, both using protocols, which were based on the amide formation between amines and carboxyl groups by means of EDC and NHS in an aqueous solution. In the first case, to the amine containing APTES surface the azide functionalised NHS ester was applied. The contact angles for the azide functionalised APTES surfaces are presented in **Table 3.5**. Here an increase in contact angle from 49° to 66° can be seen. This change demonstrates a decrease in wettability due to the bond formation between the azide linker and the silane. This confirms that the azide modification indeed occurred.

In the second case, an azide containing amine linker was added to the TMS-EDTA silanised substrate. The carboxylated substrates were initially functionalised with azide groups by putting them in a solution of EDC, NHS and AAP in H_2O. However, after using these samples no reproducible contact angles could be obtained. Most

likely a strong increased pH caused by the amine containing azide linker resulted in a damaged silane layer. By using HEPES as a buffer, the pH changes were kept under control. From this moment, the carboxyl silanised slides were dipped in a mixture containing EDC, NHS and the AAP linker in 220 mM HEPES buffer pH 6.8. After modification the contact angles increased up to 37° ±7°.

Table 3.5: Average contact angles and standard deviation (σ) of cleaned (-OH), amino-functionalised (APTES), carboxylated (TMS–EDTA), and subsequent azide functionalised glass substrates (number of measurements *n*=5).

Surface	Average Contact angle (°)	σ (°)
No treatment	25	2
-OH	<4	/
$-NH_2$	49	1
$-NH_2+N_3$	66	1
-COOH	<4	/
$-COOH+N_3$	37	7

Both types of azidified surfaces will serve as a platform to which various types of (bio) molecules will be immobilised mediated by the CuAAC reaction. In case of protein immobilisation, the hydrophilicity of the solid surface has its impact, to a certain level, on the amount of non-covalently bound proteins. For obvious reasons this is a 'side-effect' that has to be kept to a minimum.

3.3.2 Protein alkynation and labelling

Immunoglobulin G (IgG) is one of the many different types of immunoglobulins, *e.g.* IgA, IgE, IgM, that exists in mammals. The presence of accessible lysines, which are numerously present at the surface of the protein, offers the opportunity to provide the protein with alkyne functionalities. By using an alkynated NHS-ester IgG can be artificially functionalised with alkyne functionalities. By performing a native PAGE, pI changes, moderated by the formation of peptide bonds between the alkyne containing NHS-linker and the primary amines present in the lysines, were demonstrated. In **Figure 3.11** a scan of the wild-type PAGE-electrophoresis gel containing wild-type (green) and alkynated (red) bovine IgG (bIgG) is presented. When applying a certain voltage to the gel, the negatively charged proteins, wild-type and alkynated, migrate towards the anode. Due to modifications at the amino acid level, the isoelectric point (pI) of the alkynated proteins will differ from the wild-type and the migration speed towards the anode will be influenced. In this case, the pI of the alkynated IgG is lower than the pI of the wild-type IgG molecules, the latter varies from between 7 and 11. When performing the gel electrophoresis ($pH_{separating\ Gel}$ 8.8) at a pH higher than the pI of the proteins, the net charge will be negative, however the alkynated protein will be more negatively charged at this pH as compared to the wild-type species.

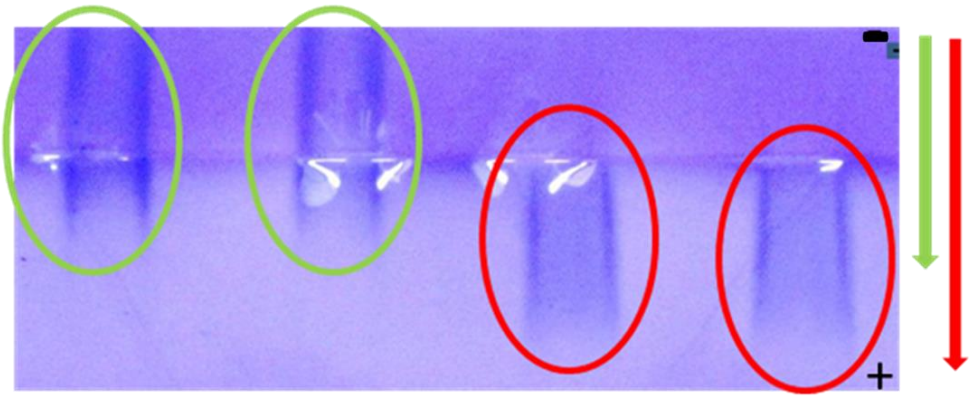

Figure 3.11: Scan of wild-type (green) and alkynated (red) IgG during native PAGE electrophoresis. The green (wild-type) and red (alkyne) arrows represent the difference in migration speed/distance through the gel towards the anode.

The distance covered by both proteins is designated with the green and red arrows next to **Figure 3.11**. For both protein species, wild-type and alkynated, two similar runs were performed. It can be concluded that the alkynation was successful, as the difference in migration speed between both species is different. However, the level of the proteins' alkynation cannot be determined from these experiments.

3.3.3 CuAAC coupling of alkynated Alexa Fluor® ^{488} to N_3-functionalised APTES surfaces

Determination of alkynated Alexa Fluor® ^{488} concentration for optimal CuAAC immobilisation

In order to optimise the CuAAC reaction using alkynated Alexa Fluor® ^{488} dyes a screening was performed involving different reagents. On an azide functionalised amino silanised glass substrate eight different spots were applied originating from

eight different 'CuAAC' solutions. Two series of four different solutions were prepared. The concentration of alkynated Alexa Fluor® ^{488} in one series was 0.5, 5, 50 or 500 µM. Both series differed in the presence (**Figure 3.12**a) or absence (**Figure 3.12**b) of copper(I), sodium L-ascorbate and TBTA in the mixture. Afterwards the fluorescence of the sample was recorded by a DIGE scanner as illustrated in **Figure 3.12**.

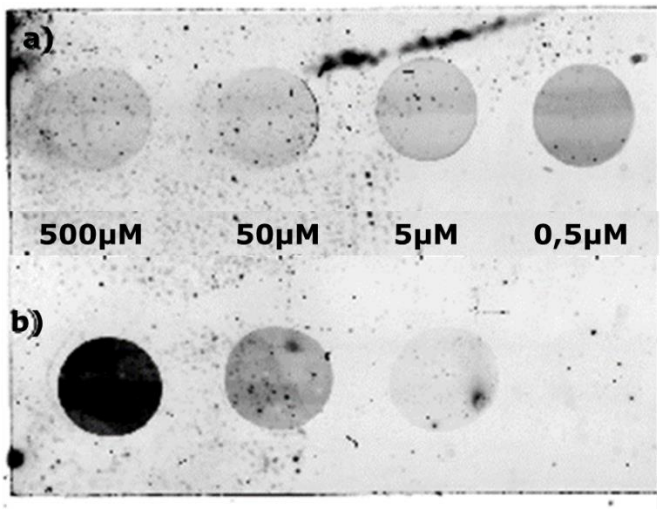

Figure 3.12: Dry fluorescence image recorded by a DIGE scanner of the azide functionalised amino silanised glass substrate after alkynated Alexa Fluor® ^{488} immobilisation *via* CuAAC in DMSO (0.5, 5, 50, 500 µM). Series a) solutions with copper (I), sodium L-ascorbate, TBTA and alkynated Alexa Fluor® ^{488} whereas series b) are solutions with only alkynated Alexa Fluor® ^{488}.

On first sight it seems that both series resulted in spots with immobilised alkynated Alexa Fluor® ^{488} molecules due to covalent coupling and/or physical adsorption on the azidified glass substrate. When lowering the concentration of alkynated Alexa Fluor® ^{488} no clear changes in fluorescence for series a) can be noticed. However, for series b), the signal decreases drastically to almost zero at

the lowest concentration. Comparing the signals from the 0.5 µM spots in series a) and b), a clear difference can be seen. Due to the absence of the CuAAC components no covalent coupling *via* CuAAC is possible in series b) and the recorded signal most likely originates from physically adsorbed dyes. By lowering the concentration, the amount of aspecific bound dye can be decreased down to the detection limit of the DIGE scanner. When measuring the same samples with the very sensitive confocal microscope an identical trend can be seen (**Figure 3.13**).

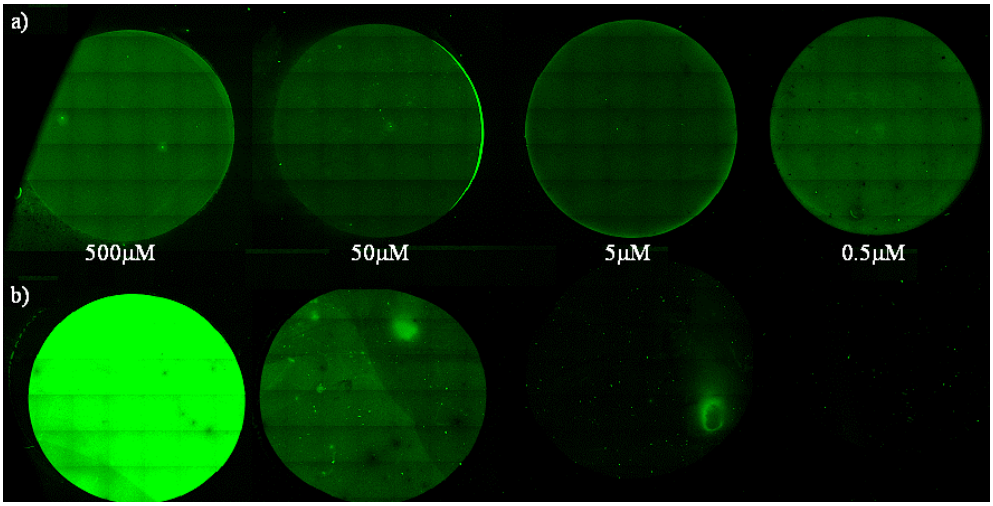

Figure 3.13: Dry fluorescent image recorded by confocal microscopy for alkynated Alexa Fluor® ^{488} containing series a) with copper(I), sodium L-ascorbate and TBTA, and series b) without CuAAC components.

These fluorescence measurements were performed under dry conditions. Most protocols suggest to perform the fluorescence measurements in solution where the excitation and emission peaks are respectively 494 nm ±3 nm (λ_{ex}) and 520 nm ± 4 nm (λ_{em}). **Figure 3.14** represents the fluorescence of the same sample in water. In order to record the fluorescence of the immobilised dyes in water, a

thin layer of water was put in between the glass substrate and the substrate holder.

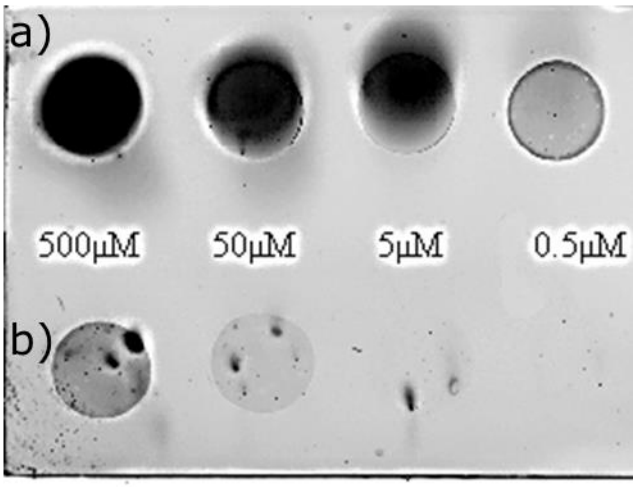

Figure 3.14: Fluorescence image in H_2O recorded by a DIGE scanner of the azide functionalised amino silanised glass substrate after alkynated Alexa Fluor® ^{488} immobilisation *via* CuAAC in DMSO (0.5, 5, 50, 500 µM). Series a) solutions with copper(I), sodium L-ascorbate, TBTA and alkynated Alexa Fluor® ^{488} and series b) solutions with alkynated Alexa Fluor® ^{488} only.

As can be seen in **Figure 3.14** the fluorescence of the CuAAC reactants containing samples in water increases significantly, whereas the signal coming from the negative controls decreases. A possible explanation for this phenomenon can be that the dye molecules that are covalently bound to the surface (series a) are closely packed together, leading to a quenching effect between the different immobilised dye molecules. Addition of a water film possibly leads to a change in the positioning of the different molecules, which leads to a reduction in quenching.

These fluorescence measurements offer the opportunity to visualize the presence of non-covalently immobilised molecules on the azidified surface and give an

indication at which concentrations physisorption can be minimised. From **Figure 3.12**, **Figure 3.13** and **Figure 3.14**, it can be concluded that further immobilisation experiments are best performed at dye concentrations between 0.5 and 5 µM. This will minimise the loss of expensive material and, in this case, the aspecific binding will be kept to a minimum. However, quantification *via* fluorescence stays difficult due to the different aspects which have to be taken into account when analysing the measured signals: Quenching, photo bleaching and auto fluorescence are all events which may influence the signal intensity, complicating an accurate quantification of immobilised molecules. Especially when more complex molecules are used for the formation of biolayers, it is appropriate to use an alternative non-destructive characterisation method to verify and quantify the amount of immobilised mass on the substrate of interest.

Determination of optimal DMSO/Sodium acetate buffer ratio for the CuAAC immobilisation of alkynated Alexa Fluor® ^{488}

In the previous experiments solutions containing at least 75 % DMSO and 25 % water were used for the immobilisation of alkynated Alexa Fluor® ^{488} on the azidified solid carriers. Unfortunately, these conditions are far too destructive and cannot be used for immobilising proteins or other biological molecules on solid surfaces. As a result, a compromise had to be found in such a way that the catalytic compounds are still soluble and the proteins of interest are not harmed and maintain their activity.

To this end, four solutions containing different ratios of sodium acetate buffer and DMSO, with or without Cu(I) catalyst were prepared. The DMSO ratios differed from 5 to 20 %, in sodium acetate buffer pH 4. The series lacking the presence of Cu(I) served as a negative control and are presented next to the minus symbol in

Figure 3.15. The four spots applied next to the plus symbol are the drops containing Cu(I). In total eight spots were applied on an azidified APTES silanised glass slide. Afterwards the fluorescence was measured, as shown in **Figure 3.15**.

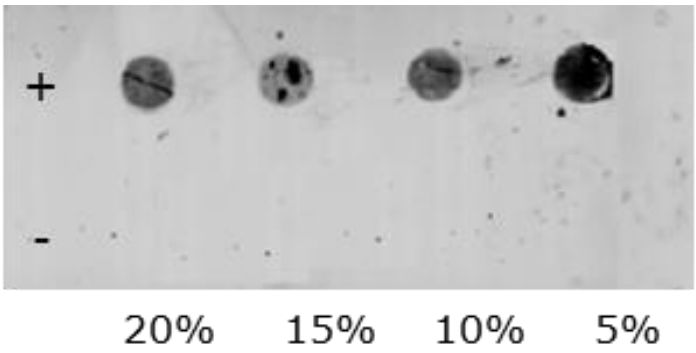

Figure 3.15: Fluorescence image, recorded by a DIGE scanner, in H_2O of four different reaction mixtures containing copper catalyst, sodium L-ascorbate and TBTA in sodium acetate buffer containing 0.5 µM alkynated fluorescent dye and respectively 5 %, 10 %, 15 % or 20 % DMSO (top row; +). Simultaneously a negative control for each mixture was applied (bottom row; -).

From the fluorescence signals in **Figure 3.15** it can be concluded that it is feasible to use solutions with only 5 % DMSO in an aqueous buffer. Lower concentrations resulted in precipitation of the ligand and the fluorescent dye. **Figure 3.15** confirms that CuAAC coupling can be performed in aqueous solutions. Up till now many protocols use higher water/solvent ratios, which could be harmful when working with biological material [17-19]. These results show that reducing the amount of organic solvent can result in a sufficient coupling. However, it is very difficult to draw conclusions about which concentration of DMSO is the most suitable for the alkynated Alexa Fluor® ^{488} immobilisation because an accurate quantitative estimation cannot be made. Notwithstanding, when comparing

Figure 3.14 and **Figure 3.15** it seems that at lower DMSO concentrations a better signal can be measured for the 0.5 µM alkynated Alexa Fluor® ^{488} (**Figure 3.15**) compared to the 3:1 DMSO/ buffer ratio in **Figure 3.14**.

The impact of the catalyst, reducing agent and ligand for CuAAC immobilisation

A screening was performed in order to further optimise the CuAAC reaction with alkynated Alexa Fluor® ^{488} dyes. In the mixtures the compound tetrakis acetonitrile copper(I) hexafluorophosphate is present to catalyse the immobilisation reaction and its oxidation state is maintained by using a reducing agent (reduction of Cu(II) to Cu(I)), *i.e.* sodium L-ascorbate. Furthermore, the ligand TBTA is added to form a complex with the produced Cu(I) to protect against fast oxidation and to prevent possible denaturation of Cu(I) sensitive proteins [20]. The reason why the copper catalyst and the reducing agent are present in the solution are pretty clear. However, the additional value of TBTA is still open for debate, especially since TBTA is one of the components which makes it rather difficult to lower the amount of DMSO even more. Therefore, the necessity of each component (Cu(I), sodium L-ascorbate and TBTA), was verified by preparing seven different mixtures of which three spots per mixture were applied on an azidified amino silanised substrate. As can be seen in **Figure 3.16**, the first three spots (column 1) originate from the mixture containing copper(II), sodium L-ascorbate and TBTA (the exact composition of the mixtures can be found in **Table 3.2**). This mixture produced the brightest fluorescence spots on the substrate. Due to the fact that all necessary components are present in the mixture it demonstrates that the immobilisation of alkynated Alexa Fluor® ^{488} occurred and the presence of all components is needed to obtain optimal immobilisation. In the

next series, column 2, no TBTA was present. This is confirmed by the less bright fluorescent spots in column 2 of **Figure 3.16**.

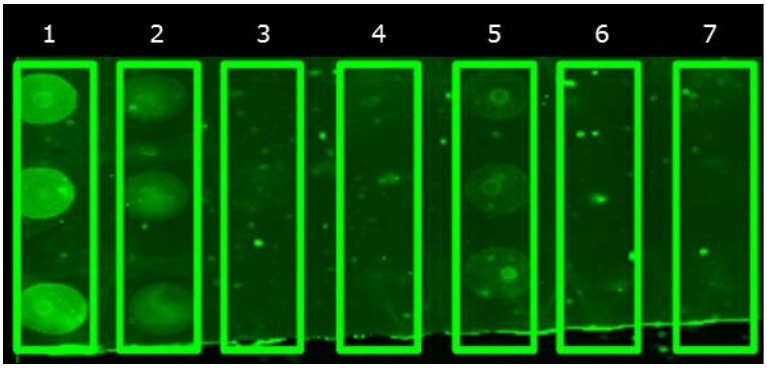

Figure 3.16: Fluorescence signal, recorded by DIGE, of seven different CuAAC mixtures as presented in **Table 3.4**. The three spots present in column 1 all contain tetrakis copper (I), NaAsc and TBTA together with alkynated Alexa Fluor ^{488} dye. Column 2-7 are control mixtures, which all lack at least one of the crucial CuAAC reagents (Cu(I), NaAsc and/or TBTA).

In the third series (**Figure 3.16**; column nr. 3), no signal could be measured due to the absence of a reducing agent or a ligand, which produces/ maintains Cu(I) levels and protects it again from further oxidation to Cu(II). Apparently, oxidation of the Cu(I) to Cu(II) occurs instantly after adding the copper to the aqueous buffer solution. In the fourth series (**Figure 3.16**, column nr. 4) copper was not present and no fluorescent spots were observed. In the fifth series (**Figure 3.16**, column nr. 5) a small fluorescent signal was detected although no reducing agent was present. This can be explained by the fact that the added copper originally is Cu(I), which can already form a complex with TBTA. Notwithstanding the amount is limited, some immobilisation occurred very fast. Once the amount of Cu(I) was consumed, no new Cu(I) could be produced, and no further immobilisation of

alkynated Alexa Fluor® ^{488} present in the reaction mixture could occur. The sixth solution (**Figure 3.16**, column nr. 6) without Cu(I) and sodium L-ascorbate, is not able to covalently immobilise alkynated Alexa Fluor® ^{488} to the azidified surface. And as shown before (**Figure 3.14** and **Figure 3.15**), there is no measurable signal for the physically adsorbed alkynated Alexa Fluor® ^{488} molecules in 95:5 sodium acetate buffer/DMSO ratio in the seventh series (**Figure 3.16**, column nr. 7). All these results prove that all three components have their value and removing one of them would have an enormous influence on the immobilised amounts.

Sodium L-ascorbate versus TCEP as a reducing agent

Several researchers who have investigated the CuAAC coupling mention that both sodium L-ascorbate and tris(2-carboxyethyl) phosphine (TCEP) can be used as reducing agents [21, 22]. In literature, a thorough comparison between both reagents has not been fully described yet. In this experiment, a comparison was made between both reducing agents. From **Figure 3.17** it can be seen that both reducing agents can be used for the immobilisation of alkynated Alexa Fluor® ^{488}. However, a distinct difference in fluorescence between both reducing agents can already be seen at the original catalyst concentration of 0.5 mM (column C_1). In addition, the original catalyst concentration was diluted two, four and ten times. When diluting down ten times the original concentration to 0.05 mM, an improved fluorescence signal can be detected for the TCEP containing solution. This indicates that TCEP performs better than sodium L-ascorbate at lower concentrations and in combination with a mixture of 0.05 mM tetrakis acetonitrile copper(I) hexafluorophosphate and 0.05 mM TBTA in order to immobilise alkynated Alexa Fluor® ^{488} in a 95:5 sodium acetate buffer/DMSO.

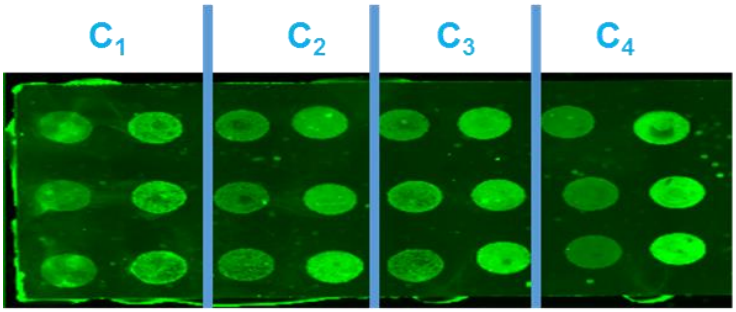

Figure 3.17: Fluorescence image recorded by DIGE of immobilised alkynated Alexa Fluor® ^{488} using CuAAC mixtures containing sodium L-ascorbate (left column of three spots) or TCEP (right column) as a reducing agent. For each reducing agent, four different mixtures (C_1: 0.5 mM tetrakis acetonitrile copper(I) hexafluorophosphate, 0.5 mM TBTA, 0.65 mM TCEP /sodium) and C_2, C_3, C_4 respectively 2, 4 and 10 times dilutions of the original CuAAC components concentrations) were prepared and spotted in triplo on the azidified surface.

3.3.4 CuAAC coupling of alkynated Alexa Fluor® ^{488} to N_3-functionalised TMS-EDTA silanised surfaces

In the previous experiments glass substrates were silanised with (3-aminopropyl) triethoxysilane (APTES). This resulted in substrates with increased contact angles of 49° ±0.5° compared to <4° for non-silanised substrates. Afterwards azide functionalities were added to these substrates, increasing their contact angles even more to values over 60°. During immobilisation reactions with biomolecules these relatively high contact angles could result in increased amounts of physisorbed molecules. Especially when working with proteins, which are more complex molecules than the smaller fluorescent dyes, the chance of aspecific immobilisation has to be reduced in order to obtain reproducible and reusable biolayers. By increasing the polarity of the substrate, hydrophobic physisorption

of proteins can be decreased. Further by using non-destructive washing solutions, like PBS, washing buffer (containing Na_2HPO_4, NaCl, EDTA and ethanolamine) and the 5 % SDS solution the larger amount of non-covalently bound molecules can be removed from the surface. The increase in polarity can be achieved by using TMS-EDTA in H_2O, a very hydrophilic, carboxyl terminated silane. After functionalising the glass surface with this silane, no contact angle could be measured (<4°). After modifying the substrate with azide functionalities this contact angle increases up to 37° ±7° (**Table 3.5**). This is only half of the angle obtained after azide functionalisation of the APTES silanised glass substrate. This can be explained by the fact that a non-azidified APTES silane layer already has a contact angle of 49° as demonstrated in **Table 3.5**. Since this environment is already more hydrophobic than the TMS-EDTA, after functionalising the carboxyl functionalities of the TMS-EDTA with azide groups, it is not surprising that this surface is still more hydrophilic than the azidified APTES surface.

To this azide functionalised carboxylated substrate four alkynated Alexa Fluor® ^{488} containing spots, with or without copper(I) catalyst, were applied. As can be seen in **Figure 3.18** (left) only the two spots, which contained CuAAC components, are lightening up while fluorescence of the control spots (**Figure 3.18**; right) are totally removed after washing with DMSO.

These results point out that both azide functionalised, APTES and TMS-EDTA silanised surfaces, respectively shown in **Figure 3.17** and **Figure 3.18**, can serve as carriers to which alkyne functionalised fluorescent molecules can be stably coupled. Keeping in mind that the objective is to functionalise surfaces with more complex biomolecules *via* CuAAC, carboxylated TMS-EDTA surfaces may well be better suited as a result of their more hydrophilic characteristics. In the upcoming

protein immobilisation experiments, the azide modified TMS-EDTA functionalised samples will be used as the base to which alkynated proteins will be applied.

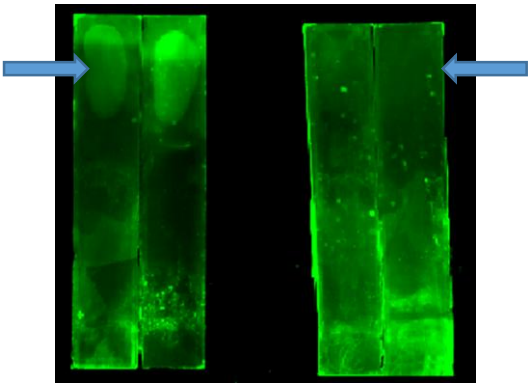

Figure 3.18: Fluorescence image of immobilised alkynated Alexa Fluor® ^{488} on azide functionalised carboxylated glass substrate recorded by DIGE (left) and the negative control without CuAAC reagents (right).

3.3.5 Coupling of fluorescent labelled proteins to N_3-functionalised glass substrates

As has been described in the previous sections, the CuAAC reaction can be used to immobilise small molecules covalently onto surfaces. Although several CuAAC reaction components, *i.e.* alkynated Alexa Fluor® ^{488}, TBTA and tetrakis acetonitrile copper(I) hexafluorophosphate have to be dissolved in rather apolar solvents (DMSO), it was possible to perform the coupling in a 95:5 sodium acetate buffer/DMSO ratio. The successful coupling was confirmed with fluorescence measurements.

Immobilisation of GFP *via* CuAAC

A molecule combining the properties of a fluorescent dye and a protein is Green Fluorescent Protein (GFP). The immobilisation of this protein to a solid carrier

would offer the opportunity to use fluorescence as an indicator whether or not GFP was present at the substrate and to confirm if the CuAAC immobilisation was successful. An advantage is that no additional labelling steps are required prior to immobilisation. However, after coupling of alkynated GFP to the azidified glass substrate, following the procedure described earlier, no fluorescent spots of the covalently immobilised GFP could be detected (**Figure 3.19**).

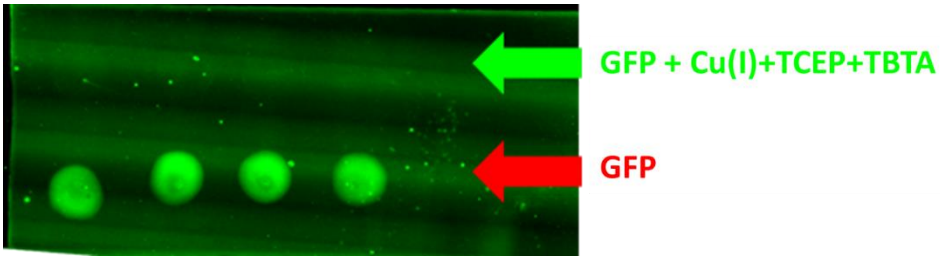

Figure 3.19: Fluorescence image, recorded by DIGE in H_2O of the coupling of alkynated GFP with (top) and without CuAAC reagents to an azidified amino silanised glass substrate (bottom).

On the contrary, the negative control spots emitted a bright fluorescence signal coming from the p-hydroxybenzylidene-imidazolidone, present in GFP. These recordings show that the amount of aspecific bound GFP is high enough to result in a very significant signal. A possible explanation may be that the presence of copper(I), TCEP and TBTA influences the fluorescence spectrum of GFP thereby disturbing the fluorescent signal. A second possibility could be that the proteins are so closely packed, they are auto-quenching themselves.

Since the negative control experiments, which lacked the presence of Cu(I), TCEP and TBTA, were still fluorescent, fluorescence spectra were recorded using a SPEX fluorescence spectrometer for the different solutions containing the CuAAC

reagents. **Figure 3.20** represents the recorded fluorescence spectra of GFP under different conditions.

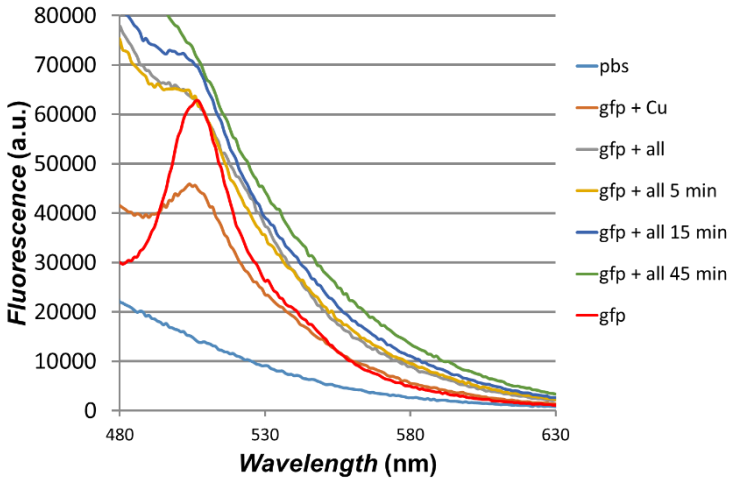

Figure 3.20: Fluorescence spectra recorded by a Spex fluorescence spectrometer for: alkynated GFP, alkynated GFP and tetrakis acetonitrile copper(I)hexafluorophosphate, GFP + all CuAAC reagents at t 0, 5, 15 and 45 min.

After excitation of GFP at 395 nm (λ_{ex}), an emission peak was recorded at 506 nm (λ_{em}). When just adding tetrakis acetonitrile copper(I) hexafluorophosphate (0.5 mM) to the solution, the fluorescence intensity decreased to almost half of the original intensity. In this mixture, the Cu(I) (coming from tetrakis acetonitrile copper(I) hexafluorophosphate) is instantly being oxidised by the presence of H_2O and forms $[Cu(H_2O)_6]^{2+}$. Literature reports describe this quenching effect of Cu(II) on GFP. However, when adding TCEP and TBTA the intensity restored itself again to the original values. This can be explained by the fact that oxidized Cu(II) ions are reduced again by TCEP to colourless Cu(I) ions, and kept in this state by the excess of TCEP and by TBTA. Both components inhibit this quenching effect by Cu(II) ions [23]. Taking these facts into account, the covalent coupling of

alkynated GFP by CuAAC accompanied by the formation of Cu(II) ions, which occurs when over time TCEP is consumed, will most likely influence the fluorescence capacity of the GFP molecules. These changes do not occur when the GFP proteins are physically adsorbed on the azide functionalised glass and no copper is present in the reaction mixtures, as can be seen in **Figure 3.19**. To rule out conformational changes and confirm that proteins indeed successfully can be coupled using the selected conditions, a second series of experiments was performed.

Immobilisation of fluorescent bovine IgG *via* CuAAC

A second option to demonstrate protein immobilisation *via* fluorescence is to artificially label an alkynated protein, in this case bIgG. The labelling was performed using a commercial labelling kit containing an ATTO^{488}-NHS ester resulting in labelled alkynated IgG molecules. It can be anticipated that most of the proteins will be labelled with a single dye, due to the fact that the fluorescent NHS-labels were added in a 1:1 molar ratio to the amount of proteins in the solution. In contrast to the coupling of GFP which occurred at pH 4, this coupling was performed in PBS at pH 7.4. It has been previously demonstrated that protein adsorption is improved when performed in a solution with a pH near the isoelectric point of the protein [24]. In **Figure 3.21** the results of the coupling of ATTO^{488} labelled alkynated bIgG to an azidified surface are shown.

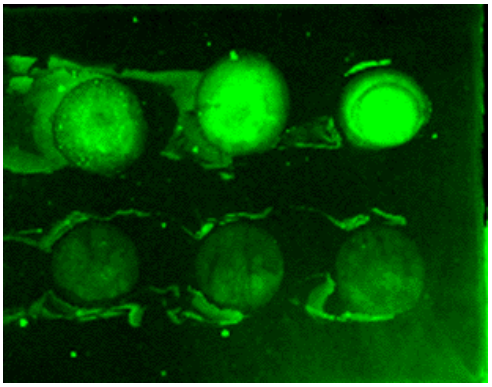

Figure 3.21: Fluorescence image recorded by DIGE of covalent immobilised (top) and physically adsorbed (bottom) ATTO^{488} labelled alkynated bIgG on an azidified glass surface.

The three spots on top of the slide represent the mixture containing Cu(II)SO_4, TCEP, TBTA and fluorescent labelled alkynated bIgG in PBS; the bottom three spots represent the ATTO^{488} labelled alkynated bIgG solution in PBS. The clear difference between both series is a strong indication for the presence of a higher amount of labelled IgG at the surface. Apparently, the presence of Cu(I) in the reaction mixture indeed allows for the covalent coupling of the labelled alkynated bIgG to the azidified surface. Notwithstanding, it is evident that fluorescence has limitations that complicate an accurate quantification. As a result, in the remainder of this thesis an alternative method, *i.e.* ellipsometry, will be utilised to validate the covalent coupling *via* CuAAC. It will be demonstrated that this technique successfully can be employed to monitor and quantify alkynated protein immobilisation at azidified surfaces.

3.4 Conclusion

The different experiments performed with the alkynated dye, alkyne Alexa Fluor® ^{488}, the alkynated fluorescent protein GFP and the alkyne functionalised and fluorescent labelled and alkynated bIgG resulted in several fundamental insights concerning the opportunities of CuAAC-mediated functionalisation of solid carriers. First two different approaches were addressed to functionalise these carriers with azide functionalities. The azidified amine silanised surface showed to have a more hydrophobic character, whereas the azide functionalised carboxylic surface resulted in a hydrophilic character of the surface. The latter will most likely be the most suited surface to use for bio-immobilisation reactions due to its hydrophilic characteristics.

The experiments performed with alkynated Alexa Fluor® ^{488} resulted in the insight that the use of a concentration of 0.5 µM of this modified dye led to a significant fluorescent signal with a very low amount of non-covalently bound dye. Furthermore, it was shown that the reaction readily can proceed with only limited amounts of DMSO present. It was found that a 95:5 ratio of sodium acetate buffer and DMSO was a good solvent ratio to perform the coupling reaction. In addition, it was found that TCEP was the most suited reducing agent in combination with a mixture of 0.5 mM tetrakis acetonitrile copper(I) hexafluorophosphate and 0.5 mM TBTA. Performing the same protocol with GFP did not result in a fluorescent spot. Likely, CuAAC-mediated immobilisation occurred but a non-fluorescent surface was obtained due to quenching. A second scenario could be that no immobilisation of alkynated GFP took place or the protein conformation changed due to the presence of TCEP. To verify that proteins indeed can be immobilised with the optimised reaction conditions, another alkynated protein, bIgG, labelled

with ATTO^{488}-NHS, was successfully immobilised on the azidified functionalised surface. These first experiments, in which a small alkynated molecule, alkyne Alexa Fluor® ^{488}, as well as a more complex molecule, bIgG, are immobilised, are very promising and provide fundamental insight in the creation of covalently biofunctionalised surface using CuAAC procedures.

3.5 References

1. Michael A. Ueber die Einwirkung von Diazobenzolimid auf Acetylendicarbonsauremethylester. J Prakt Chem 1893 (48):94–5.

2. Sustmann R. Dedicated to Professor Rolf Huisgen on the occasion of his 80th birthday-Preface. Tetrahedron. 2000;56(25):vii-viii.

3. Huisgen R. 1,3-dipolar cycloadditions past and future. Angewante Chem, International Edition English. 1963 (2):565–632.

4. Kolb HC, Finn MG, Sharpless KB. Click Chemistry: Diverse chemical function from a few good reactions. Angew Chem Int Ed Engl. 2001;40(11):2004-21.

5. Hein JE, Fokin VV. Copper-catalyzed azide-alkyne cycloaddition (CuAAC) and beyond: New reactivity of copper(I) acetylides. Chemical Society Reviews. 2010;39(4):1302-15.

6. Pakhomov AA, Martynov VI. GFP family: Structural insights into spectral tuning. Chemistry & Biology. 2008;15(8):755-64.

7. Bettati S, Pasqualetto E, Lolli G, Campanini B, Battistutta R. Structure and single crystal spectroscopy of Green Fluorescent Proteins. Biochimica et Biophysica Acta (BBA) - Proteins and Proteomics. 2011;1814(6):824-33.

8. Tan YH, Liu M, Nolting B, Go JG, Gervay-Hague J, Liu G-y. A nanoengineering approach for investigation and regulation of protein immobilization. ACS Nano. 2008;2(11):2374-84.

9. Price D. Rituximab and ME/CFS: A new trial begins. 2015, from https://emerge.org.au/rituximab-mecfs-new-trial-begins/#.WUoi4GjyjIU

10. von Maltzahn G, Ren Y, Park JH, Min DH, Kotamraju VR, Jayakumar J, *et al.* *In vivo* tumor cell targeting with "Click" nanoparticles. Bioconjugate Chemistry. 2008;19(8):1570-8.

11. Hatzakis NS, Engelkamp H, Velonia K, Hofkens J, Christianen PCM, Svendsen A, *et al.* Synthesis and single enzyme activity of a clicked lipase-BSA hetero-dimer. Chemical Communications. 2006 (19):2012-4.

12. Smith PAS, Smith PA. The chemistry of open-chain organic nitrogen compounds: WA Benjamin New York; 1966.

13. Sokalingam S, Raghunathan G, Soundrarajan N, Lee S-G. A Study on the effect of surface lysine to arginine mutagenesis on protein stability and structure using Green Fluorescent Protein. PLoS ONE. 2012;7(7) from https://doi.org/10.1371/journal.pone.0040410.

14. Hermanson GT. Chapter 13 - Silane coupling agents. In: Hermanson GT, editor. Bioconjugate Techniques (Third edition). Boston: Academic Press; 2013. p. 535-48.

15. Gunda NSK, Singh M, Norman L, Kaur K, Mitra SK. Optimization and characterization of biomolecule immobilization on silicon substrates using (3-aminopropyl)triethoxysilane (APTES) and glutaraldehyde linker. Applied Surface Science. 2014;305(0):522-30.

16. Zhang F, Sautter K, Larsen AM, Findley DA, Davis RC, Samha H, *et al.* Chemical vapor deposition of three aminosilanes on silicon dioxide: Surface characterization, stability, effects of silane concentration, and cyanine dye adsorption. Langmuir. 2010;26(18):14648-54.

17. Carvalho I, Andrade P, Campo VL, Guedes PMM, Sesti-Costa R, Silva JS, *et al.* 'Click chemistry' synthesis of a library of 1,2,3-triazole-substituted galactose derivatives and their evaluation against *Trypanosoma cruzi* and its cell surface trans-sialidase. Bioorganic & Medicinal Chemistry. 2010;18(7):2412-27.

18. Aragão-Leoneti V, Campo VL, Gomes AS, Field RA, Carvalho I. Application of copper(I)-catalysed azide/alkyne cycloaddition (CuAAC) 'click chemistry' in

carbohydrate drug and neoglycopolymer synthesis. Tetrahedron. 2010;66(49):9475-92.

19. Meldal M, Tornøe CW. Cu-catalyzed azide−alkyne cycloaddition. Chemical Reviews. 2008;108(8):2952-3015.

20. Wang Q, Chan TR, Hilgraf R, Fokin VV, Sharpless KB, Finn MG. Bioconjugation by copper(I)-catalyzed azide-alkyne [3 + 2] cycloaddition. Journal of the American Chemical Society. 2003; 125(11):3192-3.

21. Vila A, Tallman KA, Jacobs AT, Liebler DC, Porter NA, Marnett LJ. Identification of protein targets of 4-Hydroxynonenal using click chemistry for *ex vivo* biotinylation of azido and alkynyl derivatives. Chemical Research in Toxicology. 2008;21(2):432-44.

22. Wang Q, Chan TR, Hilgraf R, Fokin VV, Sharpless KB, Finn MG. Bioconjugation by copper(I)-catalyzed azide-alkyne [3+2] cycloaddition. Journal of the American Chemical Society. 2003;125(11):3192-3.

23. Hötzer B, Ivanov R, Altmeier S, Kappl R, Jung G. Determination of copper(II) ion concentration by lifetime measurements of Green Fluorescent Protein. Journal of Fluorescence. 2011;21(6):2143-53.

24. Rabe M, Verdes D, Seeger S. Understanding protein adsorption phenomena at solid surfaces. Advances in Colloid and Interface Science. 2011;162(1–2):87-106.

Chapter 4. Quantification of non-oriented protein layers by *in situ* ellipsometry

Part of this chapter is published in *'Vranken, Tom; Miszta, Adam; de Laat, Bas; Hermens, Wim; Steen Redeker, Erik; Adriaensens, Peter; Guedens, Wanda & Cleij, Thomas. In situ monitoring and optimisation of CuAAC-mediated protein functionalisation of biosurfaces In: Sensors & Actuators: B. Chemical 2017: p 992-1000. [Article - cat: A1]'*

4.1 Introduction

During the last decade several exciting examples of innovative microarrays and biosensing applications have been developed [1-4]. Typical sensing devices consist of three main parts, *i.e.* the sensing target receptor, the transducer surface and the readout system. Miniaturisation is one of the key challenges in the field of advanced biosensing devices since downscaled biosensors will facilitate multiple parallel measurements, even with smaller amounts of expensive biological receptor material [5]. Nowadays, a wide variety of target receptors is described in literature, *e.g.* DNA, phospholipids, glycosaminoglycans, enzymes, antibodies, cells and molecularly imprinted polymers (MIPs) [6-11]. Especially, the quest for sustainable coupling methods to attach proteins to functionalised surfaces is of considerable interest in biomedical, biochemical and immunological research [12-16]. For miniaturised protein-based devices, an optimal and uniform coverage of the transducer surface with proteins becomes even more crucial. The coupling reaction must be highly efficient, selective, reproducible, non-destructive and without side reactions.

Many different strategies, such as physical adsorption, affinity-based interactions and covalent couplings, have been reported to immobilise proteins to transducer surfaces [17-19]. Coupling methods based on weak interactions, *e.g.* hydrogen bonds, electrostatic, hydrophobic and van der Waals interactions, can result in oriented immobilisation but are reversible in nature, possibly leading to stability and reproducibility problems. On the other hand, covalent coupling methods based on the naturally present amino acid chemistry, although leading to stable coverage, exhibits limitations to the orientation of the protein on the surface. In either case, these methods often lead to sub-optimal sensitivity of the biosensing

devices, due to lack of uniform biomolecule orientation, reproducibility and/or stability. It is therefore important to develop methods that direct both orientation *and* stability [20-23].

In order to fulfil all requirements for miniaturisation, the proteins not only have to be coupled covalently to the transducer surface but also in a highly oriented way, *i.e.* all in the same way and having their active region accessible for the target. This demands for the introduction of a (bio) orthogonal, if possible site-specifically introduced functional group in the protein's structure. One of the most promising methods for covalent protein immobilisation is based on 'click' chemistry, *e.g.* the copper(I) catalysed 1,3-dipolar cycloaddition of azides and alkynes (CuAAC) [19, 24]. The CuAAC reaction is well known for its high specificity and efficiency, bio-orthogonal properties and lack of side reactions [25, 26]. Furthermore, the coupling reaction can be accomplished in aqueous solution under mild physiological conditions and on a variety of biomolecules and transducer supports [27-31]. However, protein functionalised surfaces created with 'click' chemistry often still suffer from reproducibility issues and insufficient and/or non-homogeneous protein coverage. This work therefore presents a full optimisation of all aspects of the 'click' chemistry reaction between proteins and surfaces. This is exemplified by the coupling of two model proteins, Protein A (SpA, a 42 kDa immunoglobulin binding surface protein of *Staphylococcus aureus*) and bovine IgG (a 150 kDa immunoglobulin; bIgG). Protein A (**Figure 4.1**), serves as model protein to optimise the reaction conditions of the CuAAC click reaction.

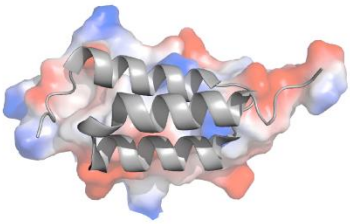

Figure 4.1: 3D-structure of Protein A with the charge distribution (red: negative; blue: positive).

SpA is non site-specifically alkynated *via* its endogenous surface lysines. The target binding efficiency is compared with well described immobilisation techniques, *i.e.* physical adsorption or EDC/NHS coupling. Next to SpA, also bIgG is alkynated *via* its endogenous lysines and later immobilised onto the azide functionalised substrates. For obvious reasons, it is important that the alkynation and immobilisation process does not induce conformational changes or influence or block the active site(s) of the protein. Therefore, the activity of SpA and bIgG after immobilisation has been assessed using binding studies with human IgG (binding the Fc domain; **Figure 4.2**) and anti-IgG (Fab domain), respectively, by ellipsometry [32].

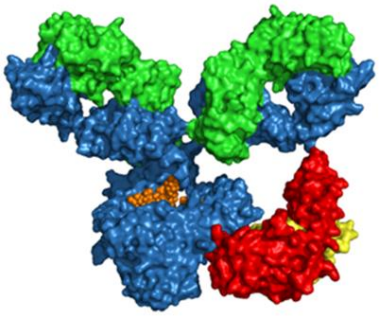

Figure 4.2: 3D-structure of the binding event of SpA (red) to human IgG at its Fc domain (blue, lower part).

4.2 Materials & Methods

4.2.1 Materials

Zeba micro spin desalting columns (7K MWCO, 0.5 mL), SpA (Cowan strain, recombinant, expressed in *E. coli*) and human IgG were obtained from Thermo Scientific. Carboxylated, hydrophilic silicon slides, PVC covered slides [33] and 'washing buffer' (WB) were obtained from Synapse B.V., Maastricht, The Netherlands. Copper(II) sulphate pentahydrate, 1-ethyl-3-(3-dimethylaminopropyl) carbodiimide (EDC), *N*-hydroxysuccinimide (NHS), bromopropylamine hydrobromide and sodium azide were purchased from Acros. Tris[(1-benzyl-1H-1,2,3-triazol-4-yl) methyl] amine (TBTA), tris(3-hydroxypropyltriazolylmethyl) amine (THPTA), diethylene glycolamine, sodium L-ascorbate (NaAsc), 4-(2-hydroxyethyl)-1-piperazineethanesulfonic acid (HEPES), sodium dodecyl sulphate (SDS),2-(*N*-morpholino) ethane sulfonic acid (MES), sodium acetate trihydrate and 5-hexynoic acid tris(2-carboxyethyl) phosphine (TCEP) were obtained from Sigma-Aldrich.

4.2.2 Solutions

Solutions were 0.27 M potassium dichromate in 25 % H_2SO_4 ;220 mM HEPES buffer pH 6.8; 10 mM alkyne NHS in acetonitrile; 1 M diethylene glycolamine pH 7.5; PBS buffer pH 7.4: 137 mM NaCl, 27 mM KCl, 10 mM Na_2HPO_4, 2 mM KH_2PO_4; 0.1 M glycine-0.2 M NaCl pH 2.5; 0.01 M sodium acetate buffer pH 4; 0.5 % SDS in H_2O; 0.01 M MES buffer pH 4; 0.05 M Tris-0.1 M NaCl buffer pH 7.5; washing buffer pH 7.5: 0.2 M Na_2HPO_4, 0.2M NaCl, 0.15 M EDTA, 0.05 M ethanolamine. Buffers were prepared with Milli-Q water.

4.2.3 Instruments

Contact angle measurements were performed with a dataphysics OCA 15+ goniometer (Filderstadt, Germany). Contour ellipse fitting of the water droplets was done by the SCA 1.0 software. The droplet size was 1 µL dispensed at 0.1 µL/s. Ellipsometry was performed on an ellipsometer having eight cuvettes (400 µL/cuvette) equipped with magnetic stirrers, monitoring time-dependent changes in polariser angle, analyser angle and reflected light intensity (see **Figure 2.3**) [32]. A reference for the surface mass was recorded for each slide before the start of the binding monitoring.

4.2.4 Functionalisation of silicon substrates

Cleaning of silicon substrates

First the samples were put in piranha for 5 minutes. Next they were flushed abundantly with H_2O and dipped in a 6 % HF in H_2O. After abundantly flushing again with H_2O, the samples were put in glass tubes containing 250 µL of potassium dichromate in 25 % H_2SO_4 at 70 °C for 30 minutes, covering a limited part of the silicon samples, which will later be measured by ellipsometry (±8 mm). After flushing the samples with H_2O and ethanol, and drying them with nitrogen, the samples were ready for silanisation.

Silanisation of silicon substrates

The clean samples were put on a Petri dish and 10 µL drops of a 6 v/v % TMS-EDTA solution in 0.2 M sodium acetate buffer pH 4 were applied to the samples. The samples were incubated for 1 hour in an oven at 110 °C. Afterwards the white layer, which appeared on the slide, was removed by washing with H_2O. The slides

were ready for further use, *i.e.* azidification, after being dried in a nitrogen atmosphere. Contact angles were measured.

Azidification of the carboxylated silicon slides

The linker, 3-azido-1-aminopropane (AAP), synthesised as described in the literature [34], was attached to the carboxylated silicon slides using EDC/NHS chemistry. The slides were immersed into a mixture of EDC (0.2 M), NHS (0.045 M) and AAP (0.23 M) in HEPES buffer for 3 hours. Remaining NHS esters on the surface of the slides were neutralised with diethylene glycolamine for 45 min, after which the slides were rinsed with Milli-Q water and dried in a nitrogen atmosphere. The presence of azides on the slides was demonstrated by measuring the contact angle.

Care should be taken when working with EDC. This rather unstable product should be stored in the freezer and after frequently being used, it has to be replaced by fresh product. The 3-azido-1-aminopropane linker should also be stored after flushing the container with nitrogen and refreshed every month. Frequent contact with CO_2 influences the quality of the linker, resulting in a decreased quality of the biolayers obtained after CuAAC.

4.2.5 Random alkynation of SpA

SpA was alkynated by the reaction of an NHS linker with lysine [35-37]. The alkyne NHS ester, 2,5-dioxopyrrolidin-1-yl-hex-5-ynoate, was synthesised according to a literature procedure [38]. The proteins were alkynated by adding the alkyne-NHS ester to a SpA solution of 17.7 µM in PBS yielding alkyne-SpA (A-SpA). Appropriate NHS ester concentrations were added to both proteins leading to a theoretical functionalisation level of 16 % of the present lysines (63 for SpA

[35, 36]; 17.7 µM SpA solution equals a lysine concentration of 1.12 mM. To functionalise 16 % of present lysines the final concentration of added alkyne NHS has to be 178 µM.) In addition, a theoretically fully (100 %) alkynated SpA (fA-SpA) was obtained by adding a 1.5 molar excess (to the total number of lysines) of the alkyne NHS ester. An alkynated SpA batch with a single alkyne functionality was obtained by adding 1/63 molar ratio to the total number of lysines of alkyne NHS ester to a 17.7 µM SpA solution in PBS. After 3 hours the reaction mixtures were filtered using a Zeba micro spin desalting column. Chemical modification by alkynation was demonstrated by native PAGE, visualising the changes in electrophoretic mobility caused by the alterations in the overall charge of the proteins.

According to the previous described procedures, 16 % of the lysines present in the protein structure of bIgG were functionalised with alkyne functionalities. Since bIgG has a higher amount of endogenous lysines (±83) [39], the amount of added alkyne-NHS was increased in order to maintain equal ratio's as mentioned for SpA.

To ensure the quality of the alkyne functionalised proteins, A-SpA/A-bIgG batches were prepared a few hours before usage. Unused proteins were not stored in the freezer but kept at 4 °C since freezing and thawing seemed to influence the alkynated proteins and the reproducibility rates of the CuAAC immobilisation.

4.2.6 Optimisation of CuAAC coupling conditions using A-SpA

A screening of the 'click' reaction conditions was performed by using different combinations of: reducing agents (TCEP *versus* sodium L-ascorbate), ligands (water soluble THPTA versus the apolar TBTA) and buffers (PBS pH 7.4 versus

sodium acetate buffer pH 4) and measuring the amount of immobilised SpA as the average surface mass (ASM or Γ). The following mixtures were prepared: *Mixture 1*: 1 µM A-SpA, 0.5 mM $CuSO_4$, 2.5 mM sodium L-ascorbate and 1 mM THPTA in sodium acetate buffer or PBS; *Mixture 2*: 1 µM A-SpA, 0.5 mM $CuSO_4$, 0.85 mM TCEP and 1 mM TBTA in sodium acetate buffer or PBS containing 2.5 % DMSO; *Mixture 3*: 1 µM A-SpA, 0.5 mM $CuSO_4$, 0.85 mM TCEP and 1 mM THPTA in sodium acetate buffer or PBS; *Mixture 4*: 1 µM A-SpA, 0.5 mM $CuSO_4$, 2.5 mM sodium L-ascorbate and 1 mM TBTA in sodium acetate buffer or PBS containing 2.5 % DMSO. All mixtures contained 1 µM A-SpA and 0.5 mM $CuSO_4$. DMSO is added to the reaction mixtures containing TBTA, as this ligand is not soluble in water. 64 azidified slides were placed in the 8 different reaction mixtures for 18 hours at room temperature without stirring resulting in 8 samples for each immobilisation condition. After the reactions, the Γ was determined by ellipsometry analysis. The different reaction conditions are given in **Table 4.1**.

Table 4.1: Reaction mixtures used for the immobilisation of SpA in either sodium acetate buffer pH 4 or PBS pH 7.4. All mixtures contain 1µM of protein.

Mixture	Reducing agent (mM)		Ligand (mM)		Cu Catalyst (mM)	
1	NaAsc	2.50	THPTA	1.00	$CuSO_4$	0.50
2*	TCEP	0.85	TBTA	1.00	$CuSO_4$	0.50
3	TCEP	0.85	THPTA	1.00	$CuSO_4$	0.50
4*	NaAsc	2.50	TBTA	1.00	$CuSO_4$	0.50

*contains 2.5% DMSO.

In addition to the coupling reaction of A-SpA to the azidified slides, three control experiments were simultaneously performed: 1) reaction between azidified slides and wild-type SpA, 2) carboxylated slides and A-SpA 3) carboxylated slides and wild-type SpA. Reaction time and concentrations of the other reactants were left unchanged.

Washing of the samples after immobilisation was performed in three subsequent steps using different buffers. PBS was used to remove the protein solution containing the reagents and the excess of protein on the surface. In order to interrupt the electrostatic interactions, the Washing Buffer was used to rinse the samples. As a final step, a SDS solution was prepared and used in order to remove the hydrophobic interactions.

4.2.7 CuAAC protein immobilisation in different buffers, with varying protein concentrations or in a different reaction volume (drop method)

To follow the 'click' reaction in real-time and to determine the rate of immobilisation, in a first experiment the surface mass Γ of A-SpA using *Mixture 1* in acetate buffer and *Mixture 2* in PBS was monitored after 0 s, 1800 s (0.5 h) and 65000 s (18 h). This experiment could show whether there is a difference in immobilisation reaction time between performing the reaction in PBS or in acetate buffer.

In addition, to determine the influence of the protein concentration on the CuAAC coupling, in a second experiment five additional A-SpA solutions were tested, *i.e.* 0.034 µM, 0.068 µM, 0.102 µM, 0.136 µM and 0.500 µM. The immobilisation was performed in *Mixture 1* (*cf.* **Table 4.1**) in acetate buffer *in duplo* for every protein concentration for 30 minutes. The Γ after coupling as well as after the washing steps was determined by ellipsometry. Furthermore, the hIgG binding capacity of the obtained A-SpA layers was tested as described in 4.2.8.

To test the effect of the reaction volume on the immobilisation efficiency, in a fourth experiment immobilisation reaction was performed *via* a drop method. For this, eight azide functionalised slides were put horizontally in a water vapour saturated environment at room temperature. Subsequently one drop (30 µL), containing 1 µM A-SpA in *Mixture 1* in acetate buffer was applied on each slide. A reference was measured before applying the protein-containing droplet. After 30 minutes, the ASM Γ was measured during the different washings steps.

Additionally, the binding activity of the A-SpA functionalised slides to hIgG was measured as described in 4.2.8.

4.2.8 Comparison of CuAAC with physisorption and EDC/NHS coupling and their activity towards IgG

For physical adsorption, PVC slides were put into a 1 µM SpA solution in Tris-NaCl buffer for 1.5 hours. After immobilisation the ASM on the slides was measured while flushing with Tris buffer. This procedure was again performed in triplicates. For covalent surface coupling by EDC/NHS, carboxylated silicon slides were put into a solution of 0.2 M EDC and 0.071 M NHS in MES buffer for 1 h. Next, the slides were put into MES buffer containing 1 µM SpA for 1.5 h, followed by flushing with WB for several minutes and measuring the ASM in MES buffer. This procedure was performed in triplicate. The methods, as described here, were standard procedure, optimised by Delbia BV., for immobilising SpA to PVC functionalised silicon slides and to carboxylated silicon samples.

It has been shown that adsorption can affect protein activity and due to random orientation of the molecules on the surface, binding sites may not be reachable [40-44]. Therefore, the effect of the immobilisation methods on the activity, as measured by the interaction and binding to an antibody, was determined. The SpA covered slides, obtained *via* physical adsorption, EDC/NHS or CuAAC chemistry (*Mixture 1* in acetate buffer) were put into cuvettes containing PBS. For each SpA covered slide a reference surface mass was recorded and human IgG (hIgG) was added to a final concentration of 0.33 µM. The interaction between the immobilised SpA and adsorbed was monitored using real-time ellipsometry.

4.2.9 Influence of alkynation level on CuAAC-mediated immobilisation

Two different A-SpA protein solutions were prepared, all containing the optimised concentrations of $Cu(II)SO_4$, sodium ascorbic acid and THPTA. Each solution contained 1 µM of SpA molecules functionalised with only one or with the maximal amount of alkynes at its surface. Both protein batches were prepared as described in 4.2.5 and were immobilised for 30 minutes in acetate buffer pH 4 without stirring at RT. Ellipsometry was used to determine the mass increase and a comparison with the A-SpA (SpA containing 16 % lysines functionalised with alkynes) layers from previous experiments was made.

4.2.10 Immobilisation of IgG and antibody recognition

Mixture 1 with alkyne functionalised bovine IgG (A-bIgG; 1 µM) and *Mixture 1* with wild-type bIgG (1 µM), both dissolved in sodium acetate buffer pH 4, were prepared. Azide functionalised silicon slides were put into both solutions for 30 minutes after running a reference measurement in PBS for each sample. Subsequently, the samples were abundantly washed in washing buffer pH 7.5 and in SDS and put in PBS containing anti-bovine IgG (0.33 µM). During the experiment the surface mass was measured in real-time by ellipsometry.

4.3 Results and Discussion

4.3.1 Azidification of the substrate and alkynation of the protein

A covalent surface protein coupling *via* CuAAC 'click' chemistry demands for the introduction of two complementary functional groups, *i.e.* one on the silicon slide and the other in the protein. The azide functionalisation of the carboxylated silicon slides was demonstrated by an average contact angle of 32.4° ± 2.9° (more hydrophobic; **Figure 4.3** b) as compared to the highly hydrophilic carboxylated slides (**Figure 4.3** a) for which no contact angle could be measured. In section 3.3.1 of chapter 3, the measured contact angles of the azide functionalised carboxyl silanised glass were higher and less reproducible as can be seen in **Table 3.5**. By slightly altering the cleaning procedure, repeatedly using the silanisation procedure and frequently replacing the used silicon samples by new slides, the contact angle's standard deviation was reduced from 7° to 3°. Furthermore, the additional treatment with an excess of diethylene glycolamine ensured the total removal of NHS esters on the silicon surface. This excludes the unwanted covalent protein binding *via* the potentially remaining NHS-esters. In addition, it contributed to the lower and reproducible contact angle of the azide slides. This lower contact angle is preferable because it implies a higher hydrophilicity. If the surface would be hydrophobic, hydrophobic interactions between protein and surface could lead to structural changes and loss in activity/functioning due to the fact that the hydrophobic interactions are mainly responsible for protein folding. [45]. In the following step, the azidified substrates were functionalised with A-SpA *via Mixture 1* in acetate buffer pH 4 (**Figure 4.3** c). This led to an increase of the contact angle to 62.4° ± 2.6°.

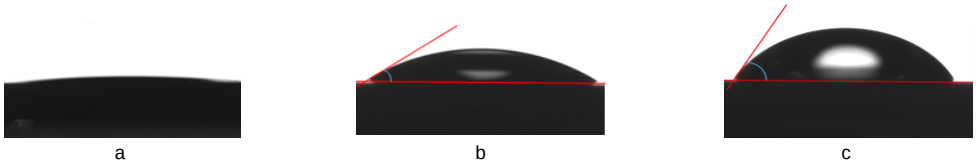

Figure 4.3: Contact angle measurements performed with H_2O on a) carboxylated, b) azide functionalised and c) A-SpA covered silicon samples.

In addition to the surface azidification, the protein SpA was complementary functionalised with alkynes *via* endogenous lysines. By alkynating the lysines, the pI of the global protein will decrease and this change can be visualised by native polyacrylamide gel electrophoresis (PAGE). **Figure 4.4** illustrates the difference between wild-type SpA (green; pI~5.4; theoretically calculated with Innovagen protein property calculator) and A-SpA (red; pI <5.4: depending on the amount of alkyne functionalities) after performing native PAGE. At pH 8.8, most of the lysines present in native SpA are still positively charged (pK_a = 10.67). When functionalising their side chain NH_3^+ groups with alkynes, the positive charges disappear by the formation of peptide bonds and the general charge of the A-SpA becomes more negative. At pH 8.8, the more negatively charged A-SpA migrates faster than SpA towards the positive pole, demonstrating a successful alkynation.

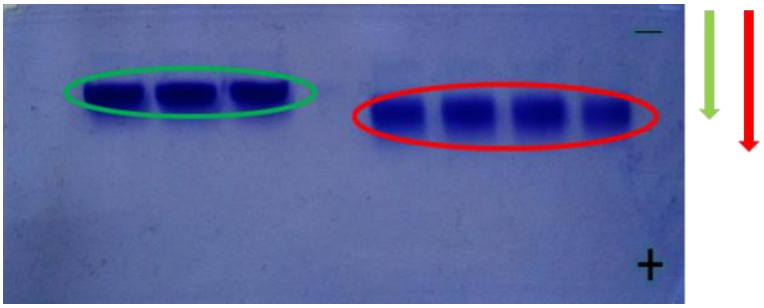

Figure 4.4: Native polyacrylamide gel electrophoresis of wild-type SpA (green; three replicate samples) and A-SpA (red; 4 replicate samples; theoretically 16 % alkynated lysines) at pH 8.8.

4.3.2 Optimisation of CuAAC conditions

The goal of this study is to couple SpA and bIgG covalently to the azidified silicon substrate *via* the CuAAC chemistry and to find the appropriate reaction conditions for this click reaction. To find the optimal conditions for protein immobilisation *via* CuAAC chemistry, SpA was used as a model protein. The reaction conditions were tested using different (combinations of) reducing agents (TCEP *versus* sodium L-ascorbate), ligands (water soluble THPTA *versus* the apolar TBTA) and buffers (PBS pH 7.4 versus sodium acetate buffer pH 4). **Figure 4.5** and **Figure 4.6** summarize the increase in surface mass as measured by ellipsometry for the different reaction mixtures in PBS pH 7.4 and acetate buffer pH 4, respectively, after 18h. Each condition was repeated on eight replicate slides.

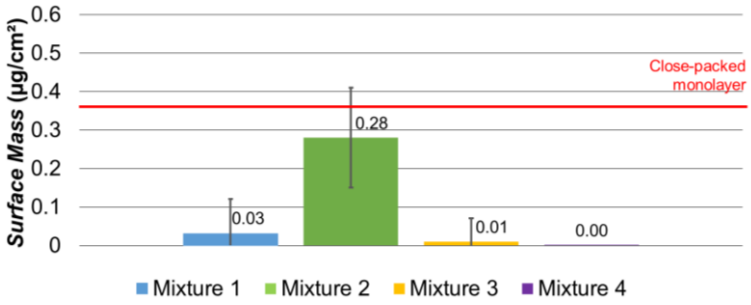

Figure 4.5: Surface mass of four different mixtures dissolved in PBS pH 7.4 as measured by ellipsometry. The red line marks the theoretical surface mass of a close-packed monolayer of SpA [46].

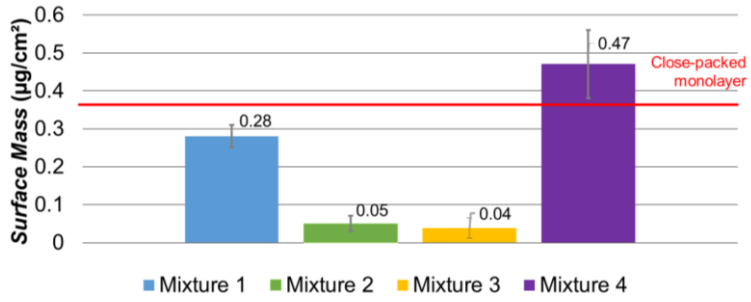

Figure 4.6: Surface mass of four different mixtures dissolved in sodium acetate buffer pH 4 as measured by ellipsometry. The red line marks the theoretical surface mass of a close-packed monolayer of SpA as stated in ref [46].

When the CuAAC reaction was performed in PBS (pH 7.4), only *Mixture 2* showed a significant binding of 0.28 µg/cm^2. However, the reproducibility was rather poor with a standard deviation of 46 %, possibly caused by the absence of electrostatic attraction (**Figure 4.5**, green). For the sodium acetate buffer pH 4 reactions in *Mixture 1* and *Mixture 4,* both yielded significant protein coverages of 0.28 µg/cm² and 0.47 µg/cm², with standard deviations of 11 % and 19 %, respectively. The better reproducibility of *Mixture 1* and *Mixture 4* can be explained by the attraction

forces between the positively charged proteins and the negative charges of the remaining, non-modified carboxylate groups at the substrate surface at pH 4 [44].

The maximal amount of protein that can be immobilised on a surface was estimated by a theoretical model [46]. This model estimates the theoretical maximal number of protein molecules per mm² in a close-packed hexagonal monolayer arrangement (CPM). With this model, the maximum surface coverage of SpA was estimated to be 0.36 µg/cm². Although this is just a model estimate assuming the proteins are hard spheres of uniform density, the three reaction conditions yielding the highest surface mass are close to this theoretical value: *Mixture 2* in PBS and *Mixture 1* and *Mixture 4* in acetate buffer. However, *Mixture 2* in PBS and *Mixture 4* in acetate buffer both contain DMSO, an organic solvent, which might result in (partial) denaturation of proteins [47, 48]. *Mixture 1* in acetate buffer is the DMSO-free alternative of *Mixture 4* in the acetate buffer and is therefore chosen as the optimal CuAAC reaction condition and is used for the subsequent reactions. It should be noted that for experiments in which the presence of DMSO is not an issue, also *Mixture 2* in PBS and *Mixture 4* in acetate buffer could be used.

To test the stability of the CuAAC covalent coupling of A-SpA to the azidified surface in *Mixture 1* in acetate buffer, four experiments were simultaneously performed in which (non-)alkynated SpA and/or non-azidified surfaces were used. Proteins were coupled to the surface for 18 hours after which the surfaces were washed with different washing solutions. During washing, the ASM was measured in real-time. **Figure 4.7** shows that only A-SpA coupled to the azidified silicon surface resisted the different washing steps. In the three control experiments, almost all protein is removed during washing. This suggests that the used CuAAC

coupling protocol of an alkynated protein to an azidified surface results in a stable and covalent bond.

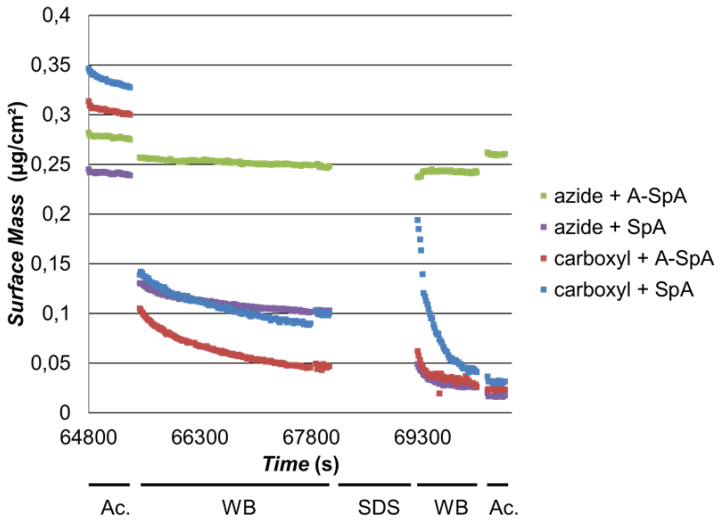

Figure 4.7: Surface mass evolution as measured by ellipsometry during consecutive washing steps with acetate buffer (Ac.); washing buffer (WB); sodium dodecyl sulphate solution (SDS); washing buffer and acetate buffer: for A-SpA which is covalently coupled to azidified silicon slides by CuAAC with *Mixture 1* in acetate buffer (green) and for control experiments accomplished under identical conditions but with carboxylated plates and/or non-alkynated SpA.

4.3.3 Protein immobilisation in different buffers, with varying protein concentrations, with varying alkynation or in a lowered reaction volume

The previous achieved SpA layers were obtained after an incubation time of 18 hours using the in the previous section selected *Mixture 1* in acetate buffer (Figure 4.6; blue) and *Mixture 2* in PBS as a comparison (Figure 4.5; green). Preliminary experiments already indicated that the immobilisation in PBS had to be performed

overnight (18 h). Due to the fact that electrostatic forces enhance the movement of (A-)SpA towards the surface, it was likely to expect that the formation of a (covalent bound) (A-)SpA layer could be enhanced as well.

To test whether the immobilisation reaction time could be shortened, surface mass measurements were also performed at 1800 seconds (30 minutes), since preliminary measurements of the immobilisation in acetate buffer showed a fast increase in surface mass during the first 30 minutes. These preliminary tests also showed that further lowering the reaction time resulted in adsorbed protein layers which were only partially covalently bond to the surface. When using *Mixture 1* in acetate buffer, it was found that the formation of the A-SpA layer was already complete after 30 minutes, which is only 2.5 % of the time that was presumed to be needed to obtain sufficient protein layers. On the other hand, when using *Mixture 2* in PBS no signs of a biolayer in development could be observed after 30 minutes and a reaction time of 18 hours was needed to obtain a biolayer of comparable mass. In addition, *Mixture 2* in PBS led to high standard deviations. This implies that *Mixture 1* in acetate buffer does not only enhances the rate of formation of the biolayer on the azide functionalised substrate [49-55] but also leads to highly reproducible layers (**Table 4.2**). The accumulation effect, initiated by the electrostatic attraction between protein and surface, has undoubtedly a boosting influence on the quality of the protein layer formed at the surface of the substrate. This electrostatic attraction will most likely influence the orientation of the individual proteins, present in the coupled biolayer.

In addition, the successful biofunctionalisation was corroborated by contact angle measurements as well. Whereas the azide functionalised slides exhibited an average contact angle of 32.4° (±2.9°) (**Figure 4.3** b), the angle increased to

62.4° (±2.6°) after treatment with A-SpA using *Mixture 1* in acetate buffer (**Figure 4.3** c). This is an indication of the chemical change caused by the formation of the A-SpA layer. Based on these experiments it can be concluded that *Mixture 1* in acetate buffer results in an optimal and reproducible coupling of A-SpA to the azidified substrate in a short reaction time of 30 min.

Table 4.2: Surface mass measurements and the corresponding standard deviations after 30 minutes and 18h of CuAAC reaction. At 30 min, a 5 min wash step with WB was performed to see the difference in surface mass.

Time	**Surface mass (µg/cm²)**			
	PBS	**S.D.[1]**	**Acetate**	**S.D.[2]**
0	0.00		0.00	
↓	**CuAAC coupling reaction**			
30 min	0.00	0.01	0.35	0.02
↓	**Wash step with WB**			
35 min	0.00	0.01	0.33	0.01
↓	**CuAAC coupling reaction**			
18h	0.38	0.18	0.37	0.03

[1]n=3, [2]n=4

Considering the future development of biofunctionalised surfaces based on antibodies, reducing the amount of protein/antibody consumption per sample is highly recommended. Therefore, five additional protein concentrations (0.034, 0.068, 0.102, 0.136 and 0.500 µM) were tested for immobilisation. After 30 minutes of immobilisation in *Mixture 1* in acetate buffer, a surface mass of 0.08 µg/cm² was achieved for the 0.034 µM solution. In case of the 0.068 µM A-SpA 0.15µg/cm² was achieved and 0.17 µg/cm² for the 0.102 µM A-SpA. The

0.136 µM A-SpA solution reached a maximum of 0.20 µg/cm² and 0.25 µg/cm² was obtained by using a 0.5 µM A-SpA solution (Figure 4.8, top left).

The measurements confirm the effect of the protein concentration on the final protein mass of the biolayers (Figure 4.8). Varying the protein concentrations from 0 to 0.102 µM results in a very steep increase in A-SpA surface mass. Further raising the A-SpA concentration results in a gradual increase in surface mass and apparent saturation around 0.30 µg/cm². This amount is in agreement with the theoretical maximum amount of SpA that can be immobilised on a surface, i.e. 0.36 µg/cm² as estimated by a theoretical model [46].

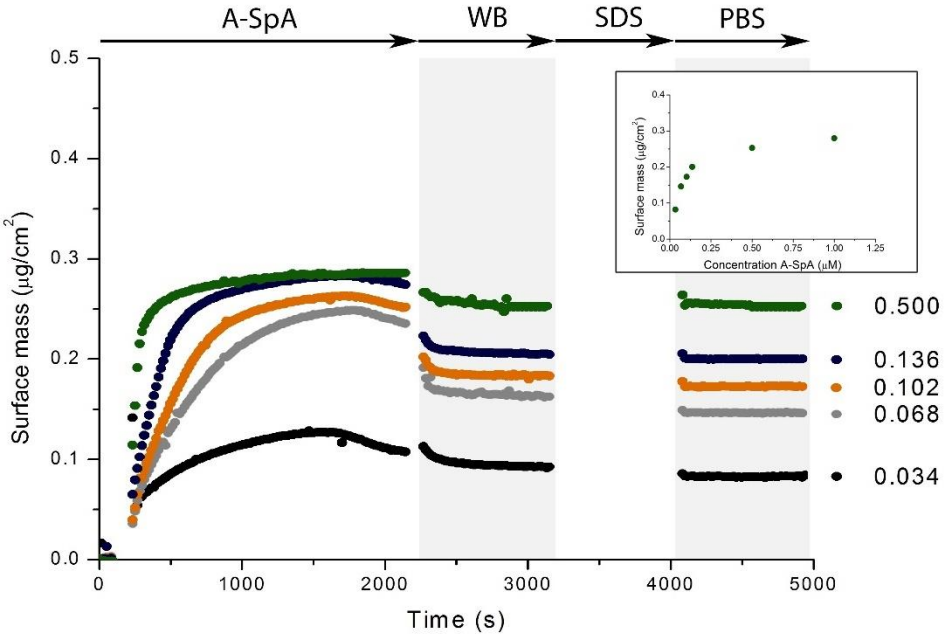

Figure 4.8: A-SpA Surface Mass evolution of CuAAC coupling using different protein concentrations, followed by subsequent washing steps with WB, SDS and PBS. The insert shows the concentration dependency of the final A-SpA surface mass.

Lowering the concentration of the reaction mixture therefore results in a lower amount of protein on the substrate. Higher protein concentrations are therefore preferred to create maximally covered surfaces.

The previous section showed that lowering the concentration of the reaction mixture influences the obtained protein layers (**Figure 4.8**). To reduce protein consumption, decreasing the reaction volume could be a second option. For the drop method experiment, a 1 µM A-SpA solution in *Mixture 1* in acetate buffer was used, but the reaction volume was reduced from 400 µl (maximum volume cuvettes) to 30 µl (**Figure 4.9**), the minimal volume to fully cover the same area of the azide functionalised silicon slides.

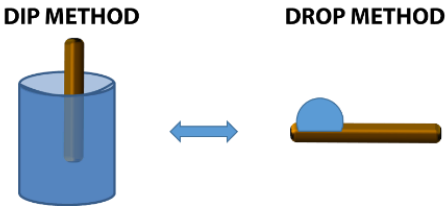

Figure 4.9: Illustrative representation of the originally used DIP method and alternative DROP method.

Interestingly, this 13-fold reduction in reaction volume still results in protein layers of 0.29 µg/cm² ± 0.03 µg/cm² A-SpA. This means a considerable reduction in protein usage to obtain dense A-SpA layers which gives the opportunity to efficiently use higher protein concentrations to get optimal surface coverage. As can be seen in **Figure 4.8**, a 0.075 µM A-SpA solution would lead to a layer between 0.15 µg/cm² and 0.17 µg/cm². However, using the same A-SpA amount dissolved in 30 µL reaction mixture, A-SpA layers of 0.29 µg/cm² ± 0.03 µg/cm²

are obtained as will be discussed in section 4.3.6. This is an improvement with respect to the method using 400 µL of 1 µM A-SpA resulting in 0.28 µg/cm² layers.

4.3.4 Comparison with other immobilising methods

The optimised surface CuAAC coupling of A-SpA was compared to other commonly used coupling procedures as shown in **Figure 4.10**. The ASM Γ of 0.28 µg/cm², resulting from the CuAAC reaction, matches a surface coverage of 78 % of a close packed monolayer, which is 0.36 µg/cm² [46]. For EDC/NHS coupling and physical adsorption, this is only 61 % and 53 %, respectively, which is significantly lower ($p=0.012 < \alpha=0.05$) than the CuAAC coupled SpA layer. The difference in ASM between the physical adsorption and EDC/NHS coupling was not significant ($p=0.310>\alpha=0.05$).

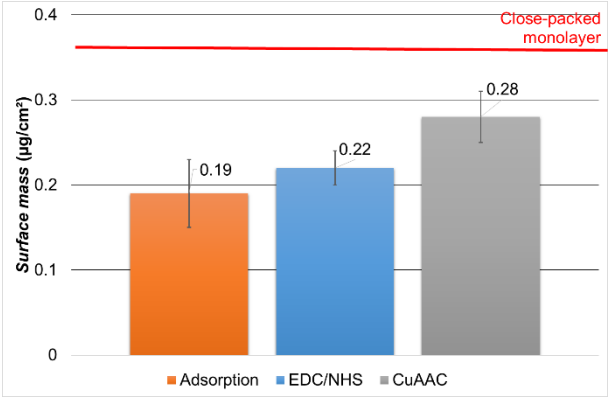

Figure 4.10: Average surface mass (ASM (Γ)) and standard deviation obtained from immobilisations of SpA to carboxylated silicon slides by physical adsorption or EDC/NHS coupling and A-SpA on azidified slides with CuAAC. The red line shows the theoretical close-packed monolayer [46].

Comparing the results of the EDC/NHS coupling of 1 µM SpA (0.22 µg/cm² ± 0.02 µg/cm²) with the results from **Figure 4.8**, it is remarkable that a 0.136 µM solution used in combination with the CuAAC coupling yields comparable surface

mass (0.20 µg/cm²), even though the reaction time is 5 times less and the protein concentration is 7 times less. One explanation for this immobilisation efficiency and higher surface mass afterclick reaction compared to EDC/NHS might be that when SpA is modified with an alkyne, a spacer was also introduced. This linker creates a suitable separation between the surface and the protein. This might reduce steric hindrance, leading to increased immobilisation mass. Hence, this indicates that CuAAC based immobilisation leads to a considerable improvement in reproducibility and surface mass.

4.3.5 Influence of alkynation level on CuAAC-mediated immobilisation

The previous reactions were all performed using A-SpA batches containing functionalised SpA with a theoretical maximum of 10 alkyne groups per SpA molecule. However, the amount of modifications will most likely affect the coupling rates. By adjusting the amount of alkyne-NHS ester, SpA species with different alkynation levels were obtained and an impression of the influence of the number of alkyne groups towards the immobilised mass was obtained by monitoring two different SpA batches during the CuAAC immobilisation and comparing them with the previous results. One batch contained SpA to which one equivalent of alkyne-NHS per SpA molecule was added, resulting in single alkynated SpA (sA-SpA). Considering future strategies involving site-directed coupling, which can only be acquired using site-specifically functionalised proteins, the sA-SpA would indicate whether proteins containing a unique alkyne functionality could be covalently coupled, within 30 minutes, to the azide functionalised solid carrier. A second protein solution contained SpA molecules functionalised with an equimolar ratio of alkyne-NHS towards the lysines present in the solution, resulting in fully

alkynated SpA (fA-SpA). The influence of the degree of alkynation towards the biolayer formation is presented in **Figure 4.11**.

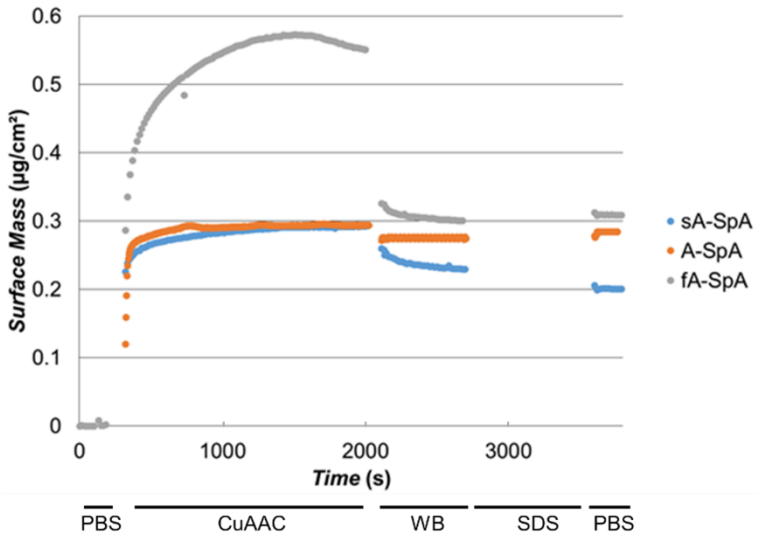

Figure 4.11: Real-time measurements of the covalently coupled, alkynated SpA using SpA species functionalised with varying ratios of alkyne-NHS (single alkynated SpA [sA-SpA], blue; random alkynated SpA [A-SpA], orange; fully alkynated SpA [fA-SpA], grey).

Figure 4.11 shows the increase in surface mass for all three different alkynated SpA batches. Initially the A-SpA (orange) and the sA-SpA (blue) curve do not differ from each other. Both resulted in layers of 0.30 µg/cm² after 2100 seconds of CuAAC. The curve of fA-SpA (grey), on the other hand, first increased rapidly towards a surface mass of 0.57 µg/cm³ before decreasing slightly towards 0.55 µg/cm² after 2100 seconds. When taking a closer look at the course of the grey curve (**Figure 4.11**) a slight bump can be seen. This might be caused by an overload of introduced alkyne groups, enhancing protein aggregation in the solution. Usually biomolecules fold in such a manner that they tend to shield their hydrophobic amino acids while exposing the polar residues towards the solvent

[56]. By overalkynation, some polar groups that form a shield to 'protect' the hydrophobic interior, were altered, leading to a reduced shielding. The spatial arrangement of amino acids, which would be expected to prevent protein aggregation, could be lost, leading to some degree of aggregation and cluster formation. During coupling, the cluster spreads and a decrease in surface mass was noticed [57]. Another explanation could be an overshoot effect by temporarily oversaturation of the surface with proteins. This effect has been explained by several researchers, having different explanations [58, 59].

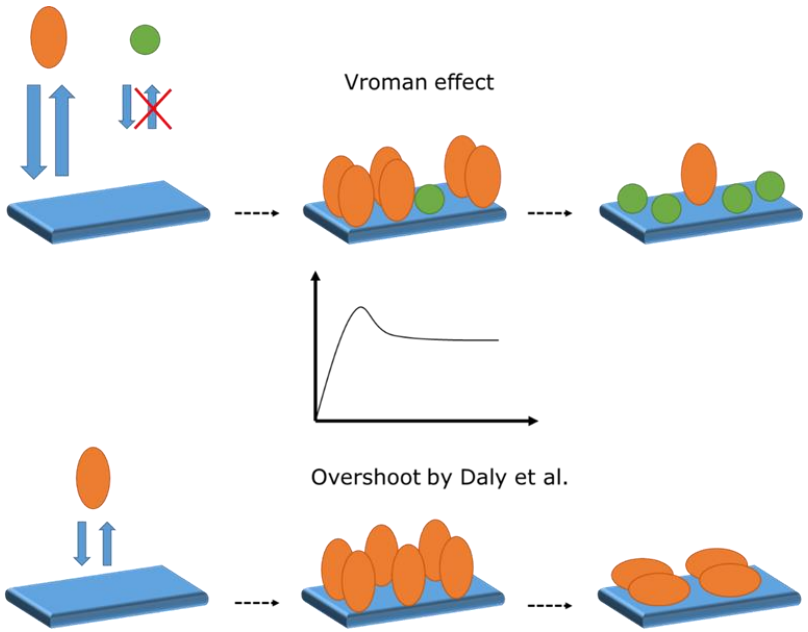

Figure 4.12: Overshoot effect which may occur during adsorption of a protein mixture containing two types of proteins marked as orange and green. (Top). The competitive adsorption of fast adsorbing proteins with low affinity and slower adsorbing proteins with a higher surface affinity causing an overshoot (Vroman effect) (Centre). Graphic representation of the overshoot during adsorption (Bottom). Reorientation effect which occurs during protein adsorption [58].

The first explanation is described by Vroman, and is called the 'Vroman effect' (**Figure 4.12**) [59]. This effect refers to the competition between rapid (orange) and slow (green) adsorbing proteins as the cause of the fast increase in surface mass. The accompanied overshoot and the stabilisation of the ASM Γ at a lower level is presented at the centre of **Figure 4.12**. After reaching a peak in surface mass, slower adsorbing proteins (with a higher affinity towards the surface) start displacing the fast adsorbing ones, resulting in a decrease in surface mass. These were findings of experiments performed with solutions containing different proteins [59]. However, it's not only the case for different proteins mixed in one solution. Experiments performed by Elofsson [60] resulted initially in a surface covered with octamers due to a fast adsorption. This caused an oversaturated surface. In time, these octamers were replaced by the slow adsorbing monomers and dimers, which had a much stronger affinity towards the surface, and the observed protein density restored to the expected value [60]. Transposing this knowledge to our results, possibly the presence of the high amounts of alkynes increases the formation of protein polymers, which are initially adsorbing to the surface. Later these polymers are being replaced by their monomers, which might result in a decrease in surface mass.

Another publication reported an identical observation but had an alternative explanation for the overshoot (**Figure 4.12**; Bottom) [58]. They performed adsorption experiments on hydrophilic surfaces using protein concentrations between 0.07 µM and 0.7 µM. The authors stated that after adsorption, reorientation from an end-on to a final side-on orientation of the proteins occurred. It is very likely that our observation can be declared by this reorientation phenomenon. When fA-SpA is adsorbing to the surface, the part which is attracted

towards the azide surface will form covalent bonds at first. Due to the flexibility of proteins in solution other alkyne functionalities present at the surface of fA-SpA are able to approach azide functionalities, resulting in covalent bonds. These additional linkages could be a credible cause of a reorientation over time.

A-SpA, containing 16 % functionalised lysines did not show such an overshoot, despite the multiple presence of alkyne functionalities. Possibly the number of alkynes has not reached the threshold leading to increased protein polymer formation or cluster formation, which could be the case for fA-SpA. A second explanation could be that the alkynation is not occurring as random as one might expect. The peptide formation between the alkyne NHS linker and the lysines could have preferential lysines, which are better reachable than others, leading to functionalised proteins of which the alkynes are located at a specific, preferred region as has been reported in the literature [44]. If this is the case, it explains that absence of the reorientation of the A-SpA.

A second way of reasoning might be the alkyne functionalisation itself *via* an alkyne-NHS ester, which lowers the isoelectric point of the SpA 5.4. Due to the different alkyne ratios, the pI of all three batches will slightly differ. The pI of sA-SpA will be the highest, followed by A-SpA and fA-SpA, respectively. At pH 4 sA-SpA will have a higher positive nett charge than A-SpA and fA-SpA. Possibly by intermolecular electrostatic (positive charged protein) repulsion the formation of a double layer is inhibited. When using a solution containing fA-SpA which has a pI lower than that of sA-SpA, the positive nett charge will be reduced, or the proteins might have no charge at all, which increases the chance of developing multiple layers as demonstrated in **Figure 4.11**.

In general, one may assume that surface masses of 0.5 µg/cm² and more, point into the direction of multilayer formation (**Figure 4.11**, grey curve). After flushing with the high ionic washing buffer and SDS, the surface mass of the fA-SpA falls back to 0.31 µg/cm² (**Figure 4.11**), demonstrating that the top layer is not covalently bound to the surface. The effect of these washing steps on the A-SpA layer is very low, demonstrating that only a very small part of the present proteins is non-covalently coupled. In case of the sA-SpA a slightly higher amount was removed pointing towards a lowered immobilisation yield. The final average surface masses of sA-SpA and fA-SpA are presented in **Figure 4.13** and amounted to 0.28 µg/cm² ± 0.03 µg/cm² (orange) for the A-SpA layer and 0.20 µg/cm² ± 0.02 µg/cm² (blue) for the s-Spa layer. Increasing the amount of alkyne groups, increased the amount of coupled proteins towards 0.31 µg/cm² ± 0.01 µg/cm² (grey).

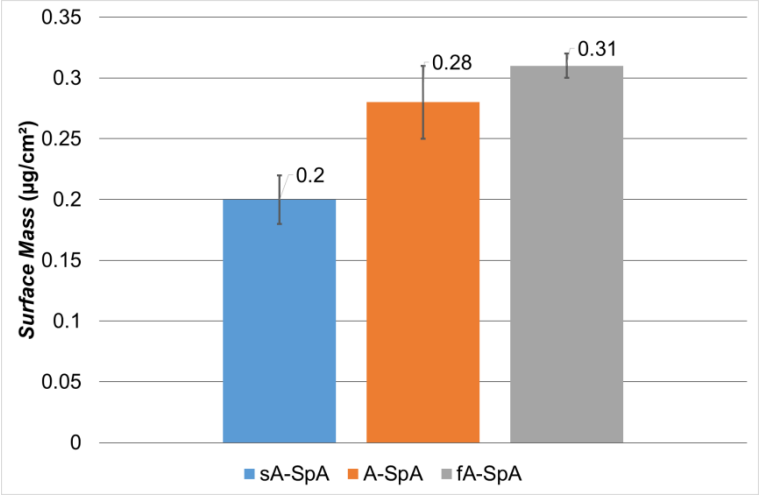

Figure 4.13: Covalently coupled alkynated SpA using SpA species functionalised with varying ratios of alkyne-NHS (sA-SpA, blue, n:3; A-SpA, orange, n:8; fA-SpA, grey, n:3).

As could be expected, reducing the amount of alkyne functionalities to a single functionality, decreased the efficiency of the immobilisation reaction. From the real-time measurements, it can be concluded that the lower amount of alkyne functionalities does not affect the adsorbed amount SpA. However, the amount of covalently immobilised SpA is reduced with 33 %. Still it is remarkable that, although the number of alkyne groups is reduced to 10 % compared to A-SpA, still 71 % of the surface mass obtained by A-SpA can be reached with sA-SpA. This corresponds to 55 % of a close packed SpA monolayer. Immobilisation of fA-SpA resulted in layers with an ASM Γ of 0.31 µg/cm².

4.3.6 Activity measurements of SpA after surface coupling

Activity of A-SpA layers obtained by CuAAC, EDC-NHS and adsorption

By measuring the binding of human IgG to the immobilised SpA, the activity of the protein after surface coupling *via* CuAAC, EDC/NHS or physical adsorption has been evaluated (**Figure 4.14**).

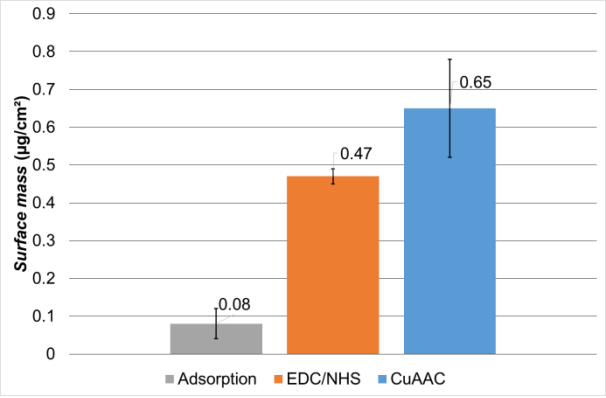

Figure 4.14: Average surface mass and standard deviation obtained after binding of human IgG to SpA functionalised slides: adsorption (grey), EDC/NHS (orange) and CuAAC (blue).

The physically adsorbed SpA is able to bind only minute amounts of hIgG, *i.e.* 0.08 µg/cm². The hIgG density of EDC/NHS coupled SpA is 0.47 µg/cm². The highest amount of hIgG binding, *i.e.* 0.65 µg/cm^2, can be observed for A-SpA layers immobilised by CuAAC. The difference between hIgG layers obtained after CuAAC immobilisation or by physical adsorption or EDC/NHS is ($p=0.034<\alpha=0.05$). This mass increase of hIgG after CuAAC is two times higher than a side-on close packed hIgG monolayer, *i.e.* 0.3 µg/cm², and is more than 40 % of fully end-on covered hIgG monolayer, *i.e.* 1.5 µg/cm². [61, 62] This indicates that the surface consists of a mixture of sideway oriented and end-on oriented hIgG molecules. After hIgG binding, the slides were flushed with an acidic glycine solution, a procedure often used to only break the specific antibody-antigen interactions in antibody purification columns. [63] After washing, the original layers of 0.28 µg/cm² were restored demonstrating the very specific binding between A-SpA and hIgG. The possibility of aspecific binding is reduced due to the obtained dense A-SpA layer (78 % of CPM), which does not allow for much 'protein-free' spaces in the biofilm. These gaps could be a possible cause for increased aspecific binding of the antibody.

Activity of SpA layers obtained from mixtures containing reduced SpA concentrations

To further study the impact of surface coverage on the hIgG binding capacity of the A-SpA, different slides with increasing A-SpA surface mass were tested. The slides initially incubated with different A-SpA concentrations (**Figure 4.8**) were incubated with hIgG and the antibody binding was followed (**Figure 4.15**).

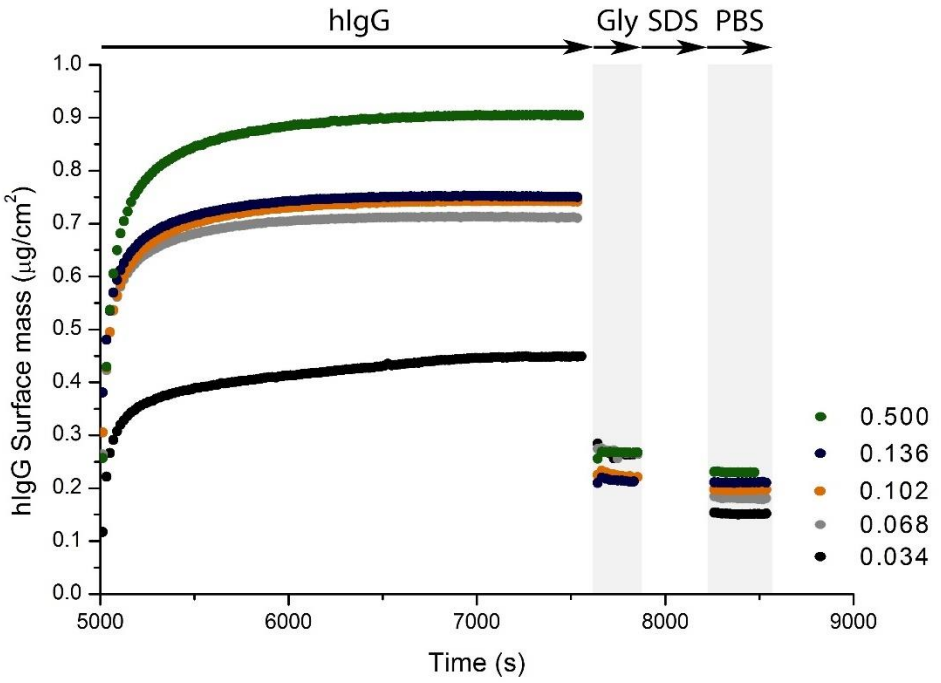

Figure 4.15: hIgG Surface Mass evolution after binding to surfaces with different amounts of A-SpA. The binding of hIgG is followed by washing with glycine, SDS and PBS.

The binding capacity towards hIgG increases with the increasing A-SpA surface mass, indicating that the improved coverage with A-SpA has a direct positive impact on the binding capacity of hIgG. Furthermore, it can be seen that the higher the initial amount of immobilised A-SpA on the azide surface (before adding IgG), the less aspecific adsorbed IgG needs to be removed by SDS after completion of the glycine washing step. This probably originates from the fact that a lower density of the initial A-SpA layers can offer the opportunity for aspecific adsorption of IgG molecules to the 'protein-free' substrate (*vide supra*). As a result, it can be concluded that the increased SpA surface mass (0.28 µg/cm²) obtained *via* CuAAC, not only leads to an increased presence of receptor (SpA)

molecules on the surface (see **Figure 4.8**), but also has the advantage of reducing aspecific binding of target molecules, in this case hIgG, to the underlying substrate. This will have a positive impact on the signal-to-noise ratio when applying this CuAAC coupling technique in sensing devices, thus improving their sensitivity and decreasing the chance of possible errors.

Activity of A-SpA layers obtained by the drop method

The second approach to reduce protein consumption and still maximise its binding capacity is to lower the volume while keeping the protein concentration constant.

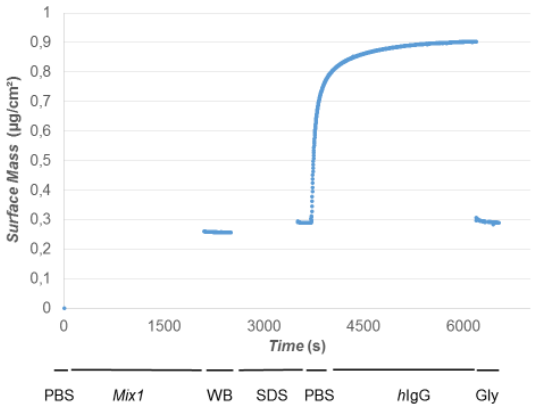

Figure 4.16: Surface mass evolution using *Mixture 1* in acetate buffer *via* drop method followed by affinity test towards hIgG.

After immobilising A-SpA from drops of 30 µl on the azide slides using CuAAC, the immobilised protein layers with an ASM Γ of 0.29µg/cm² were able to bind identical amounts of hIgG binding (0.61 µg/cm²). These results in **Figure 4.16** show that it is possible to obtain A-SpA layers with an identical activity, and with a considerably reduced amount of SpA.

Influence of alkynation on binding activity

By measuring the binding of hIgG to protein layers containing SpA molecules with varying degrees of alkynation, the influence of alkynation on the antibody binding activity was evaluated. SA-SpA with a single functionality, A-SpA with maximum 10 alkyne groups and fA-SpA with a maximum degree of alkynation were prepared and their binding activity towards hIgG were compared. It can be anticipated that the influence of one, single alkyne group towards the protein activity will be rather limited. However, the introduction of multiple alkynes could affect the proper functioning of the protein.

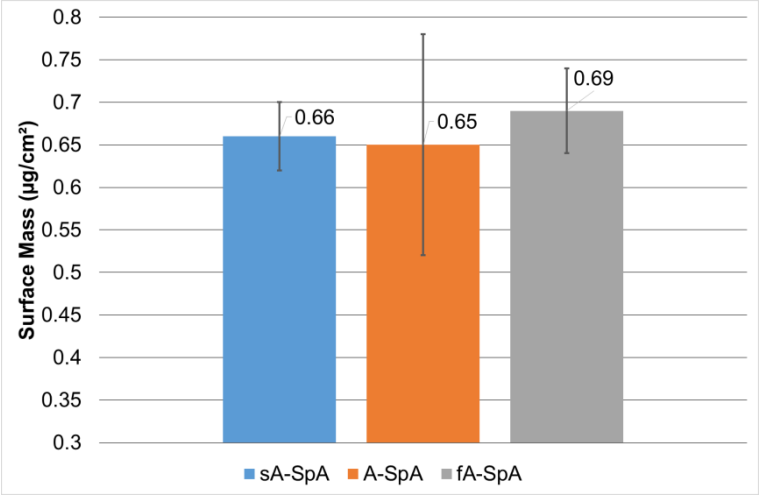

Figure 4.17: Human IgG surface mass to sA-SpA, A-SpA and fA-SpA functionalised samples.

Figure 4.17 shows the amounts of bound hIgG for each alkynated SpA species, which was previously immobilised using CuAAC. No significant difference between the different hIgG layers can be seen due to the overlap of the different standard

deviations. Remarkable is the fact that the fA-SpA is capable of binding hIgG in the same order of magnitude as A-SpA and SpA. One would expect that the introduction of multiple alkyne functionalities would affect the binding towards IgG. However, the results demonstrate that, for this particular protein, the alkynation does not negatively affect its proper functioning. The explanation lies in the amino acid sequence of SpA. Eleven amino acids are directly involved in the IgG binding of SpA [64]. These amino acids are all located in each of the four IgG binding domains. Since just one of these eleven amino acids is a lysine, alkynation will only have a minor effect on the affinity towards IgG. This can also be seen in **Figure 4.17**. Just one alteration does not necessary mean that the activity disappears. A good example for this are SpA molecules that have a fifth IgG binding domain, depending on the origin of SpA. This extra domain differs only in one amino acid residue, which in turn only has a marginal effect on its affinity towards hIgG. However, the effect of alkynation on the affinity of a protein towards its antigen or antibody might vary from one protein to another and needs to be verified for each case separately. Therefore, A-SpA with a moderate amount of alkyne functionalisations (16 %), was used in most tests (concentration dependency, drop method, etc.…) in this chapter.

4.3.7 Immobilisation of bovine IgG and antibody recognition

All previous experiments demonstrated that a highly reproducible layer of alkyne functionalised SpA on a planar azide functionalised silicon surface can be created in a straightforward manner when performing a CuAAC reaction in sodium acetate buffer pH 4. In order to prove that these coupling conditions can be used for other types of proteins, which differ in molecular weight and shape, immunoglobulin G

was covalently bound to a functionalised silicon layer. Bovine IgG is a protein of 150 kDa, which is three times larger than the previously used SpA. The isoelectric point of IgG is more basic than this of SpA, resulting in highly positively charged IgG molecules at pH 4. The general charge of the SpA molecules was only slightly positive. This could have an effect, positive or negative, on the formation of the bIgG layer. In **Figure 4.18** the adsorption of bIgG, the covalent coupling of alkynated bIgG (A-bIgG) and the recognition by anti-IgG is presented.

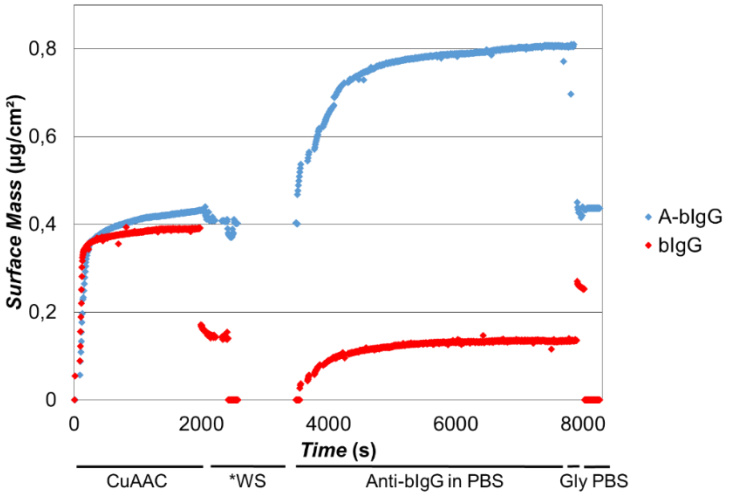

Figure 4.18: Real-time surface mass measurement of azidified silicon substrates in CuAAC solutions with A-bIgG (blue) or wild-type bIgG (red) (0-3500 s). Next recognition by anti-bIgG was evaluated (3500- 9000s). *WS: Washing steps with PBS, washing buffer and 0.5 % SDS.

Between 0 and 3500 seconds, the red curve pf the bIgG shows first an increase in surface mass due to coupling on the substrate. However, during washing in PBS, washing buffer and 0.5 % SDS, the remaining bIgG molecules were removed. On the other hand, the CuAAC mixture containing the alkynated species caused a mass increase of 0.4 µg/cm², which is 27 % of the end-on and 133 %

of a side-on close packed layer. Abundantly washing with PBS, washing buffer and SDS did not influence the present surface mass, proving its stable covalent immobilisation.

Subsequently, the slides were immersed in PBS to which anti-bovine IgG was added. The surface mass of the slides with the covalently immobilised bovine IgG, doubled after addition of anti-bovine IgG. In case of the substrates treated with wild-type bIgG, the surface mass increased with only 0.14 µg/cm². To get more information about the specificity of the interaction between anti-bovine IgG and the surface, the samples were flushed with glycine solution at pH 2.5. When there is a specific interaction between antibody and antigen, this bond can be broken using an acidic glycine solution [65]. This event is illustrated by the blue curve at time 7900 s. At this time the anti-bovine IgG is released from the surface, and the recorded surface mass restored again to its original values. This is not the case for the substrates treated with the wild-type bIgG, for which the glycine solution is not capable of removing the anti-bovine IgG molecules present on the surface. On the contrary, the surface mass seems to increase even more. This phenomenon can be addressed to parallel changes induced by the acidic environment shortening the hinge region and decreasing the compactness of the Fc domain. The Fab domain remains unchanged, even at pH 2. The mass increase detected by the ellipsometer most likely points to the swelling induced by the acidic environment as described in the literature [66].

4.4 Conclusions

The covalent coupling of SpA and hIgG on azide functionalised silicon slides has been achieved *via* the copper catalysed azide-alkyne cycloaddition. For this optimisation, the immobilisation of the proteins was followed in real-time with *in situ* ellipsometry. This allowed us to study the 'click' reaction in a time-dependent manner and to find the optimal reaction time and conditions to create covalently coupled protein surfaces with an optimal protein coverage and subsequent activity. An effective, reproducible and rapid method has been developed by combining copper sulphate, sodium L-ascorbate and THPTA in 0.01 M sodium acetate buffer at pH 4 in 30 minutes. Furthermore, a considerably improved surface mass was obtained as compared to other commonly used coupling techniques demonstrating its innovative potential for future biofunctionalisation of surfaces. After coupling, the biolayers kept their characteristics, *i.e.* the bound SpA was still able to interact with human IgG. These results confirm that this covalent coupling method can be used for proteins without inhibiting their corresponding activity. At the same time the increased surface mass resulted in a reduction in aspecific binding of target molecules, resulting in a rapid and covalent coupling strategy.

4.5 References

1. Li F, Chen W, Zhang S. Development of DNA electrochemical biosensor based on covalent immobilization of probe DNA by direct coupling of sol–gel and self-assembly technologies. Biosensors and Bioelectronics. 2008;24(4):781-6.

2. Qin GT, Santos C, Zhang W, Li Y, Kumar A, Erasquin UJ, *et al.* Biofunctionalization on alkylated silicon substrate surfaces *via* "click" chemistry. Journal of the American Chemical Society. 2010;132(46):16432-41.

3. Wang Z-H, Jin G. Covalent immobilization of proteins for the biosensor based on imaging ellipsometry. Journal of Immunological Methods. 2004;285(2):237-43.

4. van der Voort D, McNeil CA, Renneberg R, Korf J, Hermens WT, Glatz JFC. Biosensors: Basic features and application for fatty acid-binding protein, an early plasma marker of myocardial injury. Sensors and Actuators B: Chemical. 2005;105(1):50-9.

5. Chen DS, Davis MM. Molecular and functional analysis using live cell microarrays. Current Opinion in Chemical Biology. 2006;10(1):28-34.

6. Brian M P. Biosensors for chemical and biological agents of defence interest. Biosensors and Bioelectronics. 1996;11(11):1079-113.

7. Lei Y, Chen W, Mulchandani A. Microbial biosensors. Analytica Chimica Acta. 2006;568(1-2):200-10.

8. Mun S, Choi S-J. Optimization of the hybrid bilayer membrane method for immobilization of avidin on quartz crystal microbalance. Biosensors and Bioelectronics. 2009;24(8):2522-7.

9. Skidmore MA, Patey SJ, Thanh NT, Fernig DG, Turnbull JE, Yates EA. Attachment of glycosaminoglycan oligosaccharides to thiol-derivatised gold surfaces. Chem Commun (London). 2004 (23):2700-1.

10. Horemans F, Weustenraed A, Spivak D, Cleij TJ. Towards water compatible MIPs for sensing in aqueous media. Journal of molecular recognition: JMR. 2012;25(6):344-51.

11. Horemans F, Diliën H, Wagner P, Cleij TJ. Chapter 5 - MIP-based sensor platforms for detection of analytes in nano- and micromolar range. Molecularly Imprinted Sensors. Amsterdam: Elsevier; 2012. 91-124.

12. Jiang D, Tang J, Liu B, Yang P, Shen X, Kong J. Covalently coupling the antibody on an amine-self-assembled gold surface to probe hyaluronan-binding protein with capacitance measurement. Biosensors and Bioelectronics. 2003;18(9):1183-91.

13. Susmel S, Toniolo R, Pizzariello A, Dossi N, Bontempelli G. A piezoelectric immunosensor based on antibody entrapment within a non-totally rigid polymeric film. Sensors and Actuators B: Chemical. 2005;111-112(0):331-8.

14. Kohn M. Immobilization strategies for small molecule, peptide and protein microarrays. J Pept Sci. 2009;15(6):393-7.

15. Zhu Y, Gupta B, Guan B, Ciampi S, Reece PJ, Gooding JJ. Photolithographic strategy for patterning preformed, chemically modified, porous silicon photonic crystal using click chemistry. ACS Applied Materials & Interfaces. 2013;5(14):6514-21.

16. Gautrot JE, Huck WTS, Welch M, Ramstedt M. Protein-resistant NTA-functionalised polymer brushes for selective and stable immobilization of histidine-tagged proteins. ACS Applied Materials & Interfaces. 2009;2(1):193-202.

17. Briand E, Salmain M, Compère C, Pradier C-M. Immobilization of protein A on SAMs for the elaboration of immunosensors. Colloids and Surfaces B: Biointerfaces. 2006;53(2):215-24.

18. Gao Y, Kyratzis I. Covalent Immobilization of proteins on carbon nanotubes using the cross-linker 1-Ethyl-3-(3-dimethylaminopropyl)carbodiimide—a critical assessment. Bioconjugate Chemistry. 2008;19(10):1945-50.

19. Steen Redeker E, Ta DT, Cortens D, Billen B, Guedens W, Adriaensens P. Protein engineering for directed immobilization. Bioconjugate Chemistry. 2013; 24(11):1761-77.

20. Wong LS, Thirlway J, Micklefield J. Direct site-selective covalent protein immobilization catalyzed by a phosphopantetheinyl transferase. Journal of the American Chemical Society. 2008;130(37):12456-64.

21. Wong LS, Khan F, Micklefield J. Selective covalent protein immobilization: Strategies and applications. Chemical Reviews. 2009;109(9):4025-53.

22. North SH, Lock EH, Cooper CJ, Franek JB, Taitt CR, Walton SG. Plasma-based surface modification of polystyrene microtiter plates for covalent immobilization of biomolecules. ACS Applied Materials & Interfaces. 2010;2(10): 2884-91.

23. Butler JE, Ni L, Nessler R, Joshi KS, Suter M, Rosenberg B, *et al.* The physical and functional behavior of capture antibodies adsorbed on polystyrene. Journal of Immunological Methods. 1992;150(1–2):77-90.

24. Iha RK, Wooley KL, Nystro¨m AM, Burke DJ, Kade MJ, Hawker CJ. Applications of orthogonal "click" chemistries in the synthesis of functional soft materials. Chemical Reviews. 2009;109(11):5620-86.

25. Nebhani L, Barner-Kowollik C. Orthogonal transformations on solid substrates: Efficient avenues to surface modification. Advanced Materials. 2009; 21(34):3442-68.

26. Liang L, Astruc D. The copper(I)-catalyzed alkyne-azide cycloaddition (CuAAC) "click" reaction and its applications. An overview. Coordination Chemistry Reviews. 2011;255(23-24):2933-45.

27. Gouget-Laemmel AC, Yang J, Lodhi MA, Siriwardena A, Aureau D, Boukherroub R, *et al.* Functionalization of azide-terminated silicon surfaces with glycans using click chemistry: XPS and FTIR study. J Phys Chem C., American Chemical Society (ACS). 2013;117:368-75.

28. Malvi B, Sarkar BR, Pati D, Mathew R, Ajithkumar TG, Sen GS. "Clickable" SBA-15 mesoporous materials: Synthesis, characterization and their reaction with alkynes. J Mater Chem. 2009;1:1409-16.

29. Palomaki PKB, Dinolfo PH. Structural analysis of porphyrin multilayer films on ITO assembled using copper(I)-catalyzed azide–alkyne cycloaddition by ATR IR. ACS Applied Materials & Interfaces. 2011;3(12):4703-13.

30. Seo J-s, Lee S, Poulter CD. Regioselective covalent immobilization of re-combinant antibody-binding proteins A, G, and L for construction of antibody arrays. Journal of the American Chemical Society. 2013;135(24):8973-80.

31. Bally F, Cheng K, Nandivada H, Deng X, Ross AM, Panades A, *et al.* Co-immobilization of biomolecules on ultrathin reactive chemical vapor deposition coatings using multiple click chemistry strategies. ACS Applied Materials & Inter-faces. 2013;5(19):9262-8.

32. Damen CWN, Speijer H, Hermens WT, Schellens JHM, Rosing H, Beijnen JH. The bioanalysis of trastuzumab in human serum using precipitate-enhanced ellipsometry. Analytical Biochemistry. 2009;393(1):73-9.

33. Robers M, Rensink IJ, Hack CE, Aarden LA, Reutelingsperger CP, Glatz JF, *et al.* A new principle for rapid immunoassay of proteins based on *in situ* precipitate-enhanced ellipsometry. Biophys J. 1999;76(5):2769-76.

34. Hatzakis NS, Engelkamp H, Velonia K, Hofkens J, Christianen PCM, Svendsen A, *et al.* Synthesis and single enzyme activity of a clicked lipase-BSA hetero-dimer. Chemical Communications. 2006 (19):2012-4.

35. Kalkhof S, Sinz A. Chances and pitfalls of chemical cross-linking with amine-reactive N-hydroxysuccinimide esters. Analytical and Bioanalytical Chemistry. 2008;392(1-2):305-12.

36. Basle E, Joubert N, Pucheault M. Protein chemical modification on endogenous amino acids. Chemistry & Biology. 2010;17(3):213-27.

37. Uhlén M, Guss B, Nilsson B, Gatenbeck S, Philipson L, Lindberg M. Complete sequence of the staphylococcal gene encoding protein A. A gene evolved through multiple duplications. Journal of Biological Chemistry. 1984;259(3): 1695-702.

38. Jagadish B, Sankaranarayanan R, Xu L, Richards R, Vagner J, Hruby VJ, *et al.* Squalene-derived flexible linkers for bioactive peptides. Bioorganic Medicinal Chemistry Letters. 2007;17(12):3310-3.

39. Tan YH, Liu M, Nolting B, Go JG, Gervay-Hague J, Liu G-y. A nano-engineering approach for investigation and regulation of protein immobilization. ACS Nano. 2008;2(11):2374-84.

40. Aizawa M, Yun K, Haruyama T, Yanagida Y, Kobatake E. Protein engineering for self-assembling antibody molecules in an oriented manner. Supramolecular Science. 1998;5(5–6):761-4.

41. Cho IH, Paek EH, Lee H, Kang JY, Kim TS, Paek SH. Site-directed biotinylation of antibodies for controlled immobilization on solid surfaces. Analytical Biochemistry. 2007;365(1):14-23.

42. Iwata R, Satoh R, Iwasaki Y, Akiyoshi K. Covalent immobilization of antibody fragments on well-defined polymer brushes via site-directed method. Colloids and Surfaces B, Biointerfaces. 2008;62(2):288-98.

43. Ahmed SR, Lutes AT, Barbari TA. Specific capture of target proteins by oriented antibodies bound to tyrosinase-immobilised Protein A on a polyallylamine affinity membrane surface. Journal of Membrane Science. 2006; 282(1–2):311-21.

44. Hernandez K, Fernandez-Lafuente R. Control of protein immobilization: Coupling immobilization and site-directed mutagenesis to improve biocatalyst or biosensor performance. Enzyme and Microbial Technology. 2011;48(2):107-22.

45. Kauzmann W. Some factors in the interpretation of protein denaturation. Adv Protein Chem. 1959;14:1-63.

46. Lahiri J, Isaacs L, Tien J, Whitesides GM. A Strategy for the generation of surfaces presenting ligands for studies of binding based on an active ester as a common reactive intermediate: A surface plasmon resonance study. Anal Chem. 1999;71:777-90.

47. Arakawa T, Kita Y, Timasheff SN. Protein precipitation and denaturation by dimethyl sulfoxide. Biophysical Chemistry. 2007;131(1–3):62-70.

48. Bhattacharjya S, Balaram P. Effects of organic solvents on protein structures: Observation of a structured helical core in hen egg-white lysozyme in aqueous dimethylsulfoxide. Proteins: Structure, Function, and Bioinformatics. 1997;29(4):492-507.

49. Mielecki M, Wojtasik J, Zborowska M, Kurzątkowska K, Grzelak K, Dehaen W, *et al.* Oriented immobilization of His-tagged kinase RIO1 protein on redox active N-(IDA-like)-Cu(II) monolayer deposited on gold electrode—The base of electrochemical biosensor. Electrochimica Acta. 2013;96(0):147-54.

50. Shi Q, Chen X, Lu T, Jing X. The immobilization of proteins on biodegradable polymer fibers via click chemistry. Biomaterials. 2008;29(8):1118-26.

51. Wang L, Ran Q, Tian Y, Xu J, Xian Y, Peng R, *et al.* Covalent immobilization of redox protein via click chemistry and carbodiimide reaction: Direct electron transfer and biocatalysis. Journal of Colloid and Interface Science. 2010;350(2): 544-50.

52. Ran Q, Peng R, Liang C, Ye S, Xian Y, Zhang W, *et al.* Covalent immo-bilization of horseradish peroxidase via click chemistry and its direct electro-chemistry. Talanta. 2011;83(5):1381-5.

53. Qi H, Ling C, Huang R, Qiu X, Shangguan L, Gao Q, *et al.* Functionalization of single-walled carbon nanotubes with protein by click chemistry as sensing platform for sensitized electrochemical immunoassay. Electrochimica Acta. 2012;63(0):76-82.

54. Shamsi F, Coster H, Jolliffe KA. Characterization of peptide immobilization on an acetylene terminated surface via click chemistry. Surface Science. 2011; 605(19–20):1763-70.

55. Le HT, Jang J-G, Park JY, Lim CW, Kim TW. Antibody functionalization with a dual reactive hydrazide/click crosslinker. Analytical Biochemistry. 2013;435(1): 68-73.

56. Meirovitch H, Scheraga HA. Empirical Studies of hydrophobicity. 2. Distribution of the hydrophobic, hydrophilic, neutral, and ambivalent amino acids in the interior and exterior layers of native proteins. Macromolecules. 1980; 13(6):1406-14.

57. Rabe M, Verdes D, Seeger S. Surface-induced spreading phenomenon of protein clusters. Soft Matter. 2009;5(5):1039-47.

58. Daly SM, Przybycien TM, Tilton RD. Coverage-dependent orientation of lysozyme adsorbed on silica. Langmuir. 2003;19(9):3848-57.

59. Elwing H, Askendal A, Lundström I. Competition between adsorbed fibrinogen and high-molecular-weight kininogen on solid surfaces incubated in human plasma (the Vroman effect): Influence of solid surface wettability. Journal of Biomedical Materials Research. 1987;21(8):1023-8.

60. Elofsson UM, Paulsson MA, Arnebrant T. Adsorption of β-lactoglobulin A and B in relation to self-association: Effect of concentration and pH. Langmuir. 1997; 13(6):1695-700.

61. Kennedy JF, Alanis RM. Colloidal biomolecules, biomaterials, and biomedical applications. Carbohydr Polym. 2005;62:59-60.

62. Molina-Bolívar JA, Galisteo-González F. Latex immunoagglutination assays. Journal of Macromolecular Science, Part C. 2005;45(1):59-98.

63. Yarmush ML, Antonsen KP, Sundaram S, Yarmush DM. Immunoadsorption: Strategies for antigen elution and production of reusable adsorbents. Biotechnology Progress. 1992;8(3):168-78.

64. Moks T, Abrahmsén L, Nilsson B, Hellman U, Sjöquist J, Uhlén M. Staphylococcal protein A consists of five IgG-binding domains. European Journal of Biochemistry. 1986;156(3):637-43.

65. Calmettes P, Cser L, Rajnavölgyi É. Temperature and pH dependence of immunoglobulin G conformation. Archives of Biochemistry and Biophysics. 1991; 291(2):277-83.

66. Abaturov LV, Nezlin RS, Vengerova TI, Varshavsky JM. Conformational studies of immunoglobulin G and its subunits by the methods of hydrogen-deuterium exchange and infrared spectroscopy. Biochim Biophys Acta. 1969; 194(2):386-96.

Chapter 5. Site-directed immobilisation *via* alkynated maltose binding protein and subsequent protein layer quantification by *in situ* ellipsometry

Part of this chapter is published in *'Vranken, Tom; Miszta, Adam; de Laat, Bas; Hermens, Wim; Steen Redeker, Erik; Adriaensens, Peter; Guedens, Wanda & Cleij, Thomas. In situ monitoring and optimisation of CuAAC-mediated protein functionalisation of biosurfaces In: Sensors & Actuators: B. Chemical 2017: p 992-1000. [Article - cat: A1]'*

5.1 Introduction

The question arises whether the CuAAC or 'click' chemistry in general also can offer opportunities for the site directed immobilisation of planar carriers and if so, if it is an improvement compared to conventional immobilisation procedures. It has been pointed out in the previous sections that CuAAC chemistry can be of considerable use to functionalise surfaces, *e.g.* silanised glass and silicon, with different (bio) molecules, *e.g.* dyes or proteins, such as SpA and IgG. Fluorescence measurements gave evidence of the possibility to couple alkyne functionalised dyes to azide functionalised surfaces. Furthermore, ellipsometry clearly demonstrated a very reproducible, covalent biolayer formation of alkynated SpA and IgG. This confirmed the expectations that CuAAC chemistry is a better alternative as compared to other covalent, non-oriented or random coupling procedures, such as EDC/NHS [1]. Furthermore, the high reproducibility of the biolayer formation on top of the substrate and the short reaction time are additional advantages of the proposed procedure.

However, at this stage only a few of the many advantages of the CuAAC have been explored, *i.e.* the formation of a stable covalent bond and the short reaction time. Since CuAAC has much more features to offer for the further development and improvement of biofunctionalised surfaces, its key characteristic will be exploited in this chapter *i.e.* the chemo selectivity of the coupling procedure.

Although, azide and alkyne groups are highly energetic, from a kinetic point of view they are one of the least reactive functional groups in organic chemistry and do not react intramolecularly or intermolecularly. Furthermore, they do not interfere in biological processes in living organisms as they are inert towards the endogenous functional groups, *i.e.* amines, thiols, hydroxyl groups, carboxyl

groups, under physiological circumstances [2, 3]. This chemo selectivity makes them very suitable for site-specific covalent immobilisation without intermolecularly crosslinking. Biomolecules, such as sugars, (antibody) proteins or even complete cells just do not have endogenous azide or alkyne functionalities. Artificially introducing these functionalities into the biomolecules' structure using *in vitro* or *in vivo* methods [4], will result in 'clickable' molecules.

In the previous chapter the random derivatisation of the endogenous lysines of SpA and IgG with an alkyne-NHS ester yielding alkynated SpA and IgG respectively, is described in detail [5]. Subsequently, they were deployed for the biofunctionalisation of the azidified silicon slides. Since, to a certain degree, this alkynation procedure seems to be rather determined by chance due to the multiple presence of target endogenous groups, *i.e.* lysines, it is very important that other methods are explored in order to obtain site-specifically mono-alkynated biomolecules. In addition, this functionality is preferred to be at a location, distant from the protein's active site. For enzymes this would be a location remote from the substrate binding site, for antibodies this would be at or near the Fc domains, which are the C-termini of the heavy chains.

A first commonly used strategy to obtain an oriented antibody functionalised surface, utilizes SpA molecules, as the basic layer, adsorbed on top of a hydrophobic silanised silicon layer. To these SpA molecules, IgG antibodies bind with their Fc domain, creating an IgG surface of which all antigen binding sites are oriented towards the solution [6]. A restriction of this procedure is that there is still neither a covalent bond between the IgG and SpA layer, nor between SpA and the silicon substrate. However, such procedures do result in disposable IgG based biofilms. A similar biolayer, in which a more homogeneous layer of IgG

molecules was obtained by first immobilising SpA covalently to the substrate, and afterwards introducing IgG to the SpA functionalised substrate, has been described in the literature [7]. It was also described in Chapter 4 of this thesis.

A second method to obtain oriented protein films involves post-translational modifications. Post-translational modifications occur when the proteins are undergoing specific functionalisations before being fully functional, *e.g.* phosphorylation, acetylation, glycosylation, methylation or other (enzymatic) post-translational modifications. These are all belonging to the possible modifications determining the protein folding, stability and purpose after being released into the cellular environment [8-12]. When these modifications occur at one specific location in the protein, this functionality can be used as an anchoring point. Optimally, the anchoring point is located at a remote location from the active sites. When needed, these anchoring points can be manipulated even further and serve as the unique binding spot for immobilisation towards the planar carrier.

The desired properties, *i.e.* covalent immobilisation, high yields, high selectivity, biocompatibility and a proper orientation, originating from different commonly used methods can all be achieved in one single procedure, the CuAAC immobilisation protocol. In this chapter, maltose binding protein (MBP; **Figure 5.1**), a 42 kDa soluble periplasmic protein [13], will be used as a model protein for the *in vitro*, site-specific alkynation, followed by the oriented immobilisation using the CuAAC procedure as described in 4.2.6.

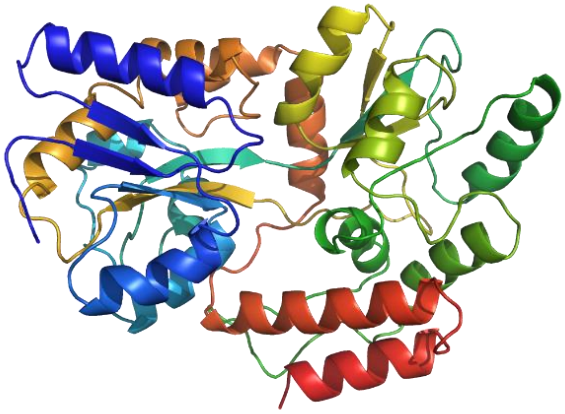

Figure 5.1: 3D-structure of maltose binding protein (MBP). An alkyne group will be site-specifically attached at the C-terminus (end of red alpha helix).

A site-specifically alkynated MBP (ssA-MBP), as well as a random alkynated MBP species (rA-MBP) and a fully alkynated MBP species (fA-MBP) will be immobilised on azidified silicon substrates as presented in **Figure 5.2** (top left: randomly oriented MBP; top right: highly oriented MBP).

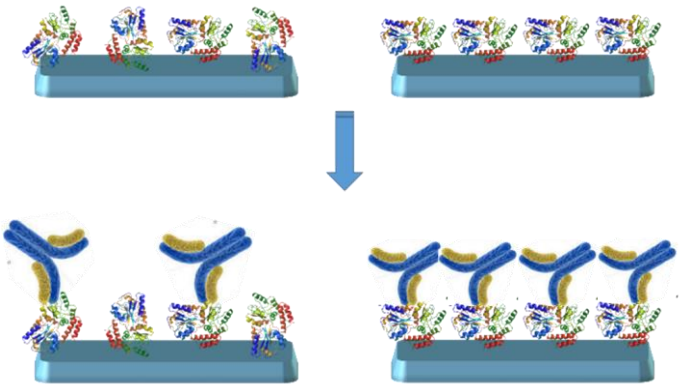

Figure 5.2: Representation of biolayers obtained by random (top, left) and site-directed (top, right) alkynated MBP immobilisation on azidified silicon substrates. Expected recognition pattern after addition of monoclonal anti-MBP to both biolayers (bottom).

The alkynation of MBP to obtain rA-MBP and fA-MBP will occur according the procedure performed earlier with SpA as described in section 4.2.5. The site-specific alkynation of MBP will make use the Intein-Expressed Protein Ligation (IPL) technique [14-19], as is schematically illustrated in **Figure 5.3**.

This Intein mediated post-translational functionalisation protocol of a protein of interest will result in a protein bearing a single alkyne functionality at its C-terminus. The technique was first described by Muir for the ligation of a phosphotyrosine-containing peptide or an unnatural amino acid to the C-terminus of recombinant proteins [15]. In IPL, a protein of interest is fused to a self-cleavable peptide sequence called Intein (or protein intron), which catalyses a N-S shift at the protein's terminus to form a thioester intermediate. By subsequently subjecting this intermediate to a thiol-functionalised (nucleophile) molecule *i.e.* MESNA, chemical ligation takes place (**Figure 5.3**, right). Due to hydrolysis the thiol containing molecule can then be removed from the target in a single step, resulting in a purified wild-type protein. The speed of hydrolysis is depending on the type of thiol reagent that has been used and the pH of the solution [21]. A bifunctional cysteine-alkyne linker that carries both a thiol group and a bioorthogonal alkyne group (**Figure 5.3**, left) could also serve as a nucleophile. By adding 2-mercaptoethanesulfonic acid (or MESNA) the modification efficiency can be increased [22]. MESNA is usually used as the primary nucleophile to produce the thioester intermediate, which in the following step undergoes the second nucleophilic attack by the cysteine-alkyne linker. This results in a covalent bond between the linker molecule and the protein's terminus, where the alkyne moiety is available to selectively react with an azide-containing molecule or surface in a CuAAC coupling reaction.

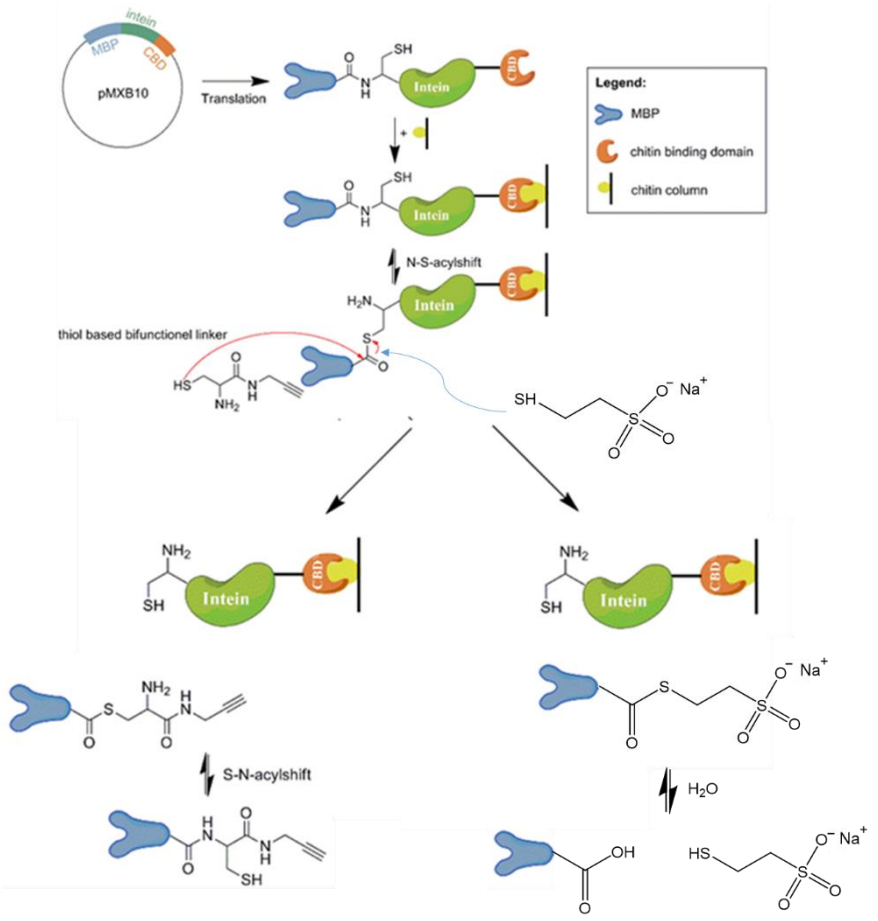

Figure 5.3: The IPL mechanism (picture adapted from Steen Redeker *et al.* [20]). The gene encoding the protein of interest is C-terminally fused to an Intein-chitin binding domain (Intein-CBD). The expressed fusion protein is purified by affinity chromatography on a chitin column. By adding a thiol nucleophile on-column cleavage of the target protein from the Intein is performed, *e.g.* cysteine-alkyne linker (left) and sodium 2-sulfanylethanesulfonate or just MESNA (right). Whereas the cysteine-alkyne linker results in the attachment of a bioorthogonal alkyne function to the C-terminus of the released protein (bottom left), MESNA – after subsequent removal by hydrolysis – results in the wild-type protein (bottom right).

In Chapter 4, a non-site-specific protein coupling method using CuAAC was described. The performances of these protein-conjugated surfaces are possibly not yet ideal. Therefore, after immobilisation of the different site-specifically alkynated MBP obtained *via* IPL or non-site-specifically alkynated MBP species, monoclonal anti-MBP antibodies will be used to verify the accessibility of the target epitopes present in all three MBP samples. By these experiments the hypothesis that an oriented biofilm will lead to an increased number of binding events by its antibody will be demonstrated.

5.2 Materials & Methods

5.2.1 Materials

Zeba micro spin desalting columns (7K MWCO, 0.5 mL), SpA (Cowan strain, recombinant, expressed in *E. coli*), bacterial protein extraction reagent (B-PER), DNase I and Luria Bertani (LB) medium containing were obtained from Thermo Scientific. 1-ethyl-3-(3-dimethylaminopropyl) carbodiimide (EDC), *N*-hydroxy-succinimide (NHS), diethylene glycolamine (98 %), copper(II) sulphate penta-hydrate, bromopropylamine hydrobromide and sodium azide were purchased from Acros. Tris(3-hydroxypropyltriazolylmethyl) amine (THPTA), sodium L-ascorbate (NaAsc), 4-(2-hydroxyethyl)-1-piperazineethanesulfonic acid (HEPES), monoclonal anti-maltose binding protein antibody (clone-17), 2-(*N*-morpholino) ethanesulfonic acid (MES), sodium acetate trihydrate and tris(hydroxymethyl)aminomethane (Trizma®base) were obtained from Sigma-Aldrich. The IMPACT™ (Intein Mediated Purification with an Affinity Chitin-binding Tag) system, Chitin beads and pMXB10 vector were purchased from New England Biolabs.

5.2.2 Solutions

Used solutions were 10 mM alkyne NHS in acetonitrile; PBS buffer pH 7.4: 137 mM NaCl, 27 mM KCl, 10 mM Na_2HPO_4, 2 mM KH_2PO_4; 0.1 M glycine-0.2 M NaCl pH 2.5; 0.01 M sodium acetate buffer pH 4; 0.5 % SDS in H_2O; 30 mM sodium 2-sulfanylethanesulfonate (MESNA); Column buffer pH 8.5: 20 mM HEPES, 500 mM NaCl, 1 mM EDTA. washing buffer pH 7.5: 0.2 M Na_2HPO_4, 0.2 M NaCl, 0.15 M EDTA, 0.05 M ethanolamine. Buffers were prepared with Milli-Q water.

5.2.3 Instruments

Ellipsometry was performed on a custom made ellipsometer equipped with eight cuvettes and magnetic stirrers, monitoring time-dependent changes in polariser angle, analyser angle and reflected light intensity [23] as previously illustrated in **Figure 2.3**. A reference surface mass was recorded for each slide before the start of the binding monitoring.

5.2.4 Non-site-specific ('random') alkynation of MBP

In analogy with the SpA alkynation a 5.8-fold molar excess of the alkyne NHS ester was added to a MBP solution in PBS (3.5 μM), leading to a theoretical maximum random alkynation of 16 % of the available lysines (37 lysines / MBP) [24]. Furthermore, a batch of fully alkynated MBP (fA-MBP) was obtained by adding a 54-fold molar excess of the alkyne NHS ester to a second MBP solution (3.5 μM). After 3 hours both reaction mixtures, containing rA-MBP or fA-MBP were filtered using Zeba micro spin desalting columns.

5.2.5 Site-specific alkynation of MBP

For the site-specific introduction of the alkyne group in MBP, the Intein-expressed protein ligation (IPL) technique was employed to obtain recombinant MBP bearing

an alkyne group at the C-terminus *via* the IMPACT™ method [25-27]. Hereto, a fusion protein was expressed from the plasmid pMXB10, containing the MBP fused in-frame to the Mxe gyrase A Intein and chitin binding domain at the C-terminus. 300 mL of Luria Bertani (LB) medium containing ampicillin was inoculated with 3 mL of an overnight single colony culture of the *Escherichia coli* strain BL21 (DE3), transformed with the plasmid pMXB10. Cultures were grown at 37 °C to an OD_{600} between 0.5 and 0.6. After induction with 1 mM IPTG at 37 °C for 3 hours, the cells were harvested by centrifugation at 5000 g for 10 min. The cell pellet was resuspended in 6 mL Bacterial Protein Extraction Reagent (B-PER) supplemented with 5-10 U/mL DNase I. After 15 minutes at RT, the lysate was centrifuged at 4 °C for 30 minutes at 15000 g and the supernatant was collected. Next, 4 mL chitin beads were washed with 10 bed volumes of column buffer. The washed chitin beads and the supernatant were poured together and incubated for 1 hour at 4 °C while inverting. Afterwards, the mixture was divided over two separate columns, followed by washing with 20 bed volumes of column buffer. The first column was incubated with 3 mL of a cleavage buffer containing 1 mM TCEP and 30 mM MESNA (**Figure 5.3**, right). The second was incubated with 3 mL of a cleavage buffer containing 1 mM alkyne functionalised cysteine (2-amino-3-mercapto-N-(prop-2-yn-1-yl) propanamide), 1 mM TCEP and 30 mM MESNA (**Figure 5.3**, left). After overnight incubation at 4 °C, both columns were eluted with 3 mL column buffer. This resulted in MESNA functionalised MBP (not alkynated MBP) and in ssA-MBP, respectively. The proteins were further purified on a Sephadex G-25 column and eluted with PBS. After purification, all proteins were stored in PBS at -20 °C until further use. The alkynated cysteine linker molecule was synthesised as described in literature [28].

5.2.6 Covalent CuAAC coupling of rA-MBP, fA-MBP and ssA-MBP

The CuAAC coupling was accomplished *via Mixture 1*, (*cf.* **Table 4.1**) consisting of 0.5 mM $Cu(I)SO_4$, 2.5 mM sodium ascorbate, 1 mM THPTA in sodium acetate buffer pH 4 during 30 minutes. The slides were prepared as described under section 4.2.4. Surface masses of immobilised rA-MBP, fA-MBP and ssA-MBP were determined by ellipsometry.

5.2.7 Activity of surface coupled A-MBP

Similarly, as has been performed with IgG for SpA in Chapter 4, monoclonal anti-MBP (0.33 µM) was added to the cuvettes containing the MBP covered slides. The interaction between the antibody and the immobilised MBP was monitored in real-time by ellipsometry.

5.2.8 Immobilisation *via* DROP method

Five different mixtures containing 1 µM of ssA-MBP were prepared. Mixture one contained copper sulphate, sodium L-ascorbate and THPTA as in the original described concentrations under *Mixture 1* in sodium acetate buffer pH 4 in **Table 4.1**. The other mixtures contained respectively 2, 4, 6, 8 and 10 times more copper, reducing agent and ligand while the protein concentration remained the same. Each sample was measured before applying 30 µL of each particular mixture. After 30 minutes the surface mass was measured while washing the ssA-MBP containing azidified silicon slides with washing buffer and SDS. The final surface mass was determined in PBS.

5.3 Results & Discussion

5.3.1 Site-specific alkynation of MBP

In order to obtain the alkyne functionality at the C-terminus of the protein, the formation of a thioester by the nucleophilic attack of the Intein N-terminal cysteine is required. In the presence of a thiol reagent *i.e.* MESNA, a thiol exchange takes place and the Intein is dissociated from the protein (**Figure 5.3**). In a subsequent ligation reaction with the alkynated cysteine, 2-amino-3-mercapto-N-(prop-2-yn-1-yl) propanamide, the thiol is exchanged followed by the generation of the peptide (**Figure 5.4**) [29].

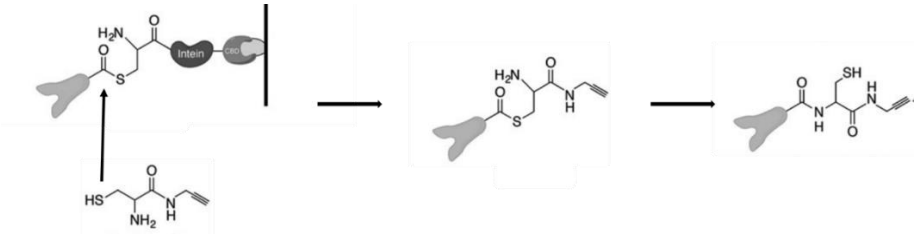

Figure 5.4: Schematic representation of the ligation reaction with alkynated cysteine.

Attempts to verify the mono-alkynation of MBP by mass spectra analysis were performed, however due to the size of MBP compared to the small modification by a single alkyne, it appeared not to be possible to determine this by mass spectra analysis. Later, a similar procedure was performed and described in literature, in order to obtain a site-specifically alkynated nanobody, demonstrating that this procedure ultimately leads to mono alkynated proteins [30, 33]. By means of electrospray ionisation-Fourier transform mass spectrometry, a mass increase of the nanobodies after alkynation was demonstrated. This corresponded to 1 cysteine-alkyne linker.

5.3.2 Covalent coupling of rA-MBP/fA-MBP/ssA-MBP

The initial MBP immobilisation occurred in an overnight experiment with ssA-MBP and a wild-type MBP species. The non-alkynated species, dissolved in *Mixture 1* in acetate buffer pH 4 as well, was used to demonstrate that physically adsorbed proteins, which are lacking an alkyne functionality, will be removed from the surface after performing the different washing steps. In **Figure 5.5** the increase in surface mass after the overnight immobilisation (65000 s) in an external holder is visualised (note: during the external immobilisation no real-time measurements can be performed). Subsequently, consecutive washing steps in washing buffer (WB) and SDS were performed, which removed the majority of the wild-type MBP (blue curve) down to a surface mass of 0.06 µg/cm², whereas a substantially higher amount of ssA-MBP, 0.32 µg/cm², remained at the azidified surface.

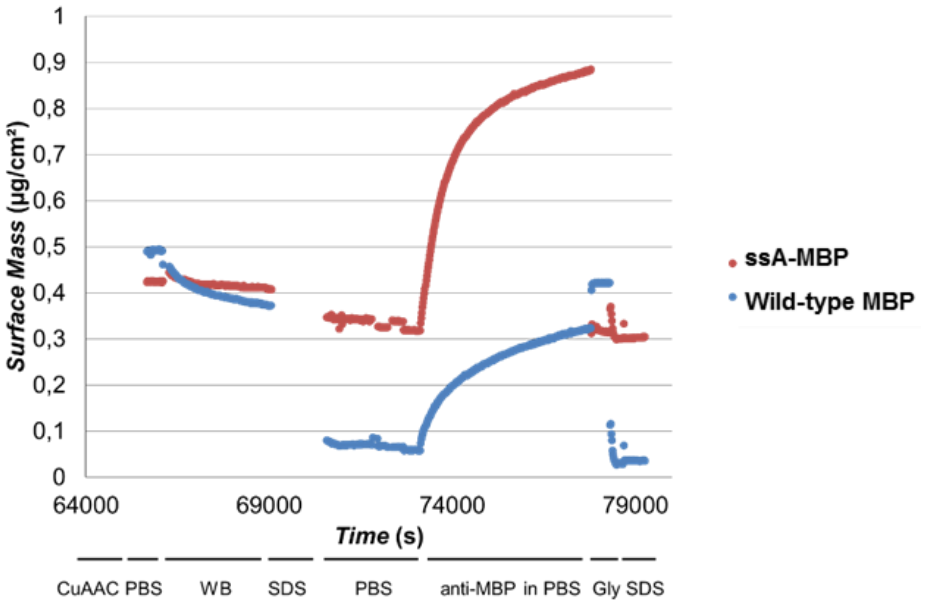

Figure 5.5: Real-time surface mass evolution measurements of azidified silicon slides immobilised with CuAAC *Mixture 1* containing ssA-MBP (red) or wild-type MBP (blue).

Next, both slides were treated with monoclonal anti-MBP, resulting in a total surface mass of 0.9 µg/cm² for the ssA-MBP functionalised surface. The amount of protein on the wild-type MBP treated sample increased from 0.06 to 0.32 µg/cm², which is 30 % of the ssA-MBP sample. By washing the samples with glycine the anti-MBP molecules were removed from the ssA-MBP layer, while the protein layer remained (and even increased in amount) at the surface of the MBP treated sample. By washing with SDS, the remaining anti-MBP antibodies could be removed while no additional influence on the ssA-MBP layer was noticed.

The previous experiment indicated that mono-alkynated proteins, such as ssA-MBP, can be immobilised using the CuAAC procedure. However, the negative control experiment with wild-type MBP still showed a certain degree of binding between the protein and the surface. The adsorbed proteins are hardly removable by the washing buffer. During earlier experiments with SpA the washing buffer was able to remove more of the physisorbed SpA. The SDS solution removed not all of the remaining non-covalently coupled MBP. Most likely the prolonged storage of MBP in acetate buffer pH 4 is harmful for the protein's stability. In addition, when storing the MBP in acetate buffer at -20 °C and subsequent unfreezing, a certain amount of MBP is not soluble anymore, demonstrating a possible conformational alteration induced by the low pH and/or the low storage temperature. To minimise such side effects, wild-type and ssA-MBP molecules were stored in PBS at -20 °C and the reaction time was reduced to 30 minutes. By lowering the reaction time and storing the ssA- and wild-type MBP proteins in PBS before using them in the coupling mixture, MBP proteins could be removed. The CuAAC procedure with *Mixture 1* in acetate buffer during a reaction time of

30 minutes using ssA-MBP, rA-MBP or fA-MBP resulted in the following MBP layers (**Figure 5.6**).

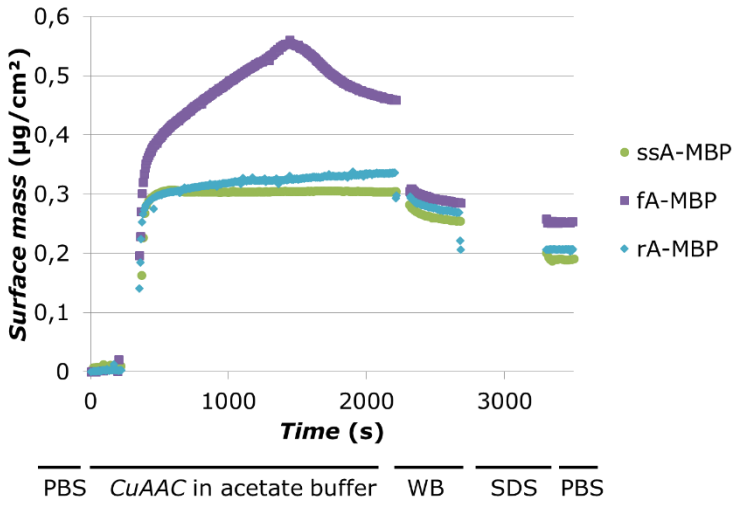

Figure 5.6: Surface mass evolution measured by real-time ellipsometry of ssA-MBP (green), fA-MBP (purple) and rA-MBP (blue) immobilised on azidified samples after CuAAC immobilisation followed by consecutive washing in washing buffer (WB) and SDS.

In all three cases, a covalently MBP layer remained at the sample surface after excessively washing with high ionic washing buffer and the denaturing SDS solution. As demonstrated in Chapter 4, both washing steps were sufficient to remove almost all non-covalently bound proteins. Comparing these values with the ones achieved during the first ssA-MBP experiment, *i.e.* 0.32 µg/cm², a decrease in surface mass can be noticed in all cases. This could be a result of the shortened reaction time or the fact that the proteins are no longer stored in acetate buffer after functionalisation, decreasing insoluble fraction. Since the ssA-MBP used in second series of experiments, was originating from a different batch, also this influence cannot be excluded.

When comparing the different alkynated MBP species one by one, the influence of the slightly higher amount of alkyne functionalities, *i.e.* 5 alkynes per rA-MBP molecule (which equals 16 % of the total amount of lysines present in MBP) instead of 1 alkyne functionality per ssA-MBP, on the resulting surface mass is rather limited. Immobilisation of fA-MBP, which is functionalised with an overload of alkyne functionalities, clearly led to the highest surface mass. When taking a closer look at the progression of this plot (**Figure 5.6**, purple), the same odd bump can be seen as in **Figure 4.11** and which could be explained by the Vroman effect or the overshoot effect as described in 4.3.5.

When fA-MBP is adsorbing, the part containing the most positive charges, will be attracted towards the azidified carboxyl silanised surface as first and this side will form the initial covalent bonds with the solid carrier. Due to the flexibility of proteins in solution other alkyne functionalities present at the surface of fA-MBP are able as well to come nearby azide functionalities, forming similar covalent bonds. These additional linkages can be the cause of an orientation change over time, leading to a decrease in final surface mass. Furthermore, a second 'side effect' of the 'overalkynation' of MBP could increase the chance of multilayer formation, as can be seen in **Figure 5.6** up to 1500 s.

Despite the presence of multiple alkyne functionalities, rA-MBP does not show this overshoot or multilayer formation (**Figure 5.6**, blue). The origin of this difference may be caused by a variety of effects as was discussed in 4.3.5. Possibly the amount of alkynes has not reached the threshold which might have led to increased protein aggregation. A second way of reasoning might be that the alkyne functionalisation by means of alkyne-NHS, which was assumed to be random, is perhaps less random as expected. Possibly certain lysines are more

accessible for peptide formation than others, leading to 'region-alkynated' proteins. Later when these proteins are covalently immobilised, their alkynated region will point towards the solid carrier surface. The chance of observing a reorientation, such as could be seen for fA-MBP, is reduced due to the higher density of alkynes at one region. Nevertheless, the above explanations remain speculations and it remains impossibly to explain accurately the difference in progression of the rA-MBP and the fA-MBP curves. In case of ssA-MBP there is one certainty, only one orientation is possible and a reorientation such as seen with fA-MBP does not occur. During the progression of the ssA-MBP plot no bump is observed (**Figure 5.6**, green), possibly pointing to an immobilisation without reorientation.

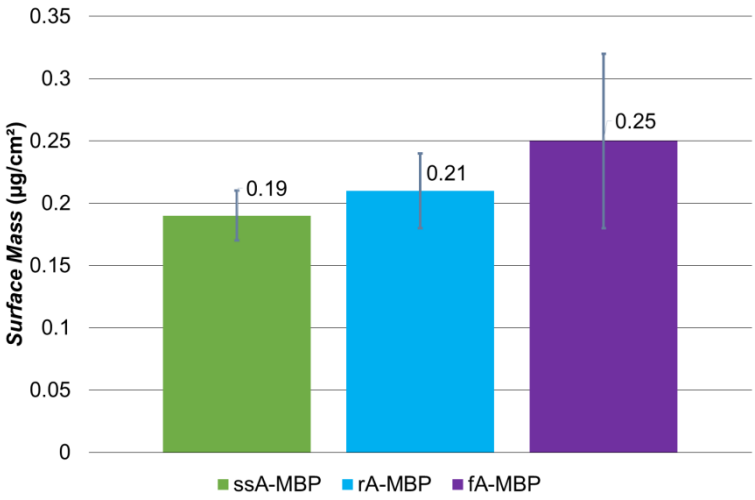

Figure 5.7: Average surface masses and standard deviation obtained from three different alkynated MBP species (ssA-MBP, rA-MBP and fA-MBP).

As presented in **Figure 5.7**, the fA-MBP solution used for the immobilisation on azidified silicon slides led to an average surface mass of 0.25 µg/cm² ±0.07 µg/cm² (*n*=3). The rA-MBP containing CuAAC solution ended up in an average

surface mass of 0.21 µg/cm² ±0.03 µg/cm² (*n*=3). An average surface mass of 0.19 µg/cm² ±0.02 µg/cm² (*n*=8) was obtained for the coupling of ssA-MBP. All three averages and their standard deviations, clearly demonstrated the presence of alkynated MBP species at the azidified surface after the different washing steps in washing buffer and SDS. By analogy with the previous experiments with SpA, the conclusion can be made that after performing the CuAAC reaction with the alkynated MBP species, and after extensively washing the slides with washing buffer and with SDS, the remaining proteins at the surface are covalently bound to the azidified silicon slide. The standard deviation and thus the reproducibility of the layers, is positively influenced by lowering the amount of alkyne functionalities. Student t-tests between the different results pointed out that there is a statistical significant difference between the ssA-MBP and the fA- MBP (two-tailed P-value: 0.042), whereas there are no statistical significant differences between ssA-MBP and rA-MBP (P-value: 0.224) or between rA-MBP and fA-MBP (P-value: 0.414). However, since all averages and standard deviations are slightly overlapping, statistically no distinction can be made. Still, the experiments pointed out that the introduction of one single alkyne group leads to an acceptable, oriented biofunctionalised surface with a high reproducibility. In a next step, the influence of the different degrees in alkynation and their immobilisation to a solid surface, on the binding activity towards their antibody, a monoclonal anti-MBP, was measured in real-time by ellipsometry using the shorter procedure.

5.3.3 Activity measurements of MBP

The different MBP covered slides *i.e.* ssA-MBP, rA-MBP, fA-MBP were put into cuvettes containing monoclonal anti-MBP dissolved in PBS. Monoclonal antibodies were chosen due to their affinity towards one single epitope, while polyclonal

antibody solutions contain a mixture of antibodies [31]. After immobilisation of MBP, certain epitopes will not be accessible while others will be. A consequence of targeting multiple epitopes, present at the surface of MBP, with a polyclonal solution will be that multiple different antibodies will be attracted and bind the exposed epitope. The amount of antibody-antigen interactions will not be changed and differences with an oriented layer will not be demonstrated.

In case of using a polyclonal solution, the present antibodies *i.e.* monoclonal anti-MBP, just target one epitope. After immobilising the target of anti-MBP, in this case ssA-, rA- or fA-MBP, certain epitopes will be accessible while others will be oriented towards the solid surface. The idea is that when immobilising ssA-MBP with their C-terminus towards the solid surface, the epitope which is targeted will be equally accessible all over the area. Since the use of rA-MBP may produce a random oriented protein surface, an influence on the antibody binding capacity should be noticeable. Furthermore, there is a chance that the targeted epitope might possess accessible lysines, which are used for peptide formation by the alkyne-NHS linker during protein alkynation. The alkynation may influence the antigen-antibody interactions, lowering the amount of bond antibody as well. In case of fA-MBP, the highest influence towards the epitope accessibility by the monoclonal antibodies, will be induced by the 'overalkynation' using alkyne-NHS. The most alkyne functionalisations will take place at the terminal amines of the lysines, often near or as a part of the target binding region. These alterations may lead to affinity changes, lowering the affinity of the antibody towards the particular epitope [32].

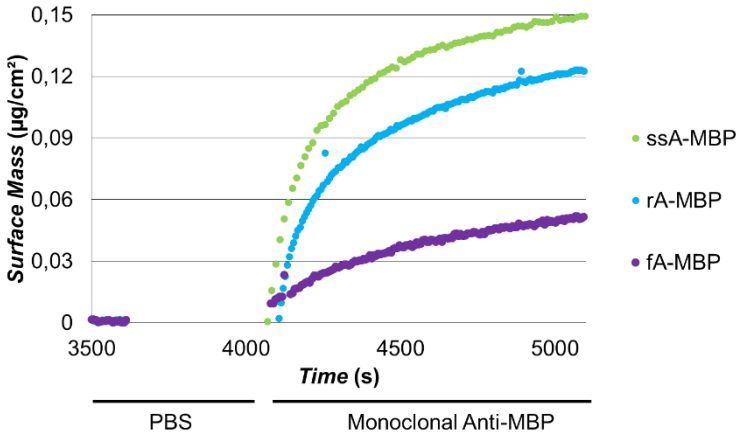

Figure 5.8: Real-time surface mass evolution of the MBP-coupled slides during the binding of monoclonal anti-MBP: ssA-MBP (green), fA-MBP (purple) and rA-MBP (blue).

In **Figure 5.8**, the evolution in surface mass of different samples, functionalised with different alkynated MBP species *i.e.* ssA-MBP, rA-MBP and fA-MBP, during immersion in a monoclonal anti-MBP solution is presented. This resulted in a considerable increase in average surface mass of 0.13 µg/cm² ±0.01 µg/cm² and 0.16 µg/cm² ±0.04 µg/cm² for respectively the rA-MBP and ssA-MBP coated slides, as illustrated in **Figure 5.9**.

As expected, in general more anti-MBP antibodies are able to bind to the ssA-MBP films than the rA-MBP and the fA-MBP samples. The identical orientation for all immobilised site-specifically alkynated proteins creates a homogeneous surface where, in this case, the epitopes are better approachable for the mono-clonal antibodies. Still, it is remarkable that the reproducibility in anti-MBP binding of the rA-MBP substrates is superior to this of the ssA-MBP layers. The origin of this phenomenon remains unclear. Notwithstanding, it can be said that the ssA-MBP sample with the lowest binding capacity of the series of 8 ssA-MBP samples (0.12 µg/cm²) is still able to bind at least as much as the average rA-MBP sample,

proving the potential improvement of a surface covered with oriented mono alkynated MBP.

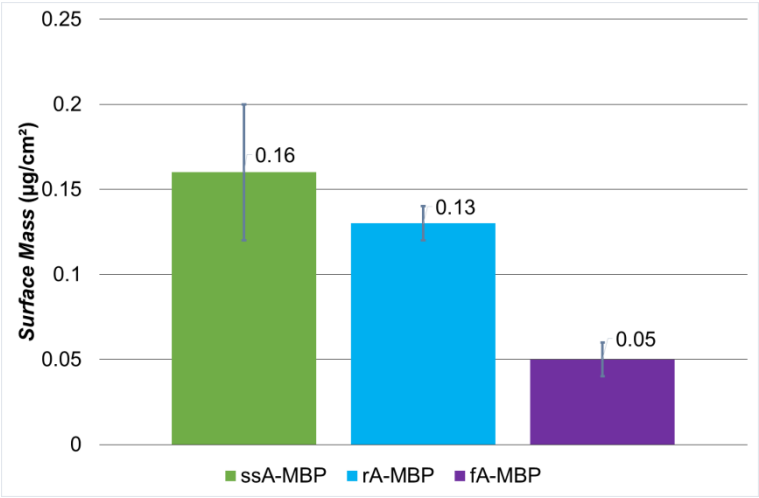

Figure 5.9: Surface mass evolution of the MBP-coupled slides during the binding of monoclonal anti-MBP: ssA-MBP (green), rA-MBP (blue) and fA-MBP (purple).

The fA-MBP functionalised samples were only able to bind a moderate 0.05 µg/cm² of anti-MBP. Despite the initial 25 % higher surface fA-MBP coverage of the samples, the availability of the epitope of interest in these samples is strongly reduced. The amounts correspond to less than 50 % of the amount, which was able to bind to the rA-MBP covered slides and less than 30 % of the amount of the ssA-MBP covered slides. A first explanation is the abundant presence of alkyne groups all over the fA-MBP surface, leading to a surface covered with randomly oriented MBP molecules. This randomly oriented immobilisation hinders the binding between anti-MBP and its target epitope. Secondly, considering the large amount of introduced alkyne groups, it is unlikely that the low amount of coupled anti-MBP is solely due to the non-orientation of the MBP layer. As mentioned before, the excessive alkynation may also well be contributing to the decreased

antibody coupling due to alterations near the anti-MBP epitope [32]. Consequently, minimizing the number of modifications is crucial in order to prevent changes which are leading towards a biosurface with reduced accessibility/activity. By reducing the number of alkyne functionalities and, if possible, introducing these groups at one specific location in every bio molecule, the accessibility of the binding sites will be maximal.

5.3.4 Immobilisation *via* the DROP method

In the previous part, ssA-MBP, rA-MBP and fA-MBP were immobilised on azidified solid carriers. This immobilisation was performed using the method as described in 4.2.6 for alkynated SpA using 400 µL of a 1 µM protein solution per sample. In section 5.2.8, a similar immobilisation procedure has been discussed in which 13 times less A-SpA was needed to obtain biofunctionalised surfaces with identical characteristics. The same procedure was performed using ssA-MBP. Due to the horizontal positioning of the silicon slides, real-time measurements could not be performed during the immobilisation by the DROP method. By determination of the surface mass before and after the CuAAC procedure, the nett mass increase was derived. The next plot shows the amounts of ssA-MBP, which was immobilised using solutions based on *Mixture 1* in acetate buffer at pH 4. The concentrations of copper, reducing agent and ligand are slightly different for each reaction mixture as they vary from 1 up to 10 times the original concentration.

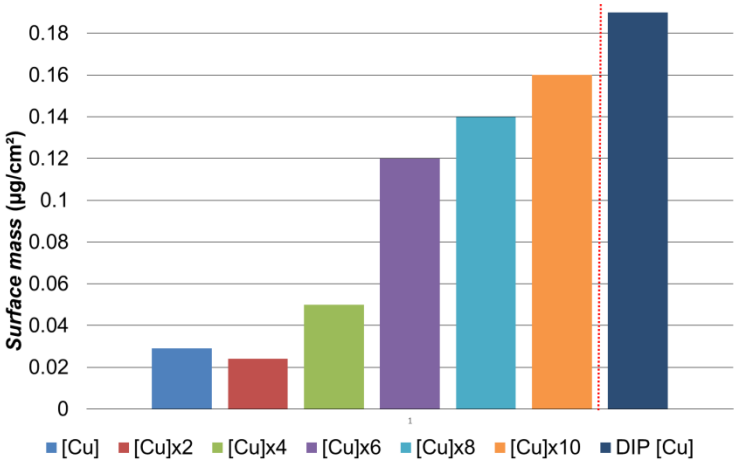

Figure 5.10: Obtained surface mass after performing the DROP method using different ssA-MBP solutions. All solutions contained 1 µM ssA-MBP and a multiple (1 up to 10 times) of the original copper catalyst, reducing agent and ligand concentration as the previously described *Mixture 1* solution in acetate buffer at pH 4. The average amount of immobilised ssA-MBP obtained *via* the earlier performed DIP method experiments is presented at the right of the red dotted line.

As depictured in **Figure 5.10** none of the obtained surface masses reached the values of the DIP method. Almost no immobilisation occurred at the concentration used during the DIP method. When gradually increasing the amount of copper, the amount of immobilised MBP increased as well. Performing the DROP method with a ten times higher amount of catalyst, reducing agent and ligand resulted in a surface mass of 0.16 µg/cm² which is not yet part of the margin of error obtained *via* the DIP method. Still, by ten times increasing the amount of catalyst during the DROP method, it is possible to reach surfaces masses near the averages achieved using the DIP method, however the amount of used protein is 13 times less. It should be noted that this preliminary test towards a lower consumption of difficult to obtain alkynated protein was not yet tested for its reproducibility.

5.4 Conclusions

The reliable and reusable platform towards a covalent intermolecular coupling between A-SpA and azide functionalised silicon slides *via* the copper catalysed azide-alkyne cycloaddition (CuAAC) was used to immobilise maltose binding protein (MBP). Higher surfaces masses could be obtained by immobilising the fully alkynated fA-MBP and random alkynated rA-MBP. However, the site-specifically alkynated ssA-MBP surfaces were able to bind more mono-clonal anti-MBP, where the surfaces covered with random alkynation species (rA-MBP, fA-MBP) led to retention of the binding capacity by its antibodies. This protocol of controlled functionalisation paves the way towards next generation biofunctionalised surfaces with improved sensitivity and selectivity caused by the covalent and oriented surface coupling of bio receptors. In the next chapter the foundation for such a sensing device will be described.

5.5 References

1. Gao Y, Kyratzis I. Covalent immobilization of proteins on carbon nanotubes using the cross-linker 1-ethyl-3-(3-dimethylaminopropyl)carbodiimide—a critical assessment. Bioconjugate Chemistry. 2008;19(10):1945-50.

2. Devaraj NK, Collman JP. Copper catalyzed azide-alkyne cycloadditions on solid surfaces: Applications and future directions. QSAR & Combinatorial Science. 2007;26(11-12):1253-60.

3. Kolb HC, Sharpless KB. The growing impact of click chemistry on drug discovery. Drug Discovery Today. 2003;8(24):1128-37.

4. van Vught R, Pieters RJ, Breukink E. Site-specific functionalization of proteins and their applications to therapeutic antibodies. Computational and Structural Biotechnology Journal. 2014;9(14):1-13.

5. Patil US, Qu H, Caruntu D, O'Connor CJ, Sharma A, Cai Y, *et al.* Labeling primary amine groups in peptides and proteins with N-hydroxysuccinimidyl ester modified Fe_3O_4@SiO_2 nanoparticles containing cleavable disulfide-bond linkers. Bioconjug Chem. 2013;24(9):1562-9.

6. Wang Z, Jin G. Feasibility of protein A for the oriented immobilization of immunoglobulin on silicon surface for a biosensor with imaging ellipsometry. J Biochem Biophys Methods. 2003;57(3):203-11.

7. Sohn Y-S, Lee YK. Site-directed immobilization of antibody using EDC-NHS-activated protein A on a bimetallic-based surface plasmon resonance chip. BIOMEDO. 2014;19(5):051209.

8. Mann M, Jensen ON. Proteomic analysis of post-translational modifications. Nat Biotech. 2003;21(3):255-61.

9. Blom N, Gammeltoft S, Brunak S. Sequence and structure-based prediction of eukaryotic protein phosphorylation sites. J Mol Biol. 1999;294(5):1351-62.

10. Yang XJ, Seto E. Lysine acetylation: codified crosstalk with other post-translational modifications. Mol Cell. 2008;31(4):449-61.

11. Lodish HB, A. Zipursky, SL. *et al*. Molecular Cell Biology. 4th ed. New York: W. H. Freeman; 2000.

12. Springer MS, Goy MF, Adler J. Protein methylation in behavioural control mechanisms and in signal transduction. Nature. 1979;280(5720):279-84.

13. Austermuhle MI, Hall JA, Klug CS, Davidson AL. Maltose-binding protein is open in the catalytic transition state for ATP hydrolysis during Maltose transport. Journal of Biological Chemistry. 2004;279(27):28243-50.

14. David R, Richter MPO, Beck-Sickinger AG. Expressed protein ligation. European Journal of Biochemistry. 2004;271(4):663-77.

15. Muir TW, Sondhi D, Cole PA. Expressed protein ligation: A general method for protein engineering. Proceedings of the National Academy of Sciences. 1998;95(12):6705-10.

16. Berrade L, Camarero JA. Expressed protein ligation: A resourceful tool to study protein structure and function. Cellular and Molecular Life Sciences. 2009; 66(24):3909-22.

17. Muir TW. Semisynthesis of proteins by expressed protein ligation. Annual Review of Biochemistry. 2003;72(1):249-89.

18. Vila-Perelló M, Liu Z, Shah NH, Willis JA, Idoyaga J, Muir TW. Streamlined expressed protein ligation using split Inteins. Journal of the American Chemical Society. 2013;135(1):286-92.

19. Karagöz GE, Sinnige T, Hsieh O, Rüdiger SGD. Expressed protein ligation for a large dimeric protein. Protein Engineering Design and Selection. 2011;24(6): 495-501.

20. Steen Redeker E, Ta DT, Cortens D, Billen B, Guedens W, Adriaensens P. Protein engineering for directed immobilization. Bioconjugate Chemistry. 2013; 24(11):1761-77.

21. Bracher PJ, Snyder PW, Bohall BR, Whitesides GM. The relative rates of thiol-thioester exchange and hydrolysis for alkyl and aryl thioalkanoates in water. Origins of Life and Evolution of the Biosphere: the journal of the Inter-national Society for the Study of the Origin of Life. 2011;41(5):399-412.

22. Zhao W, Zhang Y, Cui C, Li Q, Wang J. An efficient on-column expressed protein ligation strategy: Application to segmental triple labeling of human apolipoprotein E3. Protein Science: A Publication of the Protein Society. 2008; 17(4):736-47.

23. Damen CWN, Speijer H, Hermens WT, Schellens JHM, Rosing H, Beijnen JH. The bioanalysis of trastuzumab in human serum using precipitate-enhanced ellipsometry. Analytical Biochemistry. 2009;393(1):73-9.

24. Duplay P, Bedouelle H, Fowler A, Zabin I, Saurin W, Hofnung M. Sequences of the malE gene and of its product, the maltose-binding protein of *Escherichia coli* K12. Journal of Biological Chemistry. 1984;259(16):10606-13.

25. Chong S, Mersha FB, Comb DG, Scott ME, Landry D, Vence LM, *et al.* Single-column purification of free recombinant proteins using a self-cleavable affinity tag derived from a protein splicing element. Gene. 1997;192(2):271-81.

26. Sletten EM, Bertozzi CR. Bioorthogonal chemistry: Fishing for selectivity in a sea of functionality. Angewandte Chemie International Edition. 2009;48(38): 6974-98.

27. Noren CJ, Wang J, Perler FB. Dissecting the chemistry of protein splicing and its applications. Angewandte Chemie International Edition. 2000;39(3):450-66.

28. Lin PC, Ueng SH, Tseng MC, Ko JL, Huang KT, Yu SC, *et al.* Site-specific protein modification through Cu-I-catalyzed 1,2,3-triazole formation and its implementation in protein microarray fabrication. Angewandte Chemie International Edition. 2006;45(26):4286-90.

29. Ghosh I, Considine N, Maunus E, Sun L, Zhang A, Buswell J, *et al.* Site-specific protein labeling by Intein-mediated protein ligation. Heterologous Gene Expression in Ecoli: Humana Press. Evans JTC, Xu M-Q, editors; 2011:87-107.

30. Ta DT, Redeker ES, Billen B, Reekmans G, Sikulu J, Noben JP, *et al.* An efficient protocol towards site-specifically clickable nanobodies in high yield: Cytoplasmic expression in *Escherichia coli* combined with intein-mediated protein ligation. Protein Engineering, Design & Selection. 2015;28(10):351-63.

31. Lipman NS, Jackson LR, Trudel LJ, Weis-Garcia F. Monoclonal versus polyclonal antibodies: Distinguishing characteristics, applications, and informa-tion resources. Ilar J. 2005;46(3):258-68.

32. Li Y, Urrutia M, Smith-Gill SJ, Mariuzza RA. Dissection of binding interactions in the complex between the anti-lysozyme antibody HyHEL-63 and its antigen. Biochemistry. 2003;42(1):11-22.

33. Billen B, Vincke C, Hansen R, Devoogdt N, Muyldermans S, Adriaensens P, Guedens W. Cytoplasmic versus periplasmic expression of site-specifically and bioorthogonally functionalised nanobodies using expressed protein ligation. 2017; 133:25-34.

Chapter 6. CuAAC mediated *Staphylococcus aureus* protein A immobilisation for QCM measurements

6.1 Introduction

Various (bio) sensor applications have been introduced by the scientific community for targeting different types of toxic and non-harmful molecules. These can vary from common biomolecules, such as glucose [1] and (poly)saccharides [2, 3] to complete systems, such as viruses [4], bacteria [5] or cancer cells [6]. Until now, a limited number of these devices have become a true commercial success. From an economic point of view, the devices have to satisfy several crucial requirements. First of all, the consuming market has to be big enough and the consumer must be willing to pay for the test. Furthermore, from a technical point of view the sensor has to be stable, reliable, selective, have an acceptable response time, a predetermined range, a good life-time and it must be user-friendly [7].

One of the most well-known biosensors is the pregnancy test. The application is based on antibodies, which can bind a hormone called human Chorionic gonadotropin (hCG), present in the urine of pregnant women. The principle is straightforward, the device user-friendly and the market large. This type of tests offers qualitative results, which meet the needs of the consumer. For quantitative information one has to apply to a doctor to receive additional information. Another example of commercialised biosensors which are able to give a very accurate quantification of biomolecules present in human body fluids are glucose sensors.

Besides the healthcare industry, biosensors are utilised for food, environmental and bio threat analysis [8]. Most common targets in food analysis are glucose [9] and lactose [10]. Nitrate [11] and dioxins [12] are examples of targets for environmental testing, while *Salmonella* [13] and *Vibrio cholera* [14] bacteria are

potential threats for society which could be detected by using specifically manufactured sensors.

In order to develop sensors capable of quantifying the number of binding events, different types of non-destructive analytical methods are being used. Many applications are based on changes in optical parameters. Spectroscopy registers interactions with electromagnetic radiation, varying from infrared to ultraviolet, and analysis of these results will lead to an accurate quantification. These interactions can be, amongst others, reflectance, absorbance, fluorescence and luminescence. Also other non-destructive methods based on electrochemical, acoustic and calorimetric changes induced by binding of the target, do provide information in a quantitative manner. Piezoelectric mass quantification, which registers frequency changes of a certain resonant material in order to determine the amount of bound material, is the detection method which will be used in this chapter [15]. The quartz crystal microbalance will serve as a setup for the quantification of antigen-antibody binding events. In 2007, a report was published on the influence of the immobilisation strategy on the QCM frequency response to ligand binding experienced by the estrogenic receptor immobilised by a His-tag [16]. A direct and indirect immobilisation strategy, using a thiol linker complexed with nickel charged Nitrilotriacetic acid (Ni-NTA), was used. It was observed that the QCM only provided signals when the receptor was directly immobilised to the surface without usage of a linker between receptor and the gold covered quartz crystal. However, our preference is to avoid the use of His-tags, due to the fact that they tend to cause problems during purification. For example, other histidine containing molecules might be co-eluted together with other His-tagged molecules, leading to a mixture of different His containing molecules.

Furthermore, they tend to form dimers and tetramers which will affect the formation of homogenous monolayers. In addition, the His-tagged coupled molecules are removable, for example, at low pH, which might lead to a decrease sensing quality.

An alternative procedure was also published in 2007 involving the immobilisation of SpA on a gold coated QCM crystal using a self-assembled monolayer (SAM) of thiol amine in combination with glutaraldehyde to immobilise SpA *via* its lysines [17]. Since this procedure did not allow obtaining a reproducible, covalently bound and homogenously oriented biofunctionalised sensor surface, this method does not satisfy all our need.

In 2012, an article was published on the functionalisation of plasticized PVC membranes on top of a QCM crystal using 'click' chemistry [18]. It was demonstrated that *via* CuAAC introduced modifications the adsorption rates of various proteins towards the modified surface could be altered. The introduction of new functional groups at the surface of the PVC layer using 'click' chemistry resulted in an improvement of the biocompatibility. The modified PVC layers were tested by measuring the adsorption of albumin using QCM.

In this chapter, parts of all three mentioned articles, *i.e.* immobilisation of proteins on a QCM crystal, immobilisation *via* the lysines and in combination with CuAAC, will be combined in order to functionalise a QCM crystal with SpA using CuAAC. As presented in **Figure 6.1** SpA will be used as the receptor molecule. First it will be immobilised *via* the CuAAC method as extensively described and discussed in Chapters 4 & 5. Afterwards, the binding capacity by hIgG will be quantified using frequency changes induced by mass increases on top of the quartz crystal. **Figure 6.1** shows the expected behaviour of the QCM response after CuAAC

immobilisation of alkynated SpA and the adsorption of hIgG on top of the covalent immobilised layer.

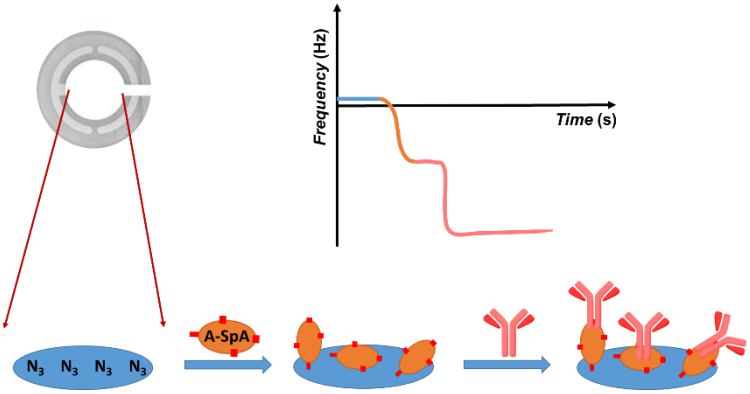

Figure 6.1: Schematic illustration of the frequency changes induced by the A-SpA immobilisation towards an azide functionalised quartz crystal followed by hIgG binding events.

In **Figure 6.1**, the blue part represents the baseline of the azidified quartz crystal. After the covalent immobilisation of SpA and specific adsorption of hIgG, the increase in mass will result in a decrease of the crystal's frequency. The goal of this chapter is to demonstrate the effectiveness of the CuAAC coupling on a platform, different from ellipsometry, that has the potential to serve as a biosensing device.

6.2 Materials & Methods

6.2.1 Materials

SpA (Cowan strain, recombinant, expressed in *E. coli*) and hIgG were obtained from Thermo Scientific. 1-ethyl-3-(3-dimethylaminopropyl) carbodiimide (EDC), *N*-hydroxysuccinimide (NHS), glycine, dodecyl sulphate sodium salt (SDS) and copper(II) sulphate pentahydrate were purchased from Acros. Tris(3-hydroxypropyltriazolylmethyl) amine (THPTA), sodium acetate trihydrate, 4-(2-hydroxyethyl)-1-piperazineethanesulfonic acid (HEPES), diethylene glycolamine and sodium L-ascorbate were obtained from Sigma-Aldrich. TMS-EDTA was purchased from ABCR GmbH & Co. KG (Germany). QCM crystals with 300 nm SiO_2 top layer were obtained from Biolin Scientific.

6.2.2 Solutions

The used solutions were 0.2 M sodium acetate buffer pH 4 (silanisation); 220 mM HEPES pH 6.8; PBS buffer pH 7.4: 137 mM NaCl, 27 mM KCl, 10 mM Na_2HPO_4, 2 mM KH_2PO_4; 0.01 M sodium acetate buffer pH 4 (CuAAC reaction); 0.1 M glycine-0.2 M NaCl pH 2.5; 0.5% SDS in H_2O. Buffers were prepared with Milli-Q water.

6.2.3 Instruments

A Q-sense E4 (Gothenburg, Sweden) Quartz Crystal Microbalance with dissipation monitoring (QCM-D) is an apparatus providing information about the adsorbed mass on a solid support and the viscoelastic properties of the adsorbed layer. This device is able to measure four QCM chips simultaneously. Changes in resonance frequency, Δf, and in dissipation ΔD, induced by the (CuAAC) immobilisation of A-SpA were monitored at a stabilised temperature of 25 °C at five different

overtones (3rd to 11th). Since the overtones are less influenced by the rubber O-ring than the basic resonance frequency they are more accurately representing the mass changes. AT cut quartz crystals, provided with a gold electrode and silicon dioxide-coating (300 nm), with a frequency of 4.95 MHz ±50 kHz, a diameter of 14 mm, a thickness of 0.3 mm and a surface roughness of less than 3 nm were used as substrate for analysis of protein immobilisation. The flow rate was set to 40 µL min^{-1}. PBS, sodium acetate buffer pH 4 containing (A-)SpA, PBS containing hIgG and Glycine were used during the different measurements.

Prior to the deposition experiments, the chips were cleaned with oxygen plasma in a Technics West Inc. reactor, type PEIIA, at 0.5 mbar, with a Power of 50 W and an oxygen flow of 35 sccm during 5 minutes. This cleaning step removed organic contamination and hydroxylised the surface of the SiO_2 covered quartz crystal to prepare it for further functionalisation steps. It should give similar results as the wet cleaning, which was used in the previous chapters.

6.2.4 Functionalisation of QCM crystals

Silanisation of the quartz crystals

Following the plasma cleaning, the clean QCM crystals were silanised. To this end, the quartz crystals were put on a Petri dish and placed horizontally in an oven at 110 °C. At the centre of each crystal, 60 µL of a 6 v/V% TMS-EDTA solution in 0.2 M sodium acetate buffer pH 4 was applied, covering the SiO_2 area in the middle of the crystal. The Petri dish was covered in order to protect the drops from turbulence caused by the fan present in the oven. After incubating the crystals for 1 hour, they were carefully washed with Milli-Q water and dried under a nitrogen flow.

Azidification of the carboxylic silanised quartz crystals

To use, the azide functionalisation procedure described in section 4.2.4, small practical adaptations were required. First of all, the crystal was placed on a Petri dish and put in a closed, with water vapour saturated container at room temperature. At the bottom of the container, water was applied on which the Petri dish was put, creating a horizontal floating platform. To the centre of the crystal, 150 µL of a mixture of EDC (0.2 M), NHS (0.045 M) and 3-azido-1-aminopropane (AAP; 0.23 M) [19] in HEPES buffer pH 6.8 were applied. After 3 hours of incubation the samples were washed with Milli-Q water and dried with nitrogen. The slides were then blocked with 150 µL of diethylene glycolamine for 45 min to neutralize possible remaining NHS esters, rinsed again with Milli-Q water and dried under a nitrogen flow.

6.2.5 Coupling procedure

The CuAAC reaction mixture in sodium acetate buffer (pH 4) contained the reagents as described in *Mixture 1* (*cf.* **Table 4.1**). The concentration of A-SpA, Cu(II)SO_4, sodium L-ascorbate and THPTA are respectively 1 µM, 1.5 mM, 7.5 mM and 3 mM. During the experiment, this solution (1 mL) was equally distributed over two crystals. One crystal was silanised with TMS-EDTA, while the other was silanised and subsequently functionalised with azide groups. The QCM-D registered frequency differences induced by the exposure to the A-SpA containing solution.

6.2.6 Activity of surface coupled A-MBP

Similarly, as has been performed with IgG for SpA in Chapter 4, a 0.33 µM hIgG solution was applied to both crystals. One azidified crystal was functionalised with

CuAAC coupled A-Spa, while the other carboxyl silanised sample was just containing a minute amount of adsorbed A-SpA that could not be removed after the washing with PBS and SDS. Subsequently, a series of dilutions *i.e.* 2 and 4 times lower in concentration, of hIgG were added to the surfaces as well. All interactions between the antibody solutions and the immobilised A-SpA layer were monitored in real-time by QCM.

6.3 Results & Discussion

6.3.1 Frequency and surface mass

The samples needed to be cleaned, silanised and functionalised with azide functionalities before the CuAAC immobilisation of A-SpA could be performed. The plasma cleaning was preferred over the acidic approach due to the SiO_2 etching which affects the quality, the lifetime and especially the frequency of the crystal [20].

During the silanisation step, the volume of the drops containing the TMS-EDTA silane was increased from 10 µL to 60 µL. The reason for this is the increase in surface area, from 24 mm² in case of the previously used ellipsometry slides to 154 mm² of the quartz crystals. Further, it was important to use a horizontal setup during silanisation to obtain a surface area which was entirely, evenly covered with the TMS-EDTA silane solution. One of the samples was not modified after silanisation, while the other sample was further modified with azide functionalities. After placing both quartz crystals in the holder, the samples were exposed to different protein solutions and buffers in order to achieve one A-SpA functionalised surface, and a crystal without covalently bound A-SpA. The latter served as

negative control in order to check for possible physisorption. The experimental results are shown in **Figure 6.2**.

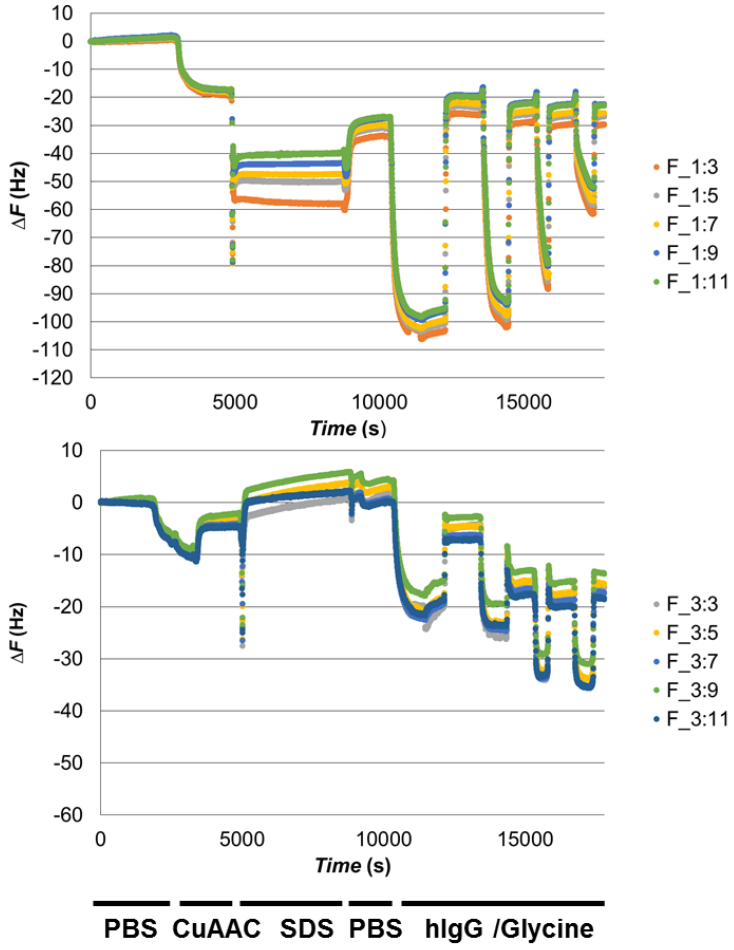

Figure 6.2: QCM frequency changes (*ΔF*) for different overtones (3, 5, 7, 9 and 11) of an azidified (top) and a carboxyl silanised (bottom) quartz crystal induced by addition of different solutions containing A-SpA (CuAAC), SDS, hIgG in different concentrations, glycine or PBS.

Initially a stable baseline was measured for both crystals in PBS buffer demonstrated by the 0 Hz frequency difference. This was done for the basic

resonance frequency F_1 and for the different overtones F_3-11. Since F_1 is being affected by the rubber O-ring, this frequency shifts for this frequency are not shown. The frequency shifts for the other overtones where normalised by dividing the actual frequency shift by the overtone number. This normalization makes it possible to compare them. Next the sodium acetate solution containing 1 µM of A-SpA was pumped over the crystals (±2000 s). A few minutes later the A-SpA CuAAC solution reached the surface and a decrease in frequency of -20 Hz and -10 Hz for respectively the azidified and the carboxyl silanised crystal was observed, which implies an increase in surface mass (**Figure 6.2**; 2000 s – 5000 s). When stopping the flow inside both cells, the frequency of the carboxyl surface increased again as can be seen by the decrease in frequency difference compared to the baseline frequency. The frequency of the azide surface remained constant at a certain point in time and was not influenced by stopping the flow. Since frequency changes are caused by either physisorption or by covalent binding, extensive rinsing with SDS was performed in order to remove the non-covalently coupled A-SpA. A washing step with 'washing' buffer (W.B.), as was performed in the previous chapters, had a negative influence on the stability of the signal. Most likely, the ethanolamine or EDTA present in the washing buffer caused a disturbance in signal which could not be removed anymore.

In the following step, rinsing with PBS resulted in a net frequency change of approximately 30 Hz for the azidified crystal while the resonance frequency of the carboxyl crystal went back to the baseline frequency. At this point (10380 s) the changes in frequency for every overtone, $\Delta F_{A\text{-}SpA}$, were used to determine the amount of A-SpA, $\Delta M_{A\text{-}SpA}$, on both crystals as is presented in **Table 6.1** and **Table 6.2**.

Table 6.1: Mass changes caused by A-SpA (($\Delta M_{A\text{-}SpA}$ (µg/cm²); t: 10380 s), hIgG (ΔM_{hIgG} (µg/cm²); t: 12162 s) and glycine solution (ΔM_{Gly1} (µg/cm²); t: 12855 s) accompanied by their belonging surface mass, for the different overtones n of the azide functionalised quartz crystal.

N	**1**	**3**	**5**	**7**	**9**	**11**	**13**
$\Delta M_{A\text{-}SpA}$ (µg/cm²)	0.75	**0.60**	**0.55**	**0.53**	**0.48**	**0.48**	**0.51**
ΔM_{hIgG} (µg/cm²)	1.20	**1.23**	**1.23**	**1.23**	**1.22**	**1.21**	**1.22**
ΔM_{Gly1} (µg/cm²)	0.51	**0.45**	**0.41**	**0.39**	**0.34**	**0.35**	**0.38**

Table 6.2: Surface mass changes (µg/cm²) caused by immobilising A-SpA (ΔFA-SpA; t: 10380 s), hIgG (ΔFhIgG; t: 12162 s) and washing with a glycine solution (ΔMgly1; t:12855 s) for the different overtones n of the carboxyl silanised quartz crystal.

N	**1**	**3**	**5**	**7**	**9**	**11**	**13**
$\Delta M_{A\text{-}SpA}$	0.26	**0.00**	**-0.02**	**0.02**	**-0.04**	**0.03**	/
ΔM_{hIgG}	0.01	**0.34**	**0.32**	**0.30**	**0.28**	**0.28**	/
ΔM_{Gly1}	1.23	**0.08**	**0.08**	**0.11**	**0.05**	**0.13**	/

Subsequently, a 0.33 μM hIgG solution in PBS was added to both crystals. Coupling between hIgG and the A-SpA containing azidified crystal and between the hIgG and the carboxyl silanised crystal occurred according to the recorded frequency changes as demonstrated in **Figure 6.2**. In case of the azide crystal the change was more explicit, *i.e.* a nett difference of approximately 70 Hz, whereas only 20 Hz for the carboxyl silanised crystal was observed. The net hIgG mass increases, ΔM_{hIgG}, (12162s) of every overtone for both crystals are being presented in **Table 6.1** and **Table 6.2**.

In the final step, glycine was used to break the specific bonds between the formed hIgG layer and the A-SpA surface. To remove the fraction of hIgG, that is aspecifically adsorbing to the crystal, the glycine solution will not be sufficient and an additional SDS washing step will be required to break the bond between hIgG and the surface. From the resulting frequency shifts after this washing step, the according mass changes (ΔM_{gly1}) were calculated and presented in **Table 6.1** and **Table 6.2**. The mass of the azide surface returns to its original values, while still a small fraction of the hIgG remains on the surface. The same steps were repeated multiple times at different concentrations. To this end, the samples were exposed again to the 0.33 μM hIgG solution and flushed again with glycine. In addition, the responses to solutions containing lower hIgG concentrations, *i.e.* 0.17 μM and 0.085 μM, and to the washing solution with glycine were measured. The differences in response for both crystals are shown in **Figure 6.3** from 15000 until 17800 seconds. This is an enlargement of **Figure 6.2**.

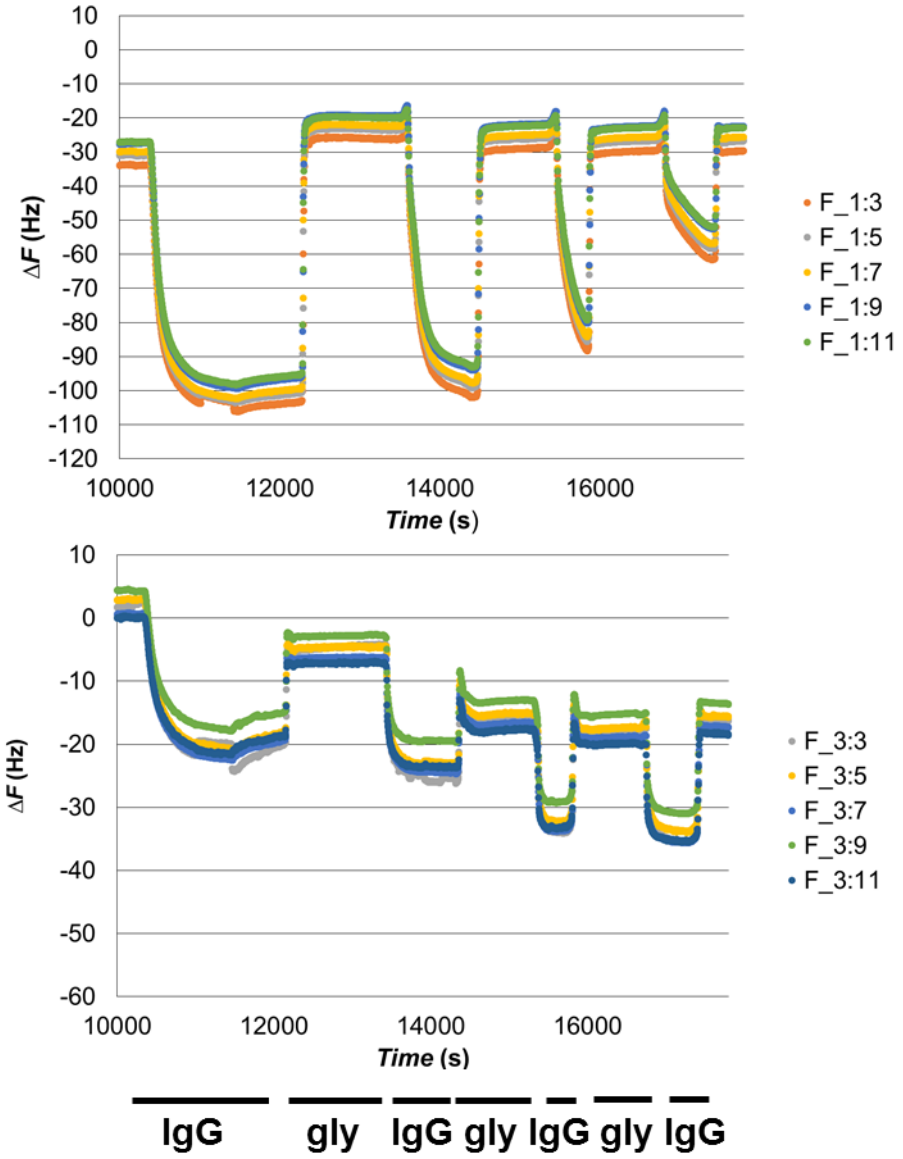

Figure 6.3: QCM frequency changes (*ΔF*) for different overtones (3, 5, 7, 9 and 11) of an azidified (top) and a carboxyl silanised (bottom) quartz crystal with A-SpA, induced by addition of hIgG (0.33 µM, 0.33µM, 0.17µM and 0.085 µM) and flushing with glycine.

It can be seen that by applying a two times diluted hIgG solution to the with A-SpA immobilised azidified surface (**Figure 6.2**; top) a smaller frequency change

is induced than was obtained for the original concentration. The frequency difference drops with 10 to 20 Hz depending on the overtone. The frequency measured for the four times diluted hIgG solution differs 40 to 50 Hz from the frequency change which occurred for the original concentration. After rinsing with glycine, the signal of the azide crystal returned to its starting value for all hIgG concentrations. On the other hand, the response of the carboxyl surface to hIgG exposure is less explicit (**Figure 6.2**; bottom). When applying the 0.33 µM solution to the carboxylated crystal, a frequency change of 20 Hz takes place. After washing the carboxyl surface with glycine the frequency changes again but does not go back to its initial frequency. Apparently, there is a small but steady accumulation of hIgG on the surface, which cannot be removed by glycine. For the lower hIgG concentrations still a difference can be noticed between the amount of specifically bound hIgG to the A-SpA covered azidified crystal and the carboxyl silanised crystal. Where the 0.17 µM and 0.085 µM hIgG solutions are causing frequency shifts of respectively 50 and 25 Hz for the A-SpA covered crystal, this shift in frequency is only 10 Hz for both concentrations on the carboxylic crystals. After all the glycine washing steps and without performing an additional flushing step with SDS, part of the hIgG, causing a 20 Hz frequency shift, remains on the carboxylated slide. In contrast, the signal for the A-SpA covered crystal returns to its baseline, which was obtained after CuAAC immobilisation of A-SpA.

The evolution in surface mass can be derived from the frequency shifts, caused by pumping the different solutions over the crystals, using the Sauerbrey equation [21]. In this equation ΔF can be: $\Delta F_{A\text{-}SpA}$, which is the frequency shift caused by the CuAAC solution containing A-SpA solution; ΔF_{hIgG} which is the frequency shift

caused by the 0.33μM hIgG solution; ΔF_{gly} which is the frequency change after flushing with glycine.

$$\Delta m = \frac{-C \times \Delta F}{n} \qquad \text{Equation 6.1}$$

In this equation C is a constant related to the sensitivity of the device to the changes in mass (C= 17.7 ng Hz^{-1} cm^{-2} for 5 MHz quartz crystal) and n stands for the overtone number. In case of a rigid layer all the calculated mass differences for every overtone should be the same. Many researchers consider proteins as soft wet materials, others state that proteins should be considered as a rigid layer due to the fact that proteins do not contain any water molecules on the inside and the interior of protein subunits and domains consist of closely packed atoms [22, 23]. From the frequency drops and the calculated mass changes coming along with each overtone, it can be seen that there is only a small difference between the different overtones, pointing towards the statement that the covalently coupled A-SpA layer results in a quite rigid layer. The A-SpA surface mass for the different overtones of the azide sample (3, 5, 7, 9 and 11 at time: 10380s) varies from 0.48 μg/cm² to 0.60 μg/cm². It should be noted that in general overtone 1 is not used because possible interference by the O-ring to which the crystal is attached. These values are quite high compared to the surface mass densities measured by ellipsometry, as was reported earlier in section 4.3.2.

When estimating the increase of hIgG on top of these A-SpA layers by the 0.33 μM hIgG solution (at 12162 s) an almost constant value is found of about 1.22 μg/cm², as is presented in **Table 6.1** (corresponds with ±49000 hIgG molecules per μm²). This hIgG layer approaches the mass of a close-packed hIgG monolayer. After rinsing with glycine, the mass on the azide surface went down

to 0.34 -0.45 µg/cm², which confirms the specific binding of the hIgG molecules to the A-SpA layer, which was also seen for the experiments recorded by ellipsometry. The additional washing step with glycine further removed some of the presumably non-covalently immobilised A-SpA molecules, which remained on the surface even after washing with SDS. Eventually, after different cycles of binding to hIgG and washing with glycine the remaining A-SpA layer had a mass of approximately 0.35 µg/cm², which is in agreement with a 0.36 µg/cm² close-packed SpA monolayer [24].

The frequency measurements of the carboxyl silanised crystal after exposure to the A-SpA containing CuAAC solution and washing with SDS, as presented in **Table 6.2**, do not show the presence of A-SpA on the surface ($\Delta M_{A\text{-}SpA}$ is close to zero). This indicates that no stable, covalent bond between the A-SpA layer and the carboxyl silanised surface was created. After exposure to the 0.33 µM hIgG solution of the crystal, a layer of physically adsorbed hIgG molecules of approximately 0.30 µg/cm² formed on the carboxyl silanised surface. Keeping in mind that a close packed monolayer of side-on oriented IgG molecules has a surface mass of 0.30 µg/cm², it seems most likely that at least a non-covalently coupled, side-on monolayer had been formed. However, most of the mass could be removed after performing several cycles of hIgG adsorption and glycine rinsing. Only an accumulating layer of adsorbed IgG molecules, which cannot be remove by glycine, remained on the COOH surface.

6.3.2 Surface thickness & visco-elasticity

Theoretical calculation of visco-elastic layer

By fitting the results from the different overtones (**Table 6.1** and **Table 6.2**) insights can be obtained about the visco-elastic properties and the thickness of the layer. Theoretically, the thickness of the monolayer can be calculated using equations, which can be found in the literature [25]. By calculating the volume of A-SpA using its molecular weight (Equation 6.2: Theoretical estimation of the protein volume based on its molecular weight) and considering the protein to be spherical, the radius of the protein can be calculated.

$$V\ (nm^3) = \left(\frac{\left(0.73 \frac{cm^3}{g}\right) \times (10^{21} nm^3/cm^3)}{6.022 \times \frac{10^{23} Da}{g}} \right) \times M\ (Da) = 1.212 \times 10^{-3} \left(\frac{nm^3}{Da}\right) \times M(Da)$$

Equation 6.2

By using the equation of the volume *V* of a sphere, which is presented in Equation 6.3, the minimal radius, R_{min}, which is needed to contain a given mass, can be calculated.

$$V = \frac{4}{3} r^3 \pi \ \rightarrow Rmin = \left(\frac{3V}{4\pi}\right)^{\frac{1}{3}} or\ Rmin = 0.066\ M^{1/3}$$

Equation 6.3

Using both formulas it is derived that the surface is covered by A-SpA with a thickness of minimum 4.8 nm (R_{min}= 2.4 nm). The thickness of the A-SpA layer can be confirmed by the calculation based on the information provided by Lahiri *et al.* [24], where an A-SpA monolayer contains 0.36 µg/cm² or 7.2 10^{-3} nmol/cm². This corresponds to a surface area of 23.22 nm² per A-SpA molecule or, given it is a sphere, a radius of approximately 2.7 nm. This means that the layer thickness is 5.4 nm. In this case, the total area which is covered by each

protein is the sum of the surface covered by the actual protein and the area created by repulsion by neighbouring, similarly charged proteins. This additional area accounts for the higher thickness derived from the second method of calculation.

Modelling of the visco-elastic layer

When comparing these 'theoretical' results with the values obtained from the computed Voigt-Kelvin, as described in section 2.4.2, the remodelled results, as depicted in **Figure 6.5**, show great similarities with the theoretical results. The remodelled results are based on frequency changes and energy dissipation of the different overtones after immobilisation (**Figure 6.4**). In **Figure 6.4** (top) can be seen that the energy dissipation before and during CuAAC immobilisation of A-SpA is less than 1 Hz. This points towards the fact that the A-SpA layer acts as a rigid layer. However, during the washing step with SDS the dissipation increased, for some overtones to a difference of 8 Hz. This can be explained by the fact that binding of SDS to the A-SpA molecules, causes partial denaturation of the proteins, which increases the damping effect on the vibration. When flushing with PBS, the dissipation decreases again but does no longer return to its original value. This could be demonstrating that washing with SDS has to be kept to a minimum in order to reduce conformational changes in the proteins as much as possible. After adding IgG, the dissipation doubles, even for the lower hIgG concentrations. The glycine step appears not to have a permanent effect on the dissipation as was the case for SDS. Nevertheless, it must be said that this washing step is not strong enough to remove all non-covalently bound proteins as was demonstrated in **Table 6.2** and is shown in **Figure 6.6**.

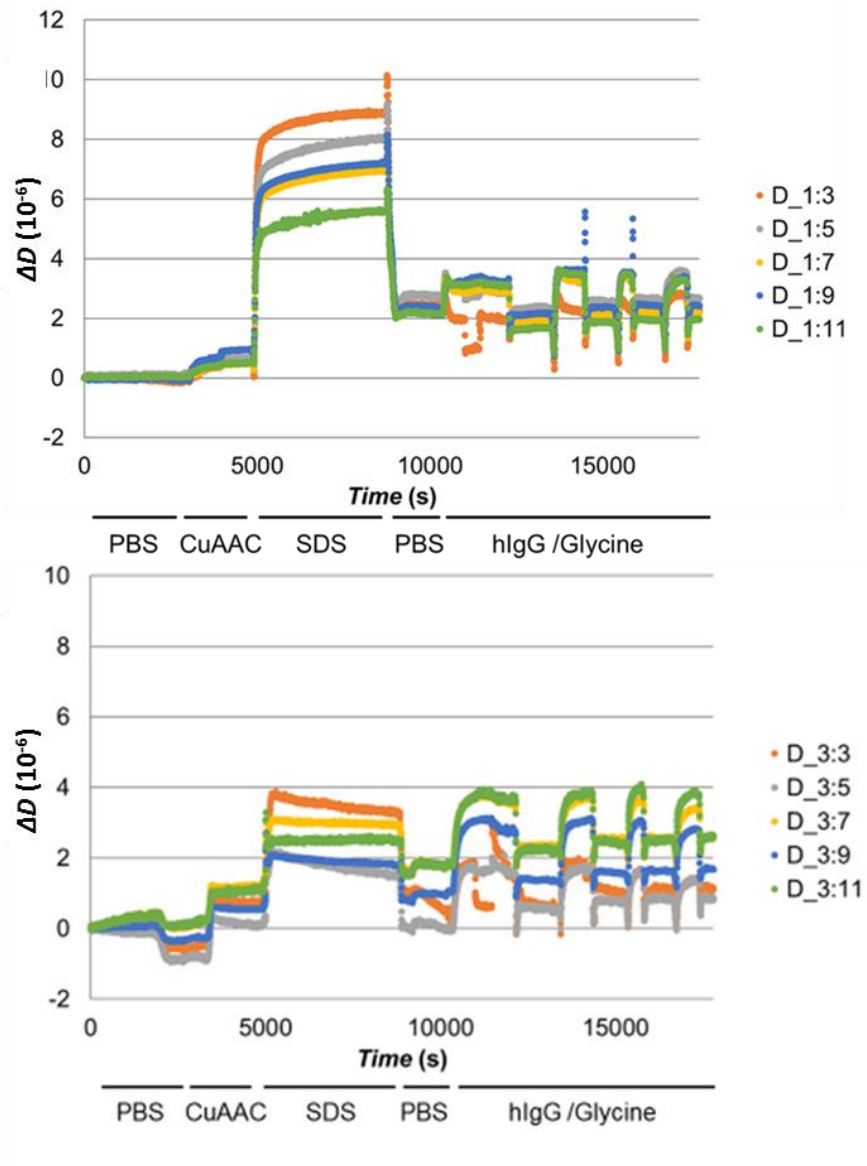

Figure 6.4: The change in energy dissipation (*ΔD*) for the different overtones (3, 5, 7, 9 and 11) of the azide functionalised (top) and the carboxyl silanised (bottom) quartz crystal induced by different solutions containing A-SpA (CuAAC), SDS, hIgG, glycine or PBS.

After remodelling, using the results of ΔF and ΔD for all the overtones, the layer thickness of the immobilised A-SpA on the azidified surface is estimated at 6 nm

after 2h46 after starting the experiment, as can be seen in **Figure 6.5** (green). This is just slightly higher than the theoretical values earlier calculated by means of Equation 6.3.

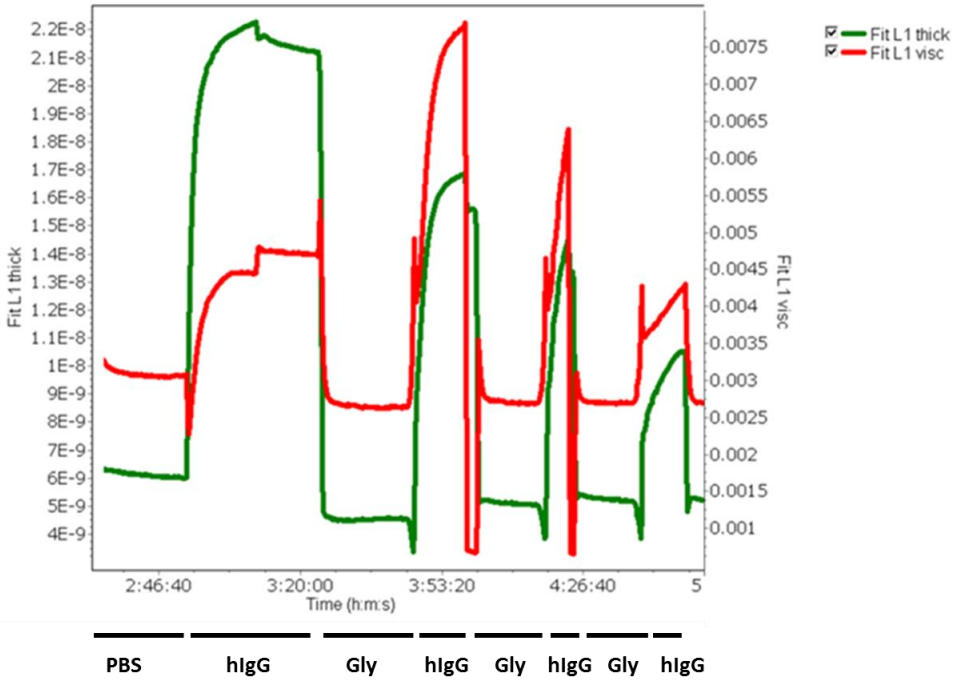

Figure 6.5: Thickness (green; m) and viscosity (red; Pa·S) of the A-SpA layer after fitting ΔF and ΔD for overtones (n: 3 and 11) after CuAAC immobilisation of A-SpA on the azide functionalised quartz crystal.

Applying 0.33 µM hIgG solution in PBS to the A-SpA covered crystal resulted in an initial increase of 16 nm in thickness. When rinsing the crystal with a glycine solution at pH 2.5, all hIgG molecules were removed. At the same time, also some A-SpA molecules were washed away, which were not yet removed after flushing with SDS. This additional washing led to an A-SpA covered surface with a thickness of ±4.5 nm. This value is in the same order of magnitude as the

theoretical thicknesses calculated using the information derived from the literature, *i.e.* 5.4 nm [24] or 4.8 nm [25] (*vide supra*).

A second exposure of the sample to the 0.33 μM hIgG solution, resulted in an increase in layer thickness up to 12 nm. These values are approaching the dimensions of a single hIgG layer, since the molecules have a dimension approaching 14.5 nm x 8.5 nm x 4 nm [26]. This suggests that the hIgG layer is a mixture of side-on and end-on oriented hIgG molecules. When decreasing the concentration further to 0.17 μM and 0.083 μM, the thickness decreased to respectively 9 and 5 nm. Apparently, the amount of bound hIgG influences the orientation on the surface, thereby influencing the thickness of the layer. The more hIgG is present in the solution, the more will be able to bind the A-SpA surface. Due to intermolecular interactions, the hIgG molecules are reorienting themselves.

Subsequently, after rinsing with glycine the hIgG molecules could be removed again, resulting in a layer thickness of 5 nm. This implies that the A-SpA surface is reusable, even after multiple binding and detaching cycles. As mentioned before, a covalent immobilisation strategy has the potential advantage of being reusable [27].

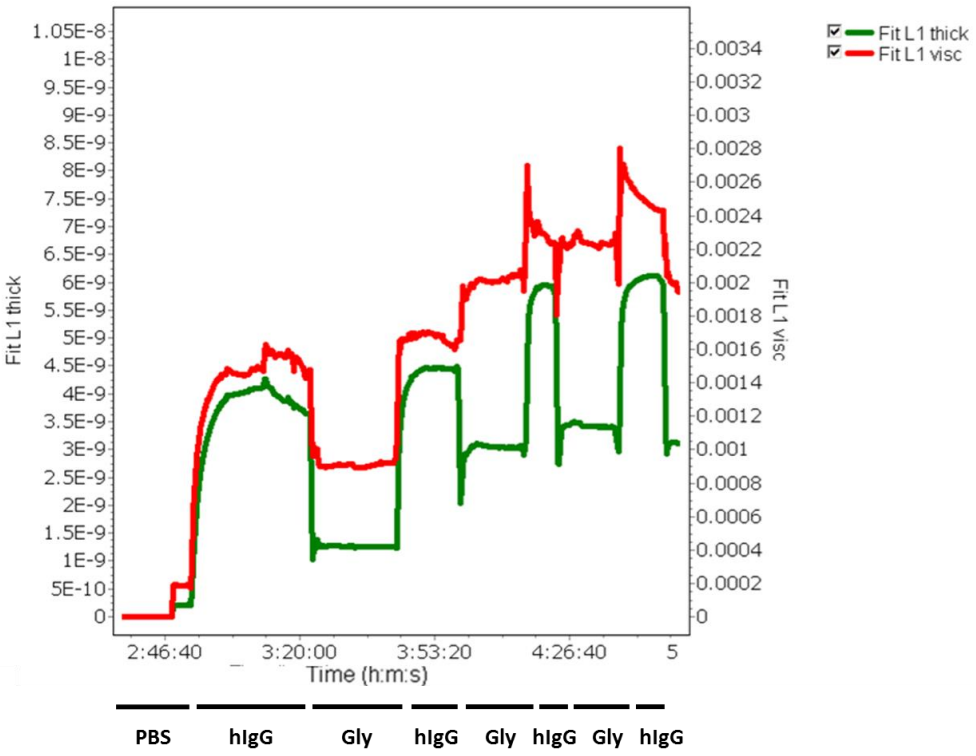

Figure 6.6: Thickness (m; green) and viscosity (Pa·S; red) of the visco-elastic layer after fitting ΔF and ΔD for the different overtones (n: 3,5,7,9 and 11) after immobilisation of A-SpA on the carboxyl silanised quartz crystal.

The layer thickness of the carboxylic surface after applying the A-SpA containing CuAAC mixture and washing with SDS, as described in section 6.2.5, is presented in **Figure 6.6**, 2h46 after starting the experiment. After remodelling all the available data, apparently no protein layer was detected on the carboxylic silanised crystal. After exposure to the 0.33 µM hIgG solution, an increase of 4.5 nm in thickness was detected, which is comparable to a hIgG layer of which the molecules are laying horizontally on the surface. After rinsing with glycine, the layer thickness went back to 1.5 nm. After four cycles comprising the addition of hIgG and the rinsing with glycine at 5h after starting the experiment, the baseline

was increased towards a thickness of 3 nm as compared to the original sample. This demonstrates that not all hIgG molecules can be rinsed off with glycine and a certain amount remains sticking at the carboxylated surface. Apparently, the increase in thickness of the carboxylated crystal is completely determined by physisorption of hIgG to the carboxylated layer. In contrast, for the surface functionalised with A-SpA, all hIgG molecules can be removed by glycine, proving its specific binding.

When comparing the visco-elasticity of the layers on top of the azide and the carboxyl functionalised quartz crystal, depicted as the red curve in **Figure 6.7**, a second difference can be seen. Whereas the visco-elasticity of the layer on top of the azide sample, before applying hIgG and after the washing with glycine remains stable around 0.003 Pa·S, the visco-elasticity of the carboxylic sample starts at 0 after being exposed to the CuAAC mixture. When going through the different cycles of hIgG exposure and glycine washing, this value gradually goes up to 0.002 Pa·S, which is only slightly lower than the value measured for the azidified surface after covalently coupling the A-SpA layer.

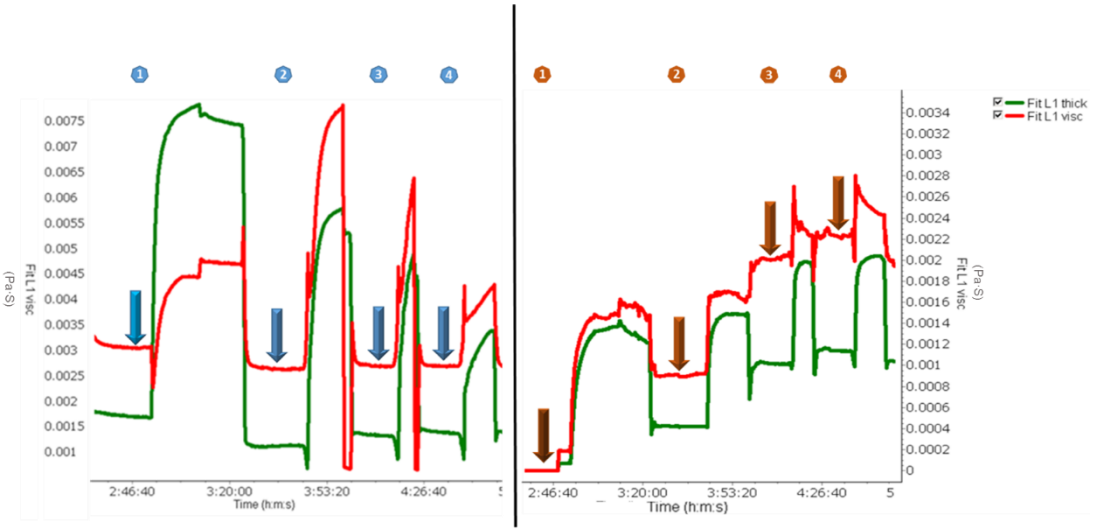

Figure 6.7: Thickness (green; unit: m) and viscosity (red; unit: Pa·S) of the visco-elastic layer after fitting ΔF and ΔD for the different overtones after immobilisation of A-SpA on the azidified (left) and carboxyl (right) silanised quartz crystal. The viscosity level was marked after each flushing step, demonstrating its evolution for both surfaces.

As expected, by flushing the azidified crystal with the glycine solution, this extra layer of hIgG could be removed, resulting in the visco-elasticity to return to 0.003 Pa·S. This is not the case for the carboxylic surface, which has remained covered with a biolayer consisting of hIgG, which is absorbing to the carboxylic surface.

6.4 Conclusions

The CuAAC immobilisation method, initially measured in real-time by null-ellipsometry, was now applied to a quartz crystal provided with a silicon oxide layer in order to perform QCM-D measurements. Differences in frequency and dissipation after performing the CuAAC immobilisation of alkynated SpA were monitored. In addition, the QCM-D response was followed during the washing steps and immobilisation of hIgG to the covalently coupled SpA layer. From these changes the surface mass and the viscoelastic properties of the formed biolayers were monitored in real time. Surface analysis by means of QCM-D demonstrated that, after remodelling the observed changes in frequency and dissipation, the layer thicknesses (5 nm) were comparable to the ones obtained from theoretical calculations. The changes in dissipation showed that the immobilised SpA layer behaves in good approximation as a rigid layer. Furthermore, it was shown that the hIgG layer, which was immobilised with its Fc domain towards the SpA layer, could be removed completely, demonstrating it specificity towards the A-SpA layer. The quartz crystal could be used for multiple hIgG binding and unbinding cycles, demonstrating its stable covalent bond with the solid crystal surface.

6.5 References

1. Wang J. Electrochemical glucose biosensors. Chem Rev. 2008;108(2):814-25.

2. Stoica L, Ludwig R, Haltrich D, Gorton L. Third-generation biosensor for lactose based on newly discovered cellobiose dehydrogenase. Anal Chem. 2006; 78(2):393-8.

3. Tasca F, Ludwig R, Gorton L, Antiochia R. Determination of lactose by a novel third generation biosensor based on a cellobiose dehydrogenase and aryl diazonium modified single wall carbon nanotubes electrode. Sens Actuators, B. 2013;177:64-9.

4. Yanik AA, Huang M, Kamohara O, Artar A, Geisbert TW, Connor JH, *et al.* An optofluidic nanoplasmonic biosensor for direct detection of live viruses from biological media. Nano Lett. 2010;10(12):4962-9.

5. Huang X-J, Choi Y-K. Chemical sensors based on nanostructured materials. Sensors and Actuators B: Chemical. 2007;122(2):659-71.

6. Eersels K, van Grinsven B, Vandenryt T, Jimenez-Monroy KL, Peeters M, Somers V, *et al.* Improving the sensitivity of the heat-transfer method (HTM) for cancer cell detection with optimized sensor chips. Phys Status Solidi A. 2015; 212(6):1320-6.

7. Kisaalita WS. Biosensor standards requirements. Biosensors and Bioelectronics. 1992;7(9):613-20.

8. Bahadır EB, Sezgintürk MK. Applications of commercial biosensors in clinical, food, environmental, and biothreat/biowarfare analyses. Analytical Biochemistry. 2015;478:107-20.

9. Wu H-P, Jung S-K, inventors; Bayer HealthCare LLC, USA, assignee. Biosensor system with signal adjustment and application for blood glucose sensors; patent WO2010077660A1. 2010.

10. Reardon KF, Dandy DS, Holcomb RE, inventors; Colorado State University Research Foundation, USA. Biosensing systems for measurement of lactose; patent WO2012071471A2. 2012.

11. Sohail M, Adeloju SB. Nitrate biosensors and biological methods for nitrate determination. Talanta. 2016;153:83-98.

12. Kitamura M, Maeda S, inventors; Yamanashi University, Japan, assignee. DRESSA: biosensing of dioxin and dioxin-like chemicals using secreted alkaline phosphatase; patent WO2005113767A1. 2005.

13. Chen Z, inventor Peop. Rep. China, assignee. A biosensor chip for rapid detection of Salmonella typhimurium; patent CN104749379A. 2015.

14. Cha HJ, Kim CS, Seo JH, Shin H, inventors; Postech Academy-Industry Foundation, S. Korea, assignee. Fabrication and use of carbohydrate chip for detection of Vibrio cholerae; patent US20130267433A1. 2013.

15. Gautschi G. Background of piezoelectric sensors. Piezoelectric Sensorics: Springer Berlin Heidelberg; 2002:5-11.

16. Baltus RE, Carmon KS, Luck LA. Quartz crystal microbalance (QCM) with immobilised protein receptors: Comparison of response to ligand binding for direct protein immobilization and protein attachment via disulfide linker. Langmuir. 2007;23(7):3880-5.

17. Boujday S, Briandet R, Salmain M, Herry J-M, Marnet P-G, Gautier M, *et al.* Detection of pathogenic *Staphylococcus aureus* bacteria by gold based immunosensors. Microchimica Acta. 2008;163(3-4):203-9.

18. Pawlak M, Mistlberger G, Bakker E. *In situ* surface functionalization of plasticized poly(vinyl chloride) membranes by 'click chemistry'. Journal of Materials Chemistry. 2012;22(25):12796-801.

19. Hatzakis NS, Engelkamp H, Velonia K, Hofkens J, Christianen PCM, Svendsen A, *et al.* Synthesis and single enzyme activity of a clicked lipase-BSA hetero-dimer. Chemical Communications. 2006 (19):2012-4.

20. Johannsmann D. Considerations for well-controlled QCM experiments: Fundamentals and modeling. The Quartz Crystal Microbalance in Soft Matter Research. 2015:377-85.

21. Sauerbrey G. Verwendung von Schwingquarzen zur Wägung dünner Schichten und zur Mikrowägung. Zeitschrift für Physik. 1959;155(2):206-22.

22. Richards FM. The interpretation of protein structures: Total volume, group volume distributions and packing density. Journal of Molecular Biology. 1974;82(1):1-14.

23. Gittes F, Mickey B, Nettleton J, Howard J. Flexural rigidity of microtubules and actin filaments measured from thermal fluctuations in shape. J Cell Biol. 1993;120(4):923-34.

24. Lahiri J, Isaacs L, Tien J, Whitesides GM. A Strategy for the generation of surfaces presenting ligands for studies of binding based on an active ester as a common reactive intermediate: A surface plasmon resonance study. Anal Chem. 1999;71:777-90.

25. Erickson HP. Size and shape of protein molecules at the nanometer level determined by sedimentation, gel filtration, and electron microscopy. Biol Proced Online. 2009;11:32-51.

26. Tan YH, Liu M, Nolting B, Go JG, Gervay-Hague J, Liu G-y. A nano-engineering approach for investigation and regulation of protein immobilization. ACS Nano. 2008;2(11):2374-84.

27. Pulido-Tofiño P, Barrero-Moreno JM, Pérez-Conde MC. Flow-through fluoroimmunosensor for isoproturon determination in agricultural foodstuff: Evaluation of antibody immobilization on solid support. Analytica Chimica Acta. 2000;417(1):85-94.

General discussion and future perspectives

Surface modifications are being applied in countless applications. When it comes to modifying these surfaces with biological materials, there are some restrictions since these molecules cannot stand the harsh conditions which are often used. An aqueous environment is one of key conditions in which the coupling should be performed. Also, the temperature has to be in an acceptable range. Since biomolecules possess several functional groups, various chemical reactions could be used to create strong bond between the surface and the biomolecule. However, not all chemical reactions can be performed without heating, in aqueous environment and are still efficient. The high amount of different functional groups makes it not difficult to find a group which will be used as the 'anchoring' molecule. The disadvantage is that, when a certain functional group has been selected, this functional group is most likely not just a single group in the entire molecule. This would mean that when coupling the molecule, different orientations are possible. If the application requires a protein layer which is still capable of performing its initial purpose, binding other target molecules, *i.e.* receptors in cells or small molecules, the orientation is crucial. Therefore, the chemistry of interest should be highly efficient, should be able to be performed in an aqueous environment, has to be performed at a temperature which the protein of interest can withstand and the functional group which will be used as an anchoring point has to be unique. In this thesis, the CuAAC demonstrated itself a chemistry, which is suited for getting the job done while meeting all previously mentioned parameters. All presented results showed that the CuAAC can be used as a reliable way to biofunctionalise surfaces for numerous applications. The CuAAC coupling could be very interesting in biomedical applications, where many different, less reliable and efficient methods currently still are being applied to modify the surface with biological molecules. Biosensors are a good example of an application which

requires a surface functionalised with biomolecules. These sensors have a large scala of potential markets in which they can be of use. Obviously, there is the clinical/medical market in which medical practitioners will be able to run tests at their cabinet. Furthermore, these sensors will be used for drug testing, clinical and home diagnostics and monitoring during surgical interventions. Biosensors could also be implemented into the industry where they could be of use in quality control, (bacterial) contamination detection, water and waste screening (*e.g.* hazardous side products) and in food and drug processing. In agriculture and veterinary medicine, an early diagnosis with biosensors could avoid the presence of infection and disease in animals and plants, disasters among farmers and the people consuming their products. In addition, the soil and groundwater could be tested on a regular basis to check and maintain or even improve their quality and thereby protecting the environment from pollution.

In times of chemical and biological warfare attacks, biosensors could be used against artificial, modified viruses and bacteria that are used by the enemy to harm human health. Drugs with very specific targets, could be modified with antibodies to very specifically address their target.

In order to develop biosensors which are sensitive and specific enough, the properties of recognition layer need to be optimal. This means an optimal orientation and accessibility of the antigen-binding parts, an optimal surface coverage density and stability. By further improving these factors, in the near future it will be possible to create biosurfaces, containing several different antibodies with all their specific antigens. CuAAC demonstrated to be a suitable chemistry to create reproducible, dens, oriented protein layers. In this work, proteins like SpA (random functionalised) and MBP (site-specifically

functionalised) were used as model proteins in order to optimise the conditions in which the covalent immobilisation using CuAAC took place. Buffers, protein concentration, ligand and catalyst concentration, the amount of alkynation and azidification were all examined in this work in order to optimise the surface coverage. The described, optimised procedure is already being applied for biofunctionalising of azidified poly (p-phenylene ethynylene) (PPE) copolymers functionalised with protein A. The PPE has the potential to be used as a transducer layer, especially since binding events can accurately be determined due to electrochemical or optical changes. Further advantages are that they can be produced at low costs, is flexible and can easily be printed [1]. Next to the immobilization of protein A, another type of receptor molecules*, i.e.* nanobodies, could be used for biosensing applications since not all target binding molecules are as stable as others. Such nanobodies, are very stable, single domain antibodies [2], and can be specifically created to interact with a predetermined target [3]. This makes them very suited for all kinds of target molecules. Vascular Cell adhesion protein (VCAM) could be one of the many possible targets. This nanobody based sensor would be able to detect and quantify the presence of VCAM, a biomarker of arthrosclerosis [4]. The first article regarding such VCAM sensors has been published and looks very promising [5]. Since these nanobodies are much smaller than regular antibodies, miniaturisation of the sensing surface without changing the detection limit could be one of the options. Since less surface area would be needed, this kind of improvements could pave the way towards multi-target biosensing devices.

Next to diagnostic tools, biofunctionalised surfaces are of interest for therapeutic use as well. By efficiently biofunctionalising drugs with antibodies, of which the orientation is well-controlled, bio conjugated medical treatment can be developed

which will only target 'sick' cells which carry the antibody's specific antigen. The optimized CuAAC immobilisation protocol would be well suited to functionalise drugs, targeting specific (cancer) cells. Furthermore, for certain drugs crossing the Blood Brain Barrier could be difficult. By creating a bio conjugated version of the drug, certain areas can be treated, which were unreachable previously [6].

Immunoaffinity chromatography is another application in which the orientation of the immobilised proteins is crucial and the described CuAAC immobilisation procedure would have great potential. This would make it possible to efficiently extract even the lowest amounts of a certain target molecule from a complex matrix, such as blood samples.

These are just a handful examples of the great potential that the optimised CuAAC procedure has in bio conjugated applications. Still, the best has yet to come…

References

1. Braeken Y, Verstappen P, Lutsen L, Vanderzande D, Maes W. Synthesis of a multifunctional poly(p-phenylene ethynylene) scaffold with clickable azide-containing side chains for (bio)sensor applications. Polymer Chemistry. 2015; 6(37):6720-31.

2. Dumoulin M, Conrath K, Van Meirhaeghe A, Meersman F, Heremans K, Frenken LGJ, *et al.* Single-domain antibody fragments with high conformational stability. Protein Science. 2002;11(3):500-15.

3. Muyldermans S, Baral TN, Retamozzo VC, De Baetselier P, De Genst E, Kinne J, *et al.* Camelid immunoglobulins and nanobody technology. Veterinary Immunology and Immunopathology. 2009;128(1–3):178-83.

4. Ley K, Huo Y. VCAM-1 is critical in atherosclerosis. Journal of Clinical Investigation. 2001;107(10):1209-10.

5. Ta D, Guedens W, Vranken T, Vanschoenbeek K, Steen Redeker E, Michiels L, *et al.* Enhanced biosensor platforms for detecting the atherosclerotic biomarker VCAM1 based on bioconjugation with uniformly oriented VCAM1-targeting nanobodies. Biosensors. 2016;6(3):34.

6. Pardridge WM. Blood-brain barrier drug delivery of IgG fusion proteins with a transferrin receptor monoclonal antibody. Expert opinion on drug delivery. 2015;12(2):207-22.

Summary

During the last decade the copper catalysed azide alkyne cycloaddition (CuAAC) reaction has demonstrated its potential use in several research areas. The unique combination of properties, such as high specificity, high yields, minute side reactions, bio-orthogonality and the mild reaction conditions, in which the coupling reaction can take place, creates many opportunities for a wide variety of applications. The CuAAC has a lot to offer for surface modification and functionalisation purposes of solid substrates. However, a reliable surface coupling protocol was not yet described and optimised until now. This thesis presents a detailed and versatile protocol, as optimised with real time *in situ* measurements, being able to modify surfaces with biomolecules using the reproducible CuAAC reaction.

For the optimisation, initially an alkynated, commercially available fluorescent dye, Alexa Fluor® ^{488}, was immobilised under various conditions to an azidified glass surface. By following the successful coupling of this fluorescent dye using fluorescence measurements, several aspects of the CuAAC immobilisation were analysed and optimised.

After the successful immobilization of the dye, an alkynated version of *Staphylococcus* protein A (A-SpA) was immobilised to the azidified surface. The reaction conditions of this CuAAC coupling were optimised by monitoring the surface mass changes in real time by means of null-ellipsometry. This resulted in a very fast, covalent, CuAAC immobilisation procedure by which very reproducible biolayers could be obtained. In this procedure, a carboxylated silicon surface was azidified with 3-azido-1-aminopropane. Subsequently, an alkynated protein was immobilized using 0.5 mM $Cu(I)SO_4$, 2.5 mM sodium ascorbate and 1mM THPTA in sodium acetate buffer pH 4.

In addition, the CuAAC can offer even more advantages due to its bioorthogonal character. For many applications that are using biomolecule layers their surfaces, an oriented coupled biolayer is preferential in order to obtain an optimal availability of the active sides. For example, it can be anticipated that orientation has a tremendous influence on the sensitivity of a sensing biolayer. This site-directed immobilisation can be achieved by modifying the biomolecules in a site-specifically manner. By applying a functionalisation method based on Intein-expressed protein Ligation (IPL), maltose binding protein was site-specifically functionalised with a single alkyne group.

By null-ellipsometry, it was demonstrated that site-specifically, mono alkynated MBP's was successfully coupled to azidified silicon substrates. However, the obtained surfaces mass of ssA-MBP were relatively lower compared to MBP species with a high degree of alkynation. Nevertheless, the binding capacity of monoclonal anti-MBP towards this site-directed immobilised layer MBP was higher. These results demonstrate that by steering the orientation of the immobilised layer, the binding capacity of the complete surface can be improved.

In addition to the ellipsometry measurements, the surface mass obtained after immobilizing A-SpA was also quantified with a QCM-D measuring device. Alkynated SpA was immobilised to an azidified, silicon oxide containing quartz crystal. Afterwards, this A-SpA functionalised surface was exposed to several cycles of hIgG binding and removing. The QCM measurements confirmed the results obtained by null-ellipsometry: the formed SpA layer had the surface mass of a close-packed monolayer. Furthermore, by performing several cycles of binding and detaching hIgG, the specific coupling of hIgG to the CuAAC immobilised A-SpA layer was demonstrated. This proved that the A-SpA

containing surface was reusable as well. All the previous observations confirm that the CuAAC reaction is actually capable of realising the high expectations of being specific, ultrafast and reliable!

Publication list & conference contributions

2017

Journal Contribution

Vranken, Tom; Miszta, Adam; de Laat, Bas; Hermens, Wim; Steen Redeker, Erik; Adriaensens, Peter; Guedens, Wanda & Cleij, Thomas (2016)**.** *In situ monitoring and optimisation of CuAAC-mediated protein functionalisation of biosurfaces.*
In: Sensors & Actuators: B. Chemical, 2017, 238, p 992-1000. [Article - cat: A1]

2016

Journal Contribution

Ta, Duy Tien; Guedens, Wanda; Vranken, Tom; Vanschoenbeek, Katrijn; Steen Redeker, Erik; Michiels, Luc & Adriaensens, Peter (2016). *Enhanced Biosensor Platforms for Detecting the Atherosclerotic Biomarker VCAM1 Based on Bioconjugation with Uniformly Oriented VCAM1-Targeting Nanobodies.*
In: Biosensors, 6 (3), (ART N° 34). [Article - cat: A2]

2015

Conference Material

Ta, Duy Tien; Vanschoenbeek, Katrijn; Vranken, Tom; Steen Redeker, Erik; Michiels, Luc; Noben, Jean-Paul; Guedens, Wanda & Adriaensens, Peter (2015). *Covalent and uniformly oriented immobilisation of the 'clickable' alkynated nanobody targeting the vascular cell adhesion molecule-1 for advanced biosensing applications.*
In: 4th International Conference on Bio-sensing Technology, Lisbon, Portugal, 10/05/2015 - 13/05/2015. [Poster - cat: C2]

TA, Duy Tien; Vranken, Tom; Steen Redeker, Erik; Noben, Jean-Paul; Guedens, Wanda & Adriaensens, Peter (2015). *Developing an Ellipsometry-based Biosensor Platform via Covalent and Oriented Coupling of the Nanobody Targeting the Vascular Cell Adhesion Molecule-1 To A Silicon Wafer.*
In: Biomedical Summit 2015, Genk, Belgium, 02/06/2015 - 03/06/2015. [Paper - cat: C2]

2014

Conference Material

Billen, Brecht; Vranken, Tom; Reekmans, Gunter; Steen Redeker, Erik; Adriaensens, Peter & Guedens, Wanda (2014). *Hydrazine-based expressed protein ligation as a tool for site-specific modification of proteins towards advanced biomaterials.*
In: Annual Meeting IAP P7/05, Louvain-la-Neuve, 19/09/2014. [Poster - cat: C2]

Billen, Brecht; Vranken, Tom; Reekmans, Gunter; Steen Redeker, Erik;

Adriaensens, Peter & Guedens, Wanda (2014). *Maltose binding protein as a model for site-specific modification by hydrazine-based expressed protein ligation for advanced biomaterials.*
In: Biomedica 2014, Maastricht, the Netherlands, 17-18/06/2014. [Poster - cat: C2]

Vranken, Tom; Miszta, Adam; de Laat, Bas; Hermens, Wim; Steen Redeker, Erik; Adriaensens, Peter; Guedens, Wanda & Cleij, Thomas (2014). *CuAAC-mediated Protein Immobilisation towards Next Generation Biosensing Devices.*
In: ChemCYS 2014, Blankenberge, 27-28/02/2014. [Presentation - cat: C2]

Billen, Brecht; Vranken, Tom; Reekmans, Gunter; Steen Redeker, Erik; Adriaensens, Peter & Guedens, Wanda (2014). *Hydrazin-based expressed protein ligation for site-specific modification of maltose binding protein.*
In: Chemcys 2014, Blankenberge, 27-28/2/2014. [Poster - cat: C2]

Billen, Brecht; Vranken, Tom; Reekmans, Gunter; Steen Redeker, Erik; Adriaensens, Peter & Guedens, Wanda (2014). *In vitro site-specific functionalisation of proteins for advanced bioactive materials.*
In: Advanced Materials for Biomedical Applications, Ghent, 17/11/2014-21/11/2014. [Presentation - cat: C2]

2013

Journal Contribution

Peeters, Marloes; Troost, Freddy J.; Mingels, Roel H. G.; Welsch, Tina; van Grinsven, Bart; Vranken, Tom; Ingebrandt, Sven; Thoelen, Ronald; Cleij, Thomas Jan & Wagner, Patrick (2013). *Impedimetric Detection of Histamine in Bowel Fluids Using Synthetic Receptors with pH-Optimised Binding Characteristics.*
In: Analytical Chemistry, 85 (3), p. 1475-1483. [Article - cat: A1 - Validation: ecoom 2014]

Conference Material

Vranken, Tom; Miszta, Adam; Hermens, Wim; Steen Redeker, Erik; Cleij, Thomas J.; Adriaensens, Peter & Guedens, Wanda (2013). *Click chemistry as a tool for protein immobilisation towards innovative biosensing applications.*
In: Engineering Functional Interfaces (EnFI), Hasselt - Belgium, 08/07-09/07/2013. [Poster - cat: C2]

Vranken, Tom; Miszta, Adam; Hermens, Wim; Adriaensens, Peter; Steen Redeker, Erik; Cleij, Thomas & Guedens, Wanda (2013). *CuAAC as protein/antibody immobilisation strategy towards advanced biosensing platforms.*
In: Belgian Polymer Group Annual Meeting (BPG), Houffalize - Belgium, 16/05-17/05/2013. [Poster - cat: C2]

2012

Conference Material

Vranken, Tom; Miszta, Adam; Hermens, Wim; Cleij, Thomas; Adriaensens, Peter; Steen Redeker, Erik & Guedens, Wanda (2012). *The covalent coupling of alkynylated proteins to functionalised carriers using the Click Azide Alkyne Cycloaddition.*
In: Belgian-German (Macro)Molecular Meeting, Advanced Materials by Modular Strategies: From Synthesis to Industrial Applications, Houffalize, Belgium, 3-4 December 2012. [Poster - cat: C2]

Nederlandstalige samenvatting

In de laatste tien jaar heeft de koper gekatalyseerde azide alkyn cycloadditie reactie (CuAAC) zijn potentieel bewezen in allerhande onderzoeksdisciplines. De unieke combinatie van verschillende eigenschappen zoals de hoge specificiteit, de hoge opbrengsten van de reactie, het klein aantal nevenreacties, de bio-orthogonale eigenschappen en de milde reactiecondities zorgen er voor dat dit type koppelingsreacties veel te bieden heeft wat betreft oppervlaktemodificaties en -functionalisaties van vaste dragers. Er is slechts één grote maar. Tot op heden zijn er nog geen betrouwbare noch geoptimaliseerde protocols om biomoleculen op een efficiënte manier aan een vaste drager te koppelen beschreven. In deze thesis wordt een gedetailleerd, generiek immobilisatie protocol voorgesteld, dat door middel van real time *in situ* metingen geoptimaliseerd is. Met dit protocol worden vaste dragers op reproduceerbare wijze gemodificeerd met moleculen van biologische oorsprong via de CuAAC koppelingsreactie.

In eerste instantie werd een gealkyneerd, commercieel beschikbaar fluorescerende molecule, Alexa Fluor® ^{488}, geïmmobiliseerd op een azide gefunctionaliseerd glasoppervlak. Aan de hand van fluorescentiemetingen werden verschillende aspecten van de CuAAC koppeling onder de loep genomen en geoptimaliseerd. Dit resulteerde uiteindelijk in een succesvolle koppeling van het fluorescerende molecule op een glasoppervlak.

Nadat deze 'dye' succesvol werd geïmmobiliseerd, werd het fluorescerend gealkyneerd protein A (A-SpA), gekoppeld op een met azides gemodificeerd oppervlak. De reactieomstandigheden van de CuAAC koppeling werden geoptimaliseerd door oppervlaktemassaveranderingen in real time te meten gebruikmakend van null-ellipsometrie. Uiteindelijk resulteerde dit in een zeer snelle, covalente, CuAAC immobilisatie procedure die zeer reproduceerbare

biolagen tot stand brengt. In deze procedure werd een gecarboxyleerd silicium oppervlak gefunctionaliseerd met 3-azido-1-aminopropaan. Vervolgens kan een gealkyneerd proteine aan de azidefunctie gekoppeld worden middels 0.5 mM $Cu(I)SO_4$, 2.5 mM natriumascorbaat en 1 mM THPTA in natriumacetaat buffer pH 4.

De CuAAC heeft, naast de mogelijkheid om op een snelle manier een covalente binding te creëren, ook nog andere voordelen door zijn bio-orthogonale eigenschappen. Voor vele applicaties waarbij biologische moleculen aangebracht worden op een specifiek oppervlak, is de oriëntatie van actieve plaats van groot belang. Een uniform georiënteerde biolaag kan er namelijk voor zorgen dat de actieve sites zo goed mogelijk beschikbaar zijn voor binding met de targetmolecule. Een goed voorbeeld hiervan is wanneer deze biologische laag gebruikt zou worden in biosensoren. Wanneer de oriëntatie optimaal is kan een grotere sensitiviteit bereikt worden. Een geörienteerde immobilisatie kan echter enkel verkregen worden indien de biomoleculen voorzien zijn van slechts één functionele groep die verantwoordelijk is voor de binding met het oppervlak. Via het 'willekeurige' alkyneringsproces (functionalisatie van endogene lysines), gebruikt voor SpA, zal deze plaatsgestuurde, mono-alkynering niet verwezenlijkt kunnen worden. Daarom werd de alkyneringsmethode, gebruikt voor SpA, vervangen door een op Inteïne-expressed Protein Ligatie (IPL) gebaseerde methode. Op die manier konden Maltose Bindende Proteins (ss-MBP) verkregen worden die slechts één alkyngroep bevatten.

In dit werk wordt aangetoond dat de plaatsspecifiek gealkyneerde MBP moleculen met succes gekoppeld kunnen worden aan een azidegefunctionaliseerd oppervlak. In vergelijking met de MBP moleculen die zonder enige vorm van oriëntatie

geïmmobiliseerd werden, resulteerde de koppeling met de plaatsspecifiek gefunctionaliseerde MBP (ssA-MBP) molecules in iets lagere oppervlakte massa's. De bindingcapaciteit van ssA-MBP daarentegen, met hun complementair proteine, anti-MBP, was echter wel verbeterd. De resultaten tonen aan dat de oriëntatie van de geïmmobiliseerde laag een cruciale rol speelt in de bindingscapaciteit van de geïmmobiliseerde biologische laag.

Als laatste, werden de massaveranderingen van A-SpA op een azide gemodificeerd siliciumoxide gefunctionaliseerd kwartskristal aan de hand van QCM-D gemeten. De QCM metingen bevestigden de aan de hand van ellipsometrie verkregen resultaten. Verder werden de stalen blootgesteld aan verschillende cycli waarin eerst hIgG werd gebonden aan het SpA oppervlak en vervolgens er weer werd afgewassen. Dit werd gedaan door eerst het staal bloot te stellen aan hIgG, en vervolgens te wassen met glycine. Zo kon aangetoond worden dat de binding tussen hIgG en de SpA oppervlak zeer specifiek gebeurde. Hieruit bleek dat de biolaag dus ook herbruikbaar was. Alle voorgaande resultaten bevestigen dat de CuAAC immobilisatie reactie niet alleen het potentieel heeft, maar dat het effectief in staat is om zijn status waar te maken in toepassingen waarbij een biologisch gefunctionaliseerd opervlak vereist is.

Dankwoord

Een dinsdagavond, 32 °C, eind juni 2017. Het ideale moment, en ook wel weer typerend vlak voor de deadline, om een dankwoord te schrijven. Als ik er zo over nadenk, heb ik toch wel een aardig lijstje van leuke/interessante collega's en vrienden opgebouwd gedurende mijn 'carriere' op de Uhasselt, waar ik toch wel het een en het ander aan te danken heb. Laten we beginnen. met het einde, maar dan ook weer niet helemaal het einde.

Gedurende het grootste deel van mijn studententijd (lees: 7 van de 13 jaar) was ik ingeschreven als doctoraatstudent/vrijwillig medewerker bij OBPC. Die laatste 'titel' heb ik, met dank aan Prof. Dr. Wanda Guedens en Prof. Dr. Thomas Cleij, gelukkig enkele malen mogen verlengen. Waarschijnlijk vaak tot ergernis van Prof. Dirk Vanderzande, die zich maar telkens afvroeg: "Wanneer gaat die bengel eindelijk eens afleggen?" (Als alles goed verlopen is, zou dat bij deze bijna gebeurd, of gebeurd moeten zijn, Dirk). Maar het is dankzij jullie twee, Thomas en Wanda, dat ik toch nog op regelmatige basis werd aangemaand tot het verder finaliseren van hoofdstuk 1, enkele maanden later hoofstuk 2 en ga zo maar door. Het was een speciaal, maar interessant traject. Ik herinner me nog een vergadering in juli 2015; "Indien we tegen september alles op papier hebben, kan het snel gaan." Helaas, die deadline hebben we net niet gehaald. In ieder geval, jullie stonden in de laatste 3 jaar helemaal centraal.

De jaren daarvoor heb ik al schipperend door gebracht tussen het lab in Maastricht van Prof. Dr. Wim Hermens, het organische scheikunde lab, het lab van Huguette en het lab van Erik, Brecht en David. Ik moet zeggen, een heerlijke tijd. Kon ik Rafael zijn, hoe zal ik het noemen, 'lectures' op een geven moment niet meer volgen, vertrok ik naar Brecht. Moest dat lab gekuist worden, kwam ik terug naar de bureau. Had Neomy daar te veel lawaai, vluchtte ik naar Maastricht. En zo ging

het dag na dag, week na week. Al weet ik nu niet meer heel zeker of ik voor jouw periode, Neomy, al richting Maastricht ging om Free zijn uiteenzettingen te ontvluchten. (Bij deze Neomy, je was niet de oorspronkelijke oorzaak).

Wanneer mijn stalen, die ik in Hasselt geprepareerd had, klaar waren om te gebruiken voor ellipsometrie experimenten, vertrok ik in mijn op-dat-moment-nog splinternieuwe Volvo C30 richting Delbia BV in Maastricht. Daar waren het Prof. Wim Hermens en Adam Miszta die mij beiden opwachtten. (Ik schrijf dit stukje niet in het Engels Adam, aangezien ik er vanuit ga dat je toch genoeg Nederlands verstaat ondertussen). Iedere dag experimenten doen, 8 uur aan het stuk oplossingen omwisselen, om zeer vaak te eindigen met de handen in het haar, onszelf afvragend wat er nu weer misgelopen was. Het zinnetje *"what do you think?"* werd wel eens vaker gesteld. Had ik al die experimenten moeten neerschrijven, dan kon ik pas tegen mijn 70ste aan het dankwoord beginnen. In ieder geval, hartelijk bedankt, Wim en Adam, om me te assisteren gedurende een twee-tal jaar. Als ik me niet vergis is hier ook mijn 'koffie verslaving' begonnen. Ook dank daarvoor!

Eens terug in Hasselt, waren het Jurgen *alias* Kesters, Pieter, Rafael, Inge, Hanne, Free, Ans, Joke, Matthias, Kathy (ik vergeet er nog wel een deel) die me telkens weer met open armen ontvingen, uitkijkend naar de spannende verhalen die ik altijd meebracht (sarcastisch). *"De experimenten lukten niet echt, maar moet ge eens weten wat mijn katten Bayleigh en Oakly weer aangevangen hebben. Die beesten zijn geweldig!".* Zo ging het dan tientalle minuten verder. Midden in mijn verhaal, kon het al eens gebeuren dat Gunther binnenstormde. "Werk, werk, werk, altijd maar werk", tot plots de handrem werd opgetrokken en Gunter toch even bleef stilstaan. De kans is groot dat ik je dan weer een of andere onnozele

opmerking naar je hoofd slingerde, waarbij je vaak dacht en waarschijnlijk ook luidop zei: *"Man, man, man, Tom jonge! Gij zijt ene Sjarel"*.

Dat brengt me naadloos bij de reden waardoor ik mijn doctoraat ben mogen beginnen. Al startte ik mijn Masterstage bij Jan Duchateau, die me eerder al enkele skills (geen voetbalvaardigheden Jan, die had ik al) had aangeleerd tijdens één van de eerste stage. Heerlijke vent die Jan, alleen jammer dat je net op dat moment veel met het schrijven van jouw PhD-thesis bezig was. Maar goed, Gunter heeft mij in de daarop volgende maanden geïntroduceerd in het functionaliseren van glazen oppervlakken en van proteines. Mede dankzij Gunter en Erik ben ik tot op dit punt geraakt. En jou Erik, moet ik zeker bedanken voor alle hulp die ik gekregen heb om het artikel gepubliceerd te krijgen. (Ik zou tekort doen aan Peter en Wanda als ik jullie hier niet zou vermelden.) Waarschijnlijk zie ik nog wel enkele zaken over het hoofd waarvoor ik ook altijd bij je terecht kon, Erik; serieuze maar veel vaker voor plezante intermezzo's.

Nu, de meeste tijd heb ik samen doorgebracht heb met Ans, Toon, Jurgen, Pieter, Inge, Hanne, Free, Sarah en Joke (sorry als ik iemand vergeet, maar ik zit met mijn deadline ;)). Ik denk dat jullie de belangrijkste reden waren voor de goeie sfeer op de bureau en daardoor kwam ik nooit met tegenzin werken. Ook Gène mag ik hier niet vergeten bij te noemen. Als er nu eens één levensgenieter is waarop ik wel een beetje jaloers op ben, dan zijt gij het! Geen enkel labo liep verkeerd onder uw toezicht. Dat in combinatie met uw eeuwenoude voetbalkennis. Wat wilt een mens nog meer?

Het thuisfront mag ik zeker niet vergeten. Ten eerste zijn er ma en pa en Wim, die natuurlijk aan de basis liggen van heel dit verhaal. Daar kan ik niet omheen. Al van kleinsaf, moesten ze alle vragen die in mij opkwamen, beantwoorden. Geen

wonder dat ze me op mijn 18e richting universiteit in Hasselt zagen vertrekken. "*Gelukkig niet op kot!".* Dan kon niet goed gekomen zijn (dat besefte ik maar al te goed). De eerste 3 jaren gingen, al bij al, vrij vlot. Een onvoldoende hoorde er al eens bij. Uit het niets kwam ik Diana tegen. Een blond meisje, blauwe ogen, afkomstig uit het naburige dorp Opgrimbie (Waarschijnlijk heeft daar nog geen kat van gehoord, tenzij het over het klooster gaat dat gebouwd is op het koninklijk domein, illegaal ook nog wel, maar goed). "Hoe kon het ook anders", zal pa op dat moment wel gedacht hebben (rara waar zou hij van afkomstig zijn?). Het leuke is dat ik vanaf dat moment, zonder herkansingen, de twee laatste jaren van mijn Master met succes kon afmaken. Maar niet alleen tijdens die laatste 2 jaren heb je een positieve invloed gehad. Ook in het finaliseren van mijn doctoraat heb jij een grote rol gespeeld. Sinds het moment dat ik begon te werken bij NineSigma, heeft ze mij ook regelmatig de vraag gesteld: *"Wanneer gaat ge nu dat eindwerk eens afmaken?"*. Mijn blik, die op die vraag volgde, was waarschijnlijk niet de meeste vriendelijke, maar het heeft er wel voor gezorgd dat ik regelmatig op een zaterdagochtend achter of voor de laptop (afhankelijk van uw referentiepunt) te vinden was, tussen het voetballen en de festivals door. Al moet ik wel zeggen, diezelfde vraag, met een lichtjes anders accent, werd me ook regelmatig (lees: dagelijks) voorgeschoteld door mijn collega's in Eindhoven Bedankt Rafael, Rick, Elma, Margot, Evi en John. Al moet ik zeggen, op een gegeven moment heb ik zelfs even aan een besmettelijke vorm van Alzheimer gedacht.

En hier ben ik dan, 7 jaar later. Waarschijnlijk mijn PhD behaald. Het duurde iets langer dan normaal maar dankzij jullie allemaal, ben ik er uiteindelijk geraakt. En nu, op naar het volgende project: *"Hoe bouw ik een huis?"*. Maar daar ga ik geen boekje over schrijven.